STScI | SPACE TELESCOPE SCIENCE INSTITUTE

Instrument Science Report WFC3 2017-22

WFC3 Anomalies Flagged by the Quicklook Team

C.M. Gosmeyer & The Quicklook Team

Last modified on May 16, 2019 [1]

Abstract

Like all detectors, the UVIS and IR detectors of the Wide Field Camera 3 (WFC3) on the Hubble Space Telescope are subject to detector and optical anomalies. Many of them can be corrected for or avoided with careful planning. We summarize, with examples, the various WFC3 anomalies, which when found are flagged by the WFC3 "Quicklook" team of daily image inspectors and stored in an internal database. We also give examples of known detector features and defects, and some non-standard observing modes. The aim of this report is (1) to educate users of WFC3 to more easily assess the quality of science images and (2) to serve as a reference for the WFC3 Quicklook team members in their daily visual inspections.

[1] J. V. Medina, May 2019 - Table 1, Section 2.3

Copyright © 2017 The Association of Universities for Research in Astronomy, Inc. All Rights Reserved.

1 Introduction

As initially conceived, Quicklook was a sub-team of Hubble's Wide Field Camera 3 (WFC3) instrument team tasked with visually inspecting all new images for quality and any unexpected behavior, with the intent that the WFC3 team would catch and diagnose anomalies before the general observers. The scope and tools of the Quicklook team have grown, however, and today "Quicklook" refers to more than just the team, but also the team-built system of software, database, and filesystem, all underlying an internal website (Bourque et al., 2016). With the website team members daily check automated calibration and stability monitors, as well as the new images. One benefit of the web browser interface to the Quicklook system is the ability to, with a click, flag an image for specific anomalies. These flags are stored as entries in a database table. Because this function was developed seven years after WFC3's installation, the Quicklook team has been returning to archived WFC3 data to completely catalog all present anomalies. We expect to finish the process in early 2018 and eventually make available non-proprietary entries of the database table. With this anomalies database table, we take a step beyond just monitoring the integrity of observations; we can also use it to obtain a deeper understanding of the behaviors of the optics and IR and UVIS detectors as they age, knowledge that can also be applied to other Hubble instruments such as the Advanced Camera for Surveys or to forthcoming space-based instruments such as those on the James Webb Space Telescope.

When we talk about the appearance of an "anomaly" that does not necessarily imply that the feature has compromised the science quality of the image or that it is unexpected or that its cause is unknown. Most of these features are very well studied and corrections and avoidances are in place. We use "anomaly" to describe certain features appearing unwanted anywhere in the frame - whether or not they impact the science target - features such as satellite trails, peculiar cosmic rays, or reflections off the filter wheel. Eight years of data show certain anomalies appearing again and again, and most of them have been named and explained. The occasional unclassified anomaly is categorized in the catch-all of "other" until enough examples are found to justify defining its own class. Table 1 lists the classified anomalies, as well as four pending-classified anomalies, that the Quicklook team flags (sub-divided by origin: detector (Section 2), light scatter and reflections (Section 3), and act-of-nature (Section 4)); Table 2 lists some known detector defects that the Quicklook team does *not* flag (Section 5); and Table 3 lists some non-standard observing modes that could be mistaken for anomalous behavior (Section 6). In the Appendix we illustrate some queries to the Quicklook database that utilize the anomalies table. In Conclusions we summarize detector studies that have been facilitated by the anomalies table.

We are assuming some familiarity with the WFC3 UVIS and IR detectors. You can get an overview from Chapter 1 of Deustua (2016) and Chapter 2 of Dressel (2017). For quick reference, Figure 1 shows schematics of the detectors.

The purpose of this report is to provide an overview, for both WFC3 observers and Quicklook team members, of what the identified detector and optical anomalies are and how they can be corrected for or avoided. We strive to consolidate into a single document information that has been scattered through the WFC3 website, instrument science reports, and handbooks, and we hope this will serve as a primary reference going forward.

Please be assured that all images shown in this report are non-proprietary. The images are FLT (`calwf3`-calibrated) files that have been stretched and converted into JPGs by Quicklook's automated software, appearing as they would on the Quicklook website.

Table 1– Anomalies on the IR and UVIS detectors as defined by the WFC3 team, flagged by daily quicklookers. Many of these names are colloquial to the WFC3 team and may not be the standard industry names, or even the same names used by other Hubble or James Webb instrument teams, for the phenomena.

Anomaly	*Detector(s)*	*Origin*	*Section*
Cosmic Ray Shower	UVIS	detector	2.1
Crosstalk	IR, UVIS	detector	2.2
Dark Vertical Stripe*	IR	detector	2.3
Data Drop-Out*	IR, UVIS	act-of-nature	4.1
Data Transfer Error	IR, UVIS	act-of-nature	4.2
Detector-Filter Ghost	IR, UVIS	scatter/reflection	3.1
Diamond Feature	IR	scatter/reflection	3.2
Diffraction Spike	IR, UVIS	scatter/reflection	3.10
Dragon's Breath	UVIS	scatter/reflection	3.3
Earth Limb/Shine	IR	scatter/reflection	3.4
Excessive Saturation	IR, UVIS	detector	2.4
Figure-8 Ghost	UVIS	scatter/reflection	3.5
Filter Ghost	UVIS	scatter/reflection	3.6
Fringing	UVIS	scatter/reflection	3.7
Guidestar Failure	IR, UVIS	act-of-nature	4.3
IR Banding	IR	detector	2.5
Light Hedge*	IR	scatter/reflection	3.8
Light Spike*	IR	scatter/reflection	3.9
Persistence	IR	detector	2.6
Prominent Blobs	IR	detector	2.7
Satellite Trail	IR, UVIS	act-of-nature	4.4
Scattered Light	UVIS	scatter/reflection	3.11
Space Trash & Asteroids*	IR, UVIS	act-of-nature	4.5

* These anomalies do not have their own column in the Anomalies table of the Quicklook database at this time and are instead flagged as "other." They may be given proper classes in a future update to the software.

Table 2– Known defects of the IR and UVIS detectors *not* flagged by daily quicklookers.

Known Defect	*Detector*	*Section*
Bad Pixel Columns	UVIS	5.5
Blobs	IR	5.1
CTE Trails	UVIS	5.2
IR Flat Field	IR	5.3
Snowballs	IR	5.4
UVIS Internal Flat Field	UVIS	5.6

Table 3– Some non-standard WFC3 modes and observations that could be mistaken for anomalous behavior.

Non-Standard Mode/Observation	*Detector*	*Section*
Bowtie	UVIS	6.1
Charge Injection	UVIS	6.2
Earth Flats	IR	6.3
Grism Bright Object Bands	IR	6.4
Grism+Spatial Scanning	IR	6.5
Moving Target	IR, UVIS	6.6
Quad Filters	UVIS	6.7
Spatial Scanning	IR, UVIS	6.8
UVIS Grism	UVIS	6.9

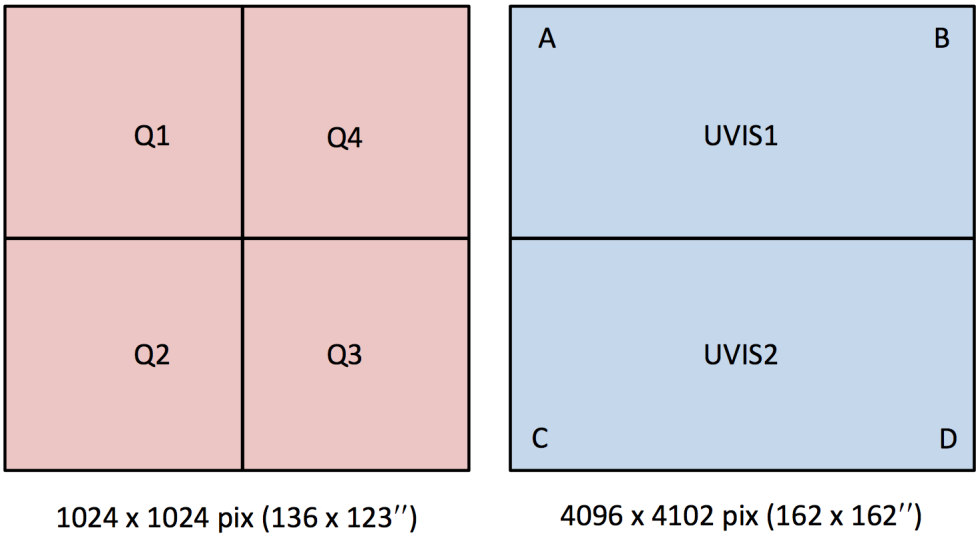

Figure 1 – Schematic of the four-quadrant IR detector (left) and the two-chip UVIS detector (right). The letters on UVIS represent the four corner amplifiers.

2 Detector Anomalies

This section discusses anomalies due to the nature of the IR and UVIS detectors themselves.

2.1 Cosmic Ray Shower (UVIS)

Some cosmic rays appear to shower across the UVIS detector. In most cases these showers resemble a contorted globular cluster and are usually only visible when the background is low, such as in a dark. They will rarely degrade the science target, except in cases of very poor luck, and like average cosmic ray streaks can be drizzled from the final image. A general discussion of cosmic rays on WFC3 is in Section 5.4.10 of Dressel (2017).

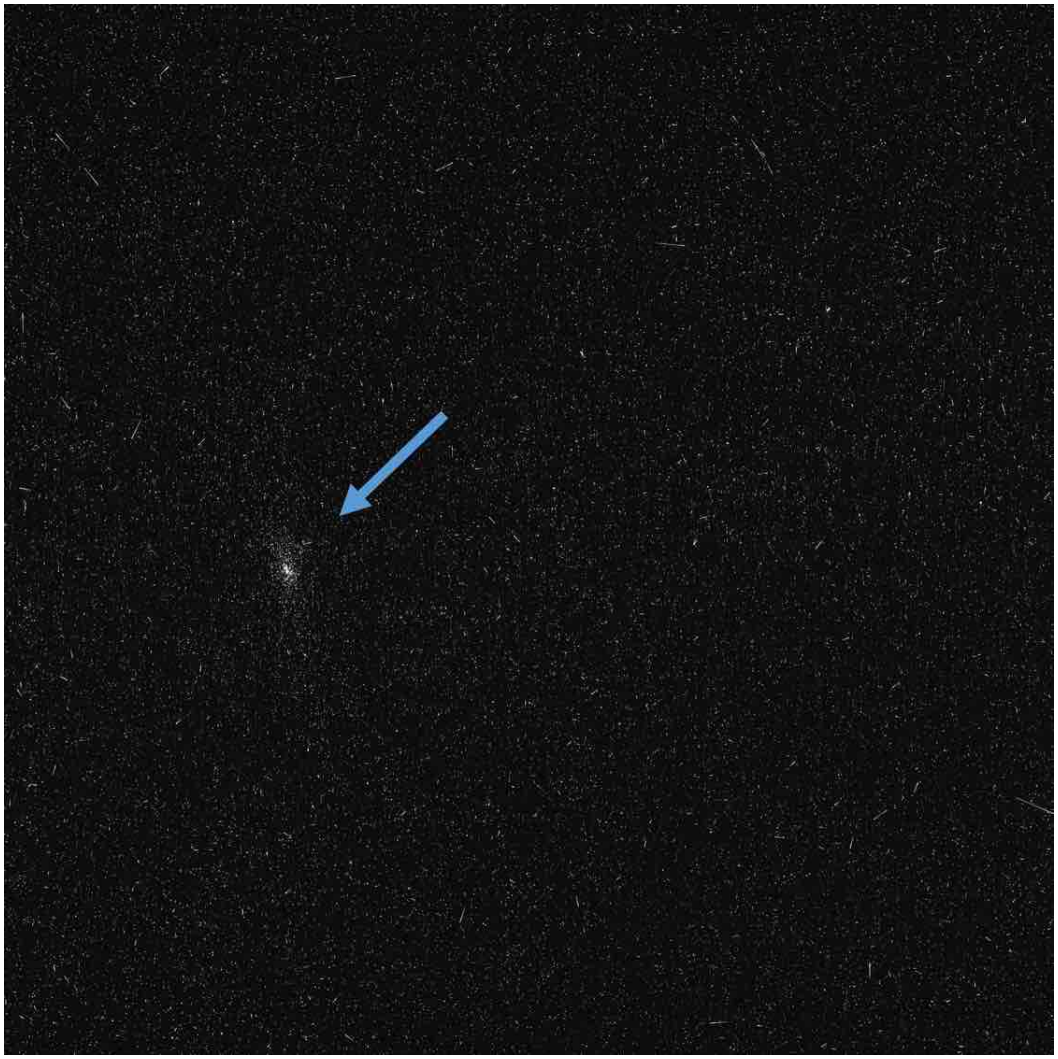

Figure 2 – Cosmic ray shower on UVIS, image `ic5m2rsbq_flt.fits`.

2.2 Crosstalk (IR & UVIS)

Crosstalk occurs between amplifiers as quadrants are read out, causing a mirror-symmetric electronic ghost of a bright source to appear on a coupled quadrant (A→B and C→D in UVIS, and 1→2 and 3→4 in IR). It's usually a subtle feature, and often you have to know what to look for to spot it. In UVIS, crosstalk is at a -2e-04 level of the source's signal in quadrants B and D, due to bright sources in quadrants A and C. Conversely, the level is -0.7e-04 in quadrants A and C due to sources in quadrants B and D (Baggett, 2009). In the IR, crosstalk appears lower than the background, a ∼1e-06 level of the source's signal (Viana and Baggett, 2010).

So that the effect is easily visible, we show an extreme example of UVIS crosstalk from a saturated comet in Figure 3. The crosstalk is the dark mirror on the far right (quad D) of the bright source on the far left (quad C). Figure 4 gives an example of IR crosstalk, the dark mirror in the upper left (quad 1) of the bright source on lower left (quad 2).

Crosstalk can be corrected on UVIS using standalone IDL and Python scripts available at `http://www.stsci.edu/hst/wfc3/tools/crosstalk`. Crosstalk on IR does not have a correction code, but it is so low it should not impact observations, especially if they are dithered.

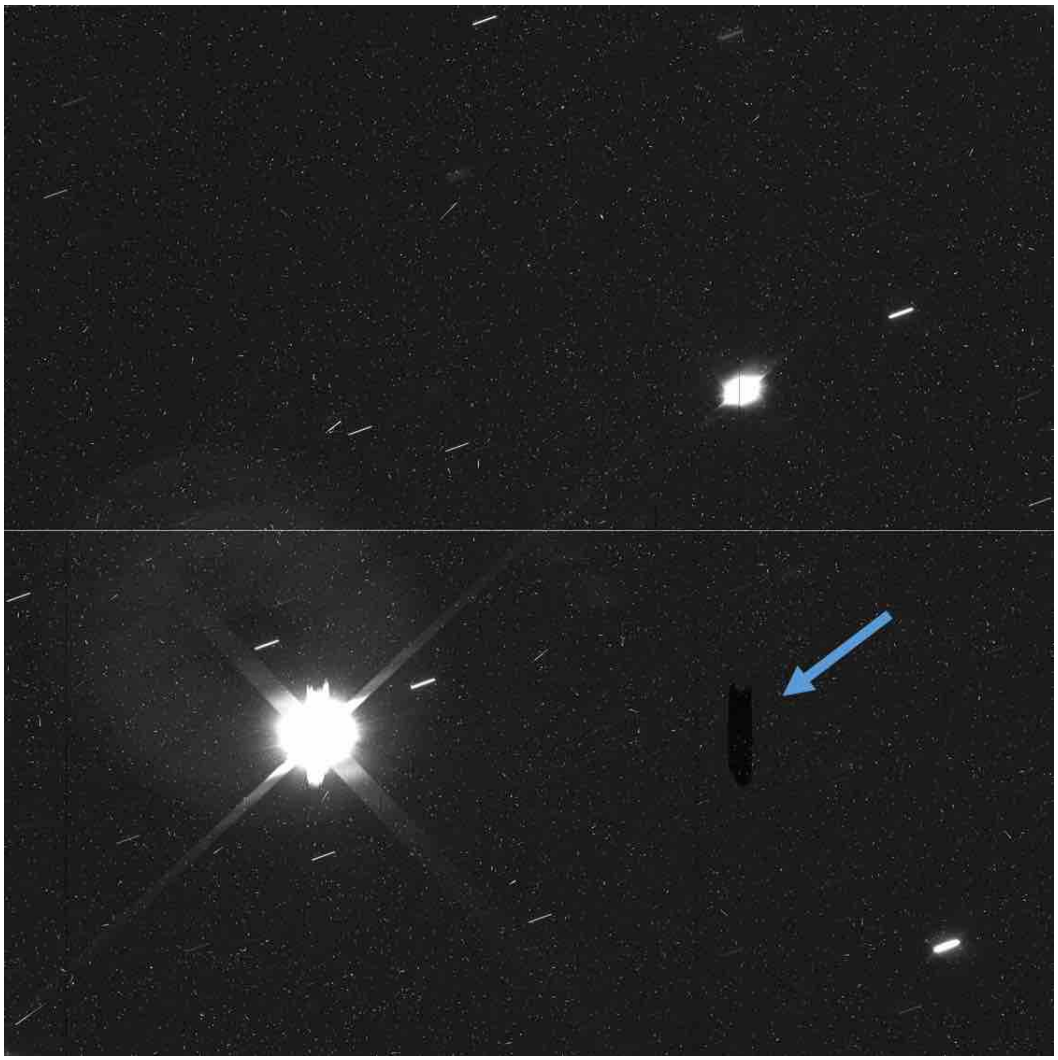

Figure 3 – Crosstalk (dark ghost on the right mirroring the bright target on the left) on UVIS image `ibcr07huq_flt.fits`*. A detector-filter ghost is also visible over the bright source.*

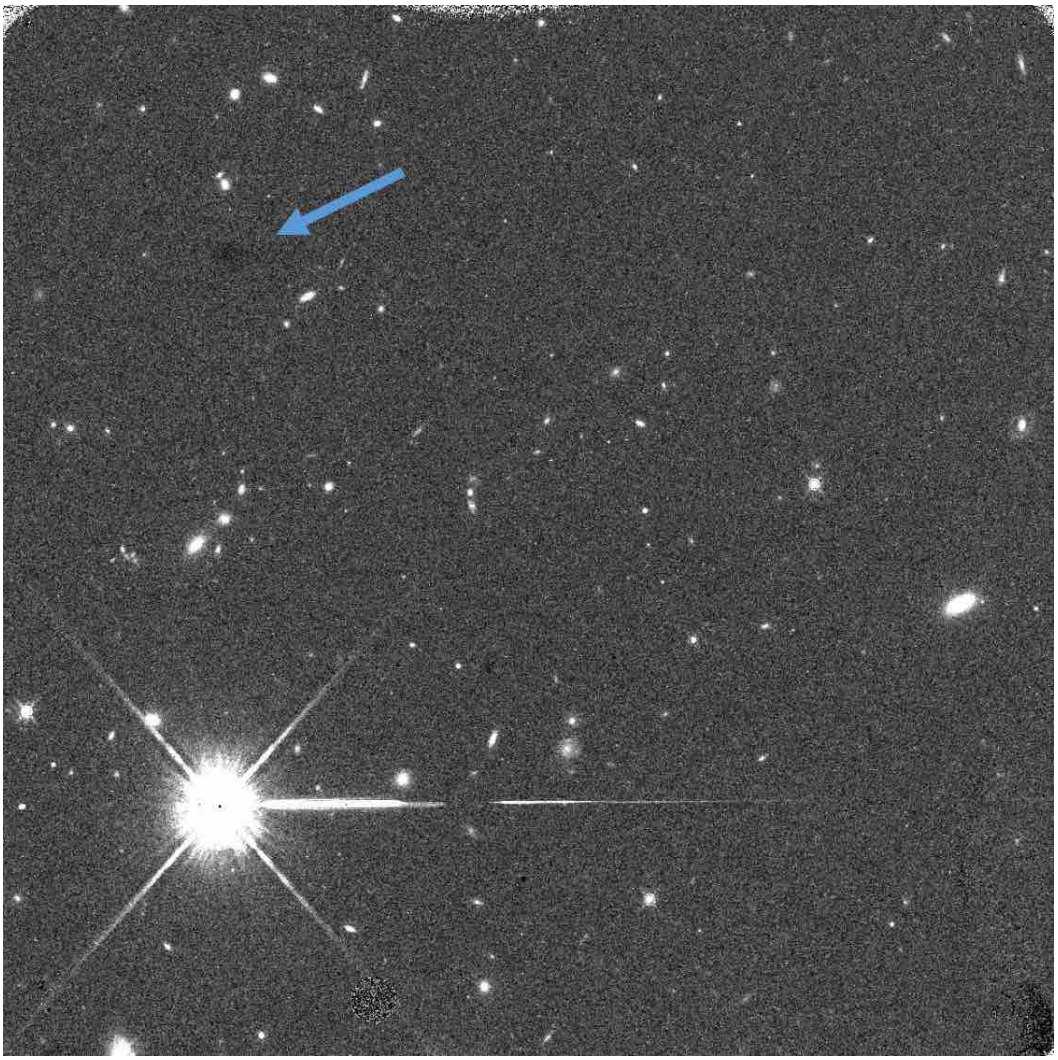

Figure 4 – Crosstalk (dark ghost on upper left mirroring bright target on lower left) on IR image `ibl91nsvq_flt.fits`*. The horizontal spikes appearing to emanate from the star are due to grism persistence.*

2.3 Dark Vertical Stripe (IR)

A dark vertical stripe will appear on the IR detector when the PSF core of a bright source lands on the Y-axis midline of the detector (regardless of where the source's position is on the X-axis). It has been observed that the column will appear darker on the side of the detector in which more of the PSF lands. The reason for why this happens is unknown, but the best way for users to prevent this artifact is to avoid having the cores of their sources land on the Y-axis midline.

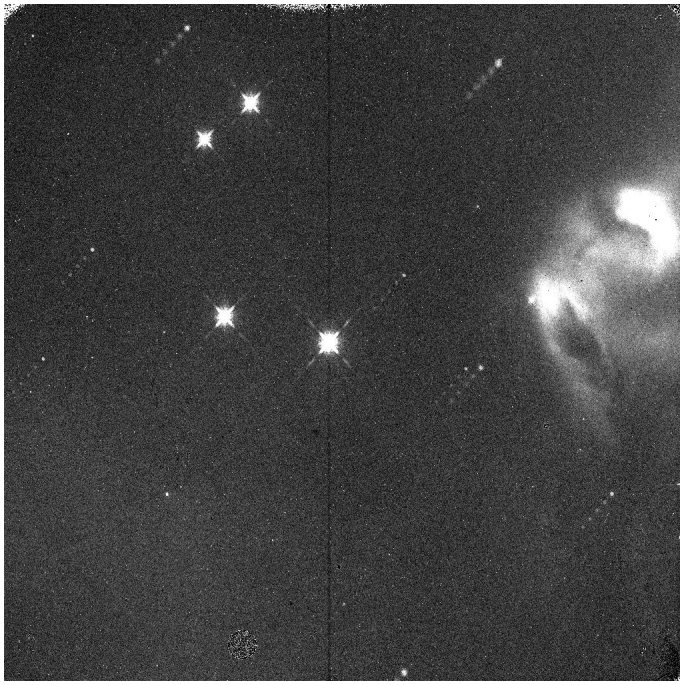

Figure 5 – Dark vertical stripe artifact on IR (`ib0lauigq_flt.fits`).

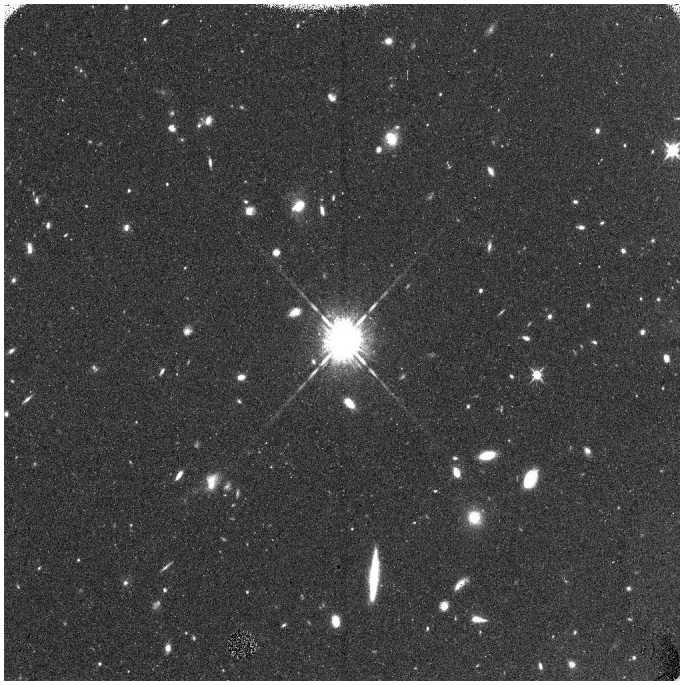

Figure 6 – Example where the dark vertical stripe is fainter in the bottom two quadrants, as a result of more of the PSF landing on the top 2 quadrants (`ibeuiqjfq_flt.fits`).

2.4 Excessive Saturation (IR & UVIS)

Saturation on UVIS ensues when charge is collected above the full well of 63000-71000 e-/pix on chip 1 or 67000-72000 e-/pix on chip 2 and spills out along columns, an effect called "blooming" (Gilliland et al., 2010). On the IR detector, saturation is defined when the linear response deviates by more than 5% (∼78,000 e-) (Section 5.7.5 in Dressel (2017)); this deviation from linearity can lead to aggressive flagging in the DQ array and, therefore, dark patches on the final pipeline-calibrated product where the saturated pixels have been masked. If not saturated entirely up the ramp, it can be possible to recover information from saturated IR images by removing the saturated reads and re-calibrating. There is no fixed criteria for what defines "excessive" saturation; the Quicklook team is encouraged to flag an image if a significant number of pixels relative to the source are impacted. For advice on selecting appropriate exposure times to avoid saturation see Section 4.2.2 in Dressel (2017).

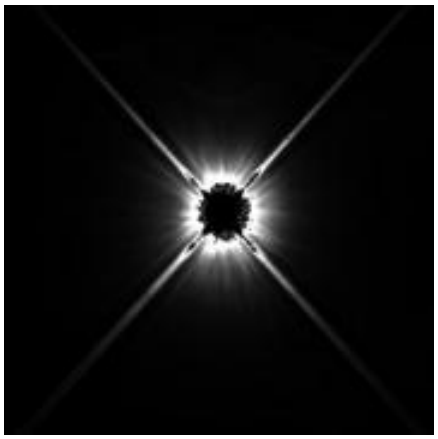

Figure 7 – Excessive saturation on IR, image `ib7910g5q_flt.fits`.

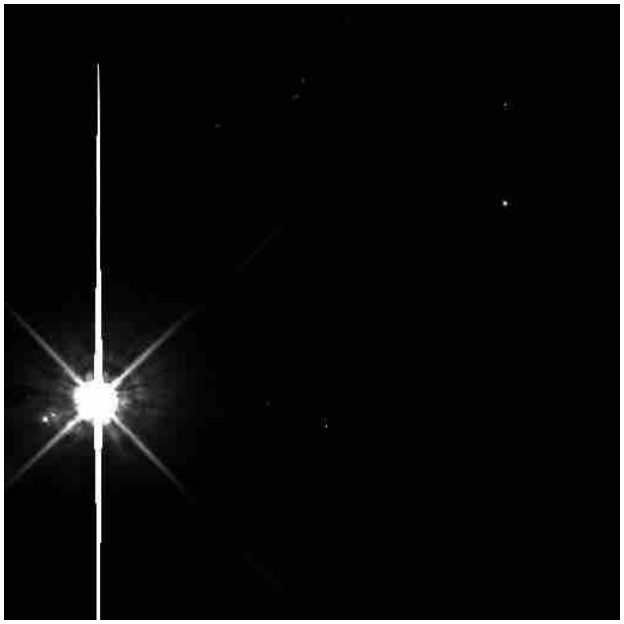

Figure 8 – Excessive saturation on UVIS subarray image `icvi45uuq_flt.fits`.

2.5 IR Banding

IR Banding is the imprint of preceding subarrays on a following larger-format image. They appear as horizontal stripes of slightly higher or lower signal on the top and bottom of the image. The height of the central band will be the height of the subarrays, either 64, 128, 256, or 512 pixels (Dulude et al., 2011). Banding can be avoided by not mixing different subarray sizes and full-frames within a single orbit. If various size formats must be used in an orbit, they should be staggered largest to smallest.

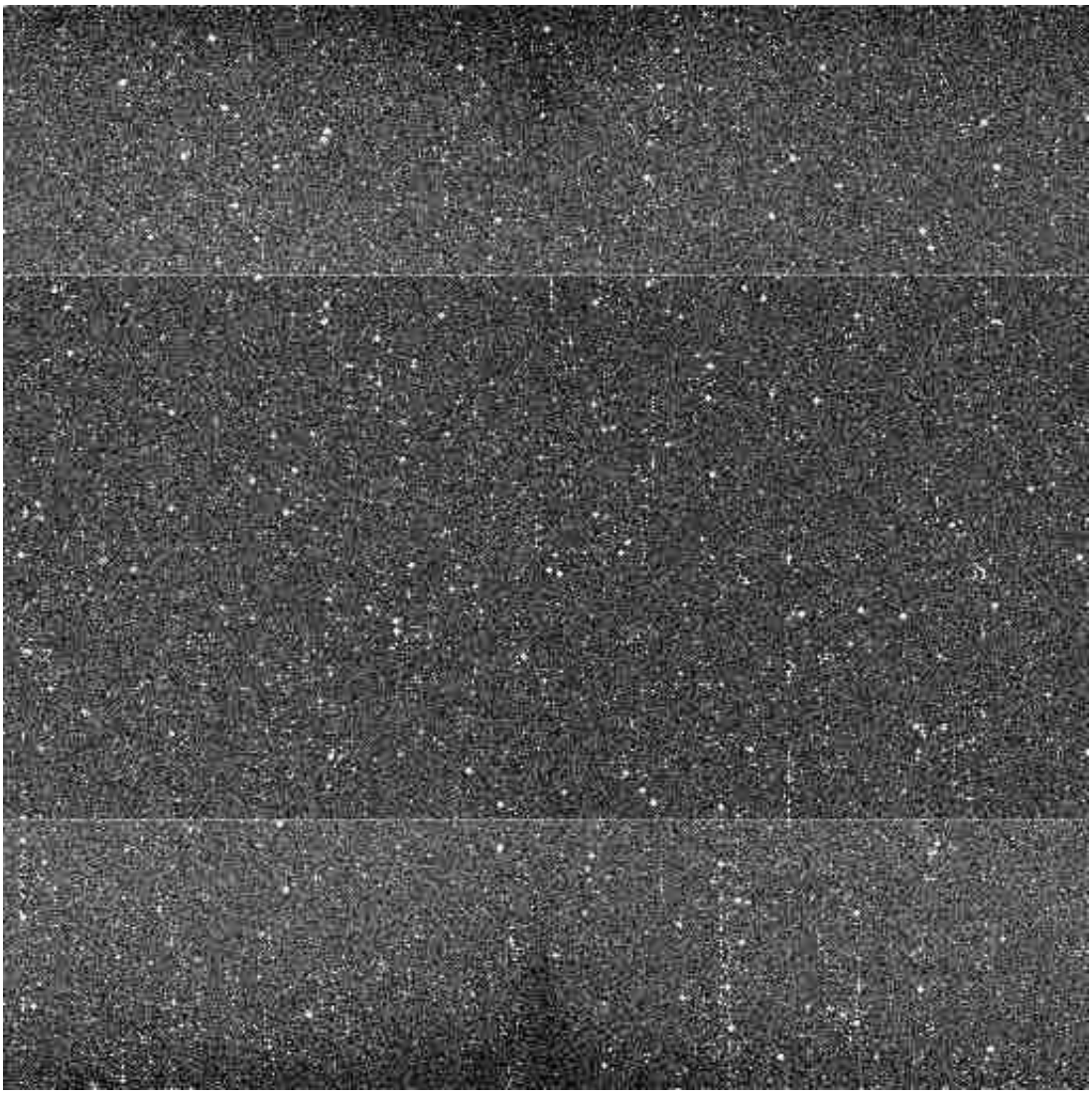

Figure 9 – IR banding on image `ibcu1dg4q_flt.fits`.

2.6 Persistence (IR)

Persistence is an unavoidable fact-of-life for the IR detector. The best strategy is to avoid taking your observations immediately after a visit that observed bright targets or had high background (such as a flat). It has been extensively documented (Long et al. (2013a), Long et al. (2013b), Chapter 8 of Deustua (2016)) and program coordinators and contact scientists do their best to retain the integrity of all programs. Depending on your science goals, some persistence can be tolerated.

Persistence can be of anything, as we illustrate in extreme examples: star fields (Figure 10), grism traces (Figure 11), scanned grism trails (Figure 12), Earth flat streaks (Figure 13), and so forth. Note that most of these examples were actually taken in calibration programs designed to study persistence and observation planners are usually very diligent about avoiding persistence blasts on science observations. For all the care of observation planners, persistence can still occur from acts of nature, such as satellite trails and cosmic rays, and days-old sources have been known to "burp" out after a high-signal flat is taken (Ryan and Baggett (2015), Gosmeyer and Baggett (2015)). Sometimes it can be difficult to tell whether you are, for example, seeing a satellite trail or a *persisted* satellite trail, and you may need to look at the individual ramps in the RAW or IMA file, or even the preceding images, to make that call.

Persistence masks can be downloaded from the Mikulski Archive for Space Telescopes (see `https://archive.stsci.edu/prepds/persist/search.php`). These can be used to check whether your target may have been subjected to persistence and whether it is a tolerable level for your science goals.

Figure 10 – A fairly extreme example of persistence in IR image `id1sa2hpq_flt.fits`*. The image is, in fact, a dark and each "star" is actually a persisting phantom of a star.*

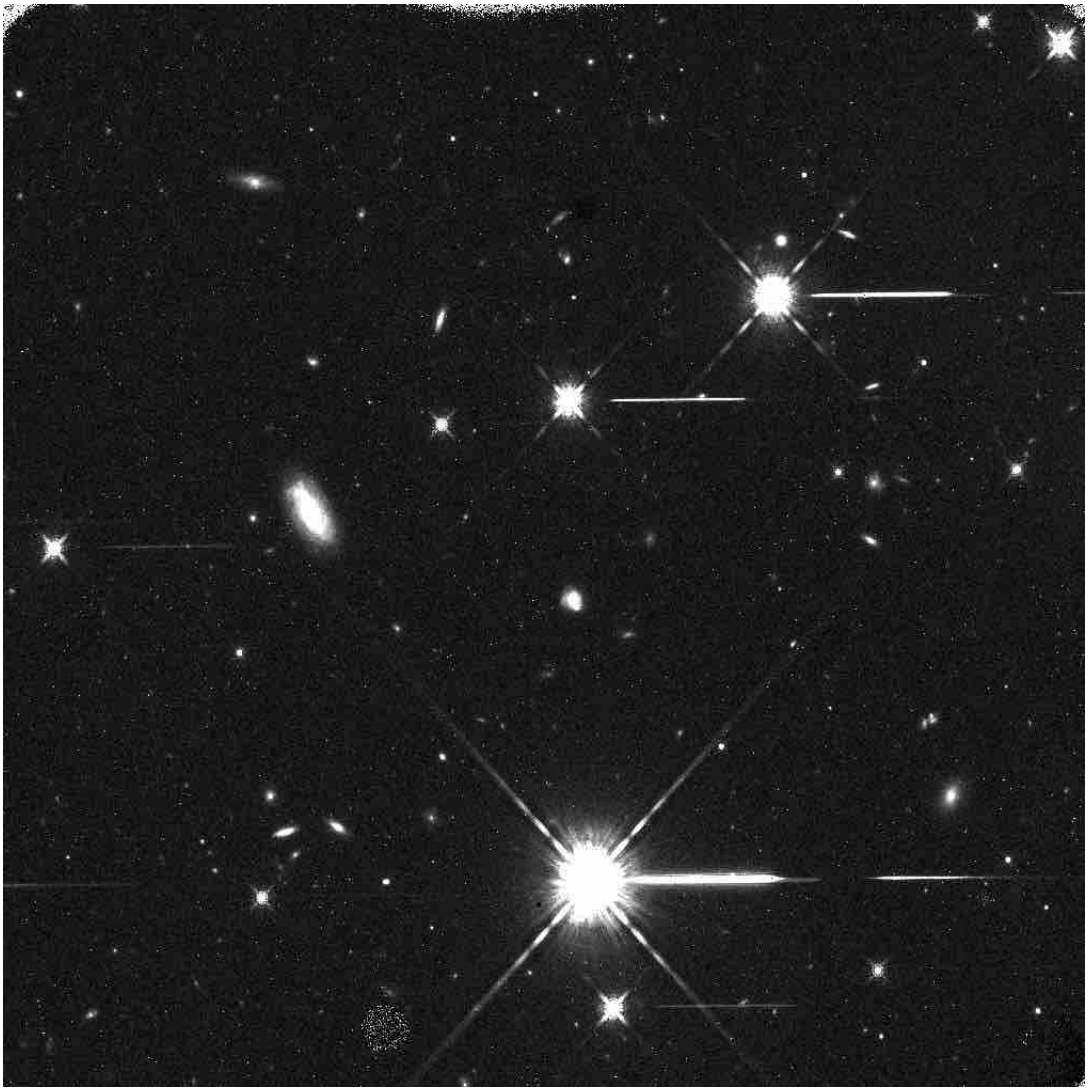

Figure 11 – Example of persisting grism traces, the horizontal features in IR image `id1k3nyns_flt.fits`.

Figure 12 – Example of persistence after a scanned grism observation in IR dark image `ic5j55grq_flt.fits`*. See Section 5.3 for a discussion of the other flatfield features.*

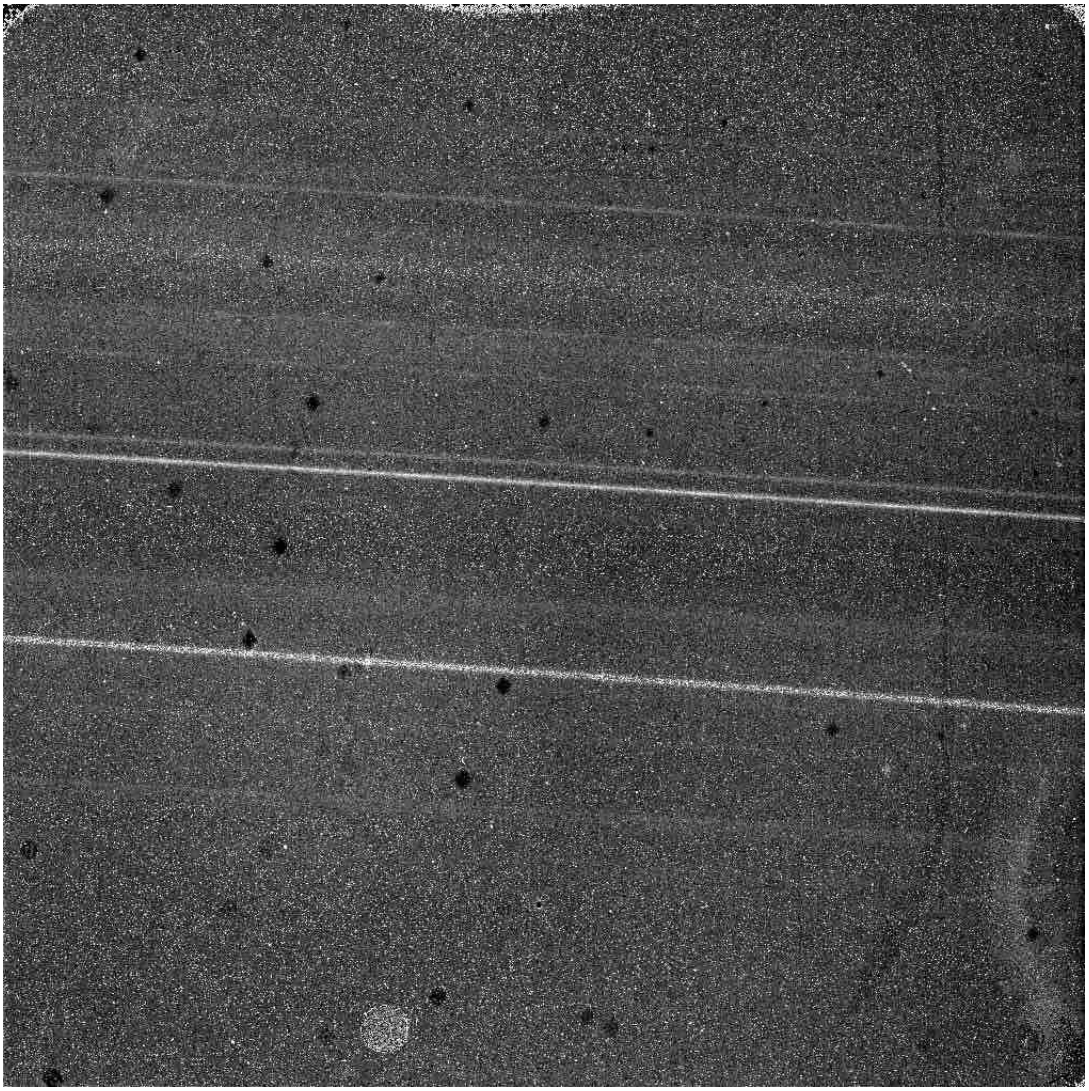

Figure 13 – Example of persistence after an Earth flat in IR image `id2984qqq_flt.fits`*. Notice also the prominent blobs.*

2.7 Prominent Blobs (IR)

This characteristic does not really originate from the IR detector, but we describe it in this section for lack of better placement. Blobs are due to roughly circular regions of particulate matter on the CSM mirror and show up most prominently in high-background IR images as small dark orbs (Durbin and McCullough, 2015). Note that the death star near the bottom edge is not a blob, but a known defect of the IR detector. We monitor blobs using Earth flats, which provide the high background required for discovering and tracking the blobs. Blobs can be corrected by dithering, and when dithering is not possible, by dividing by the epoch-specific blob flat field (McCullough et al., 2014). Blobs have a

monitoring program and automated scripts to track them, and when a new blob is found it is added to the blob mask. When "flagged" as an anomaly in the Quicklook system, however, it is for their anomalous prominence in an image. Admittedly, the prominence of the blobs in the image eligible for flagging is subjective to the quicklooker.

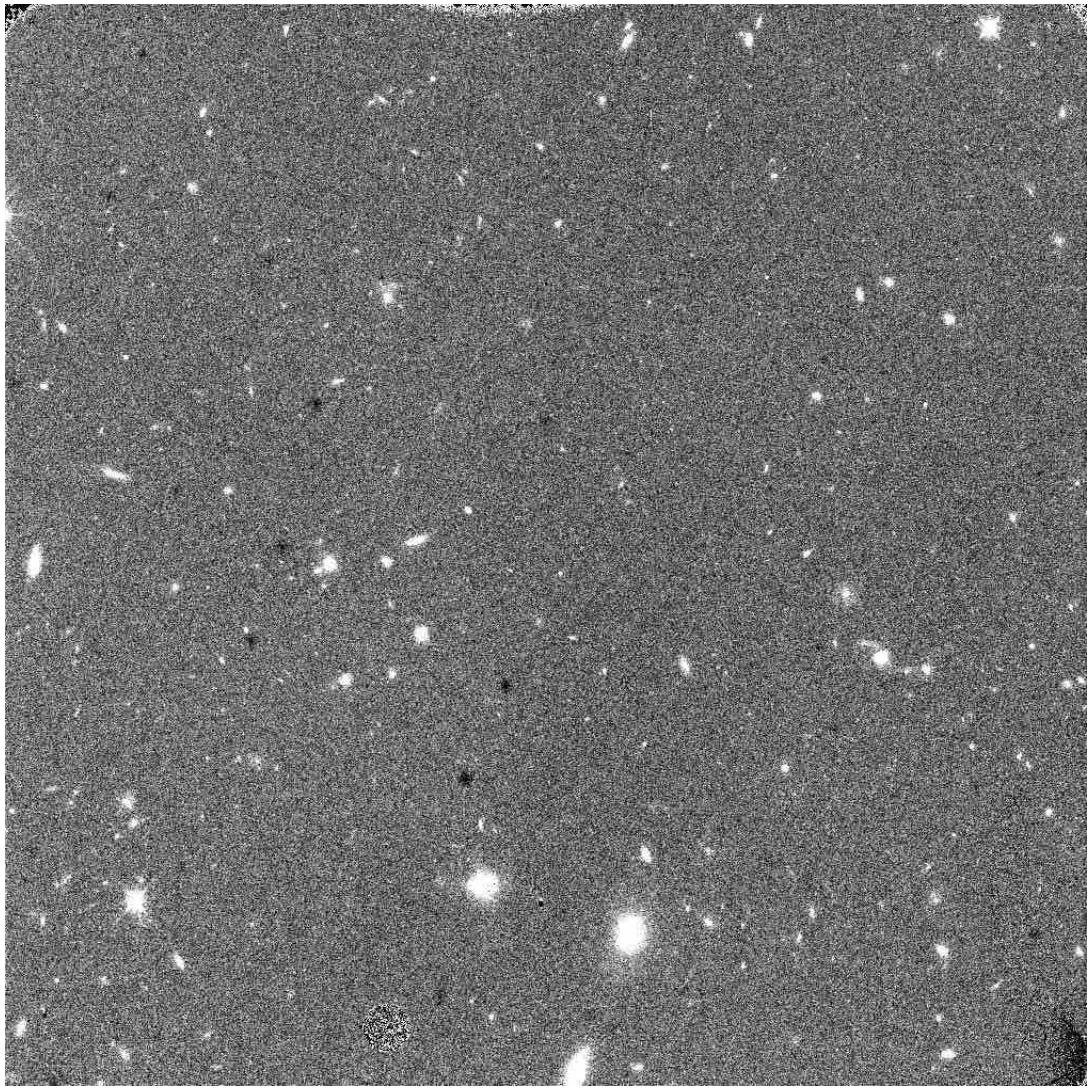

Figure 14 – Prominent blobs (black spots) in IR image `id1k9cmtq_flt.fits`.

3 Optical Anomalies

This section discusses anomalies due to scatter or reflections in the WFC3 optics from bright objects either in the scene or just off the edge of the detector.

The various UVIS ghosts are caused by reflections off the surfaces of the filter wheel and the windows on the two UVIS chips (McCullough, 2011). The primary culprit for the UVIS ghosts are the detector windows. The filters also contribute to the window-detector ghosts, and the filters themselves have their own family of ghosts. The filter ghosts used to be much worse, so much so that 10 of the filters were replaced following the TV1 ground testing (Brown, 2007). The UVIS ghosts are categorized by the Quicklook team as detector-filter ghosts, filter ghosts, and figure-8 ghosts. A single source can cause more than a single class of ghost in one image, or even multiple incarnations of the same ghost (Figure 22). The IR detector can also, in rare cases, show a detector-filter ghost and a reflection known as the diamond feature.

3.1 Detector-Filter Ghost (IR & UVIS)

A detector-filter ghost is caused by a bright source reflecting off both the filter wheel and the IR and UVIS detector windows. It appears as a large, diffuse single or double donut, quartered by the shadows of the four struts. It appears rarely; in the Quicklook database so far there are only about 140 flagged.

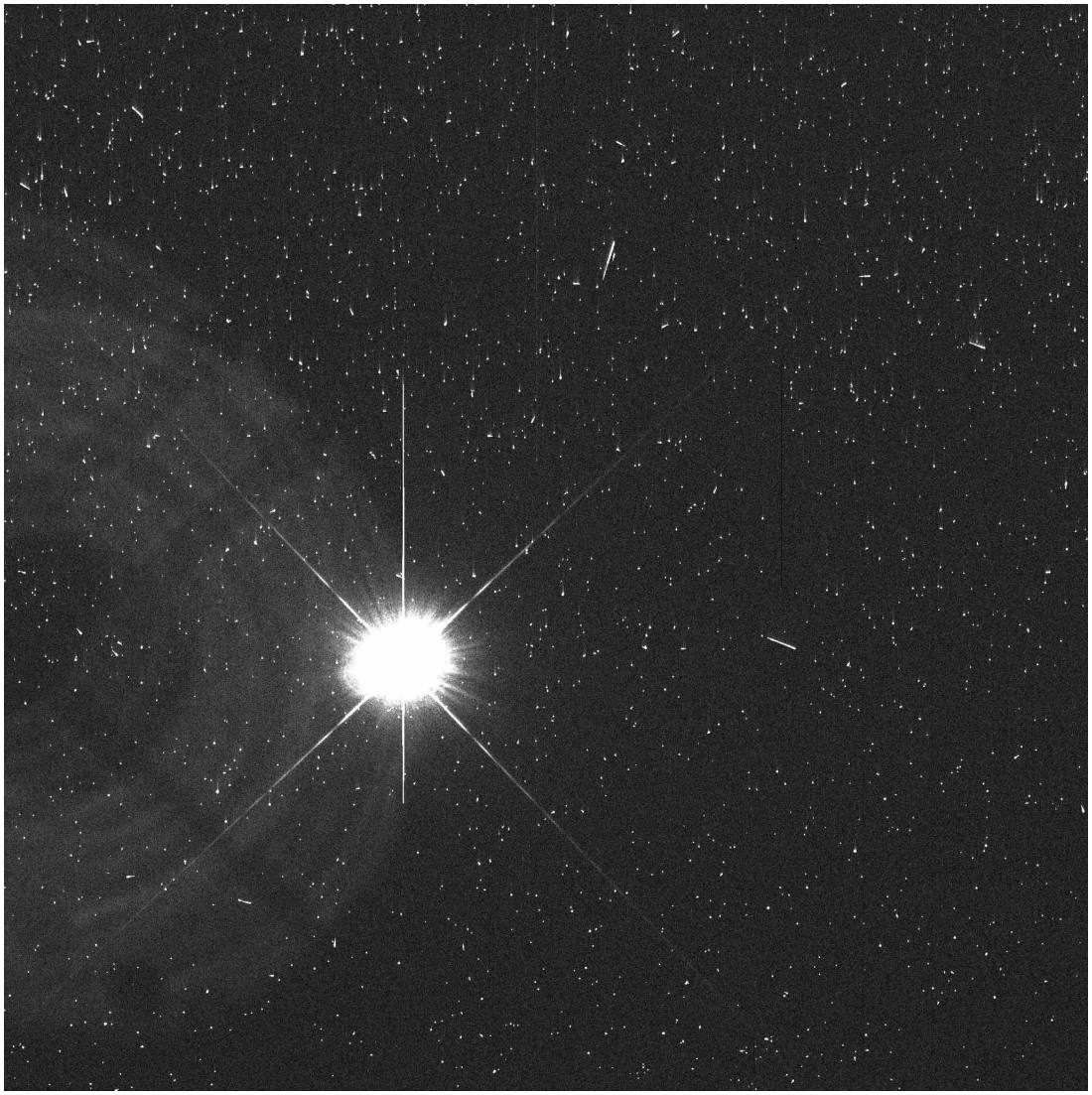

Figure 15 – Detector-filter ghost in UVIS image `id0513g5q_flt.fits`.

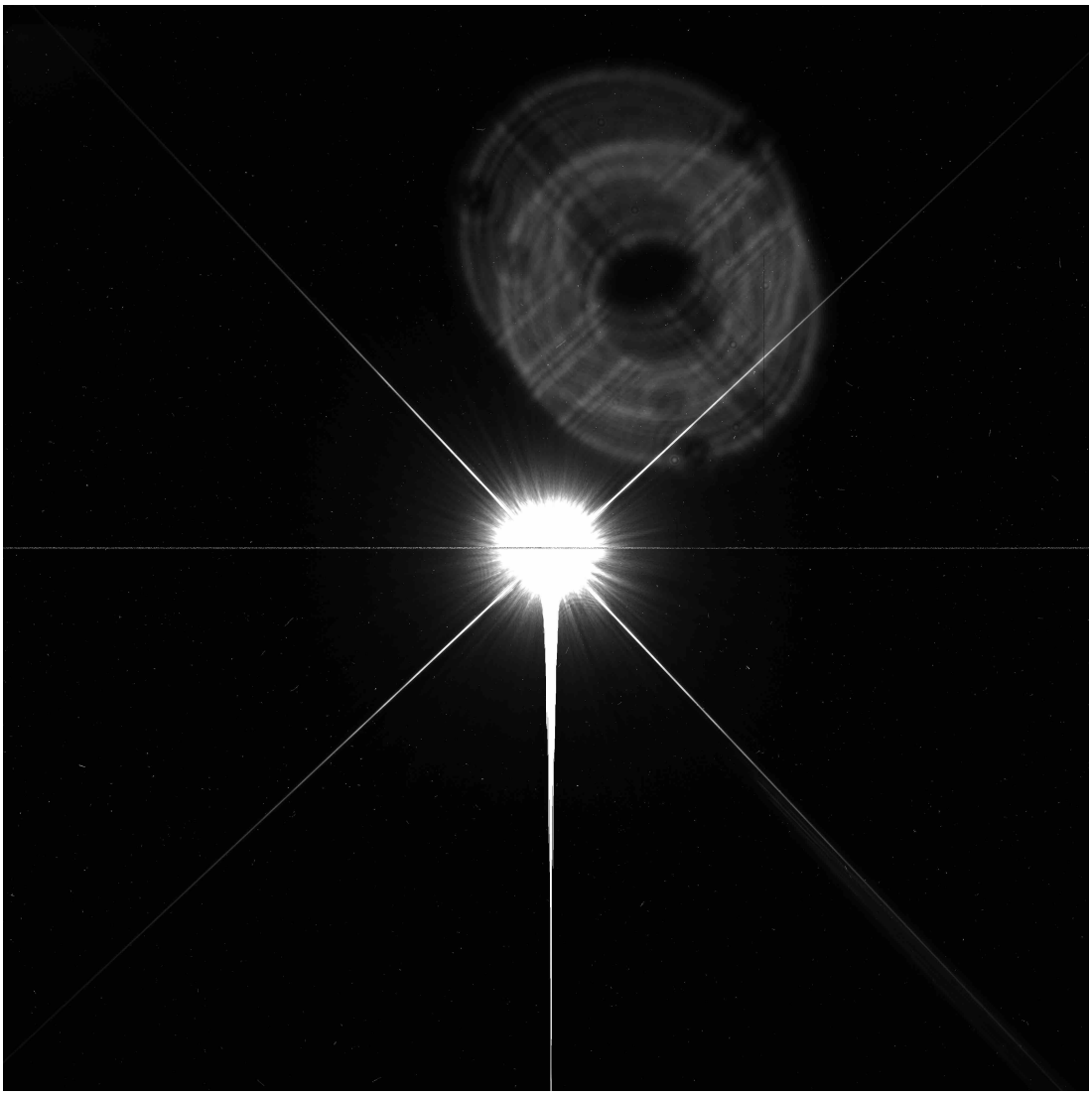

Figure 16 – Another example of a detector-filter ghost in UVIS image `ibsq56igq_flt.fits`*. This image would also be a candidate for excessive saturation.*

3.2 Diamond Feature (IR)

The diamond feature on bright sources imaged with the IR detector is due to reflection from the refractive IR corrector element (G. Hartig, private communication). In the example in Figure 17, it appears as the diamond-shaped outline balanced on top of the star's PSF. It is believed to be linked with the amount of saturation. No documents have been published on this feature and, now that there are over 200 examples in the Quicklook database, it would be a good subject for a future characterization project.

We choose an extreme case for illustration; usually the feature is subtle and you need know to look for it to spot it.

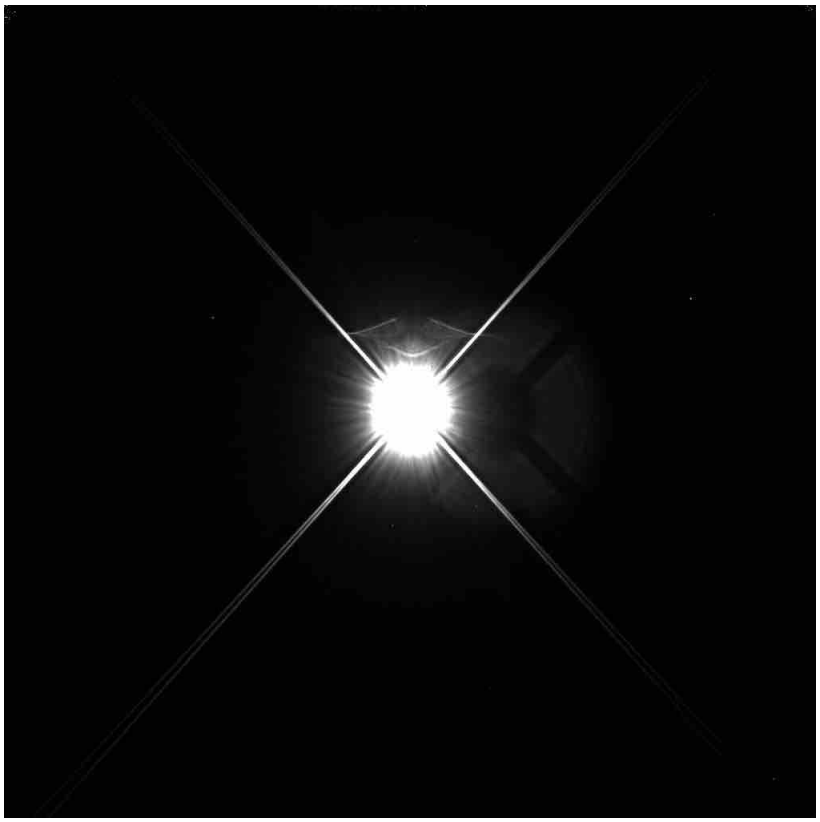

Figure 17 – Diamond feature and a rare IR detector-filter ghost in IR image `ib7911gwq_flt.fits`.

3.3 Dragon's Breath (UVIS)

Bright sources immediately outside the detector's edge can scatter onto the image, appearing much like a fountain of flame - hence, dragon's breath (Fowler et al., 2017). This light scatter is only classified as dragon's breath if it seems to originate at the edge. If it appears to float unconnected in the middle of the image it is classified simply as scattered light.

The following link contains an interactive plot to help you avoid dragon's breath and scattered light: http://www.stsci.edu/hst/wfc3/ins_performance/anomalies/bokeh_dragon.html

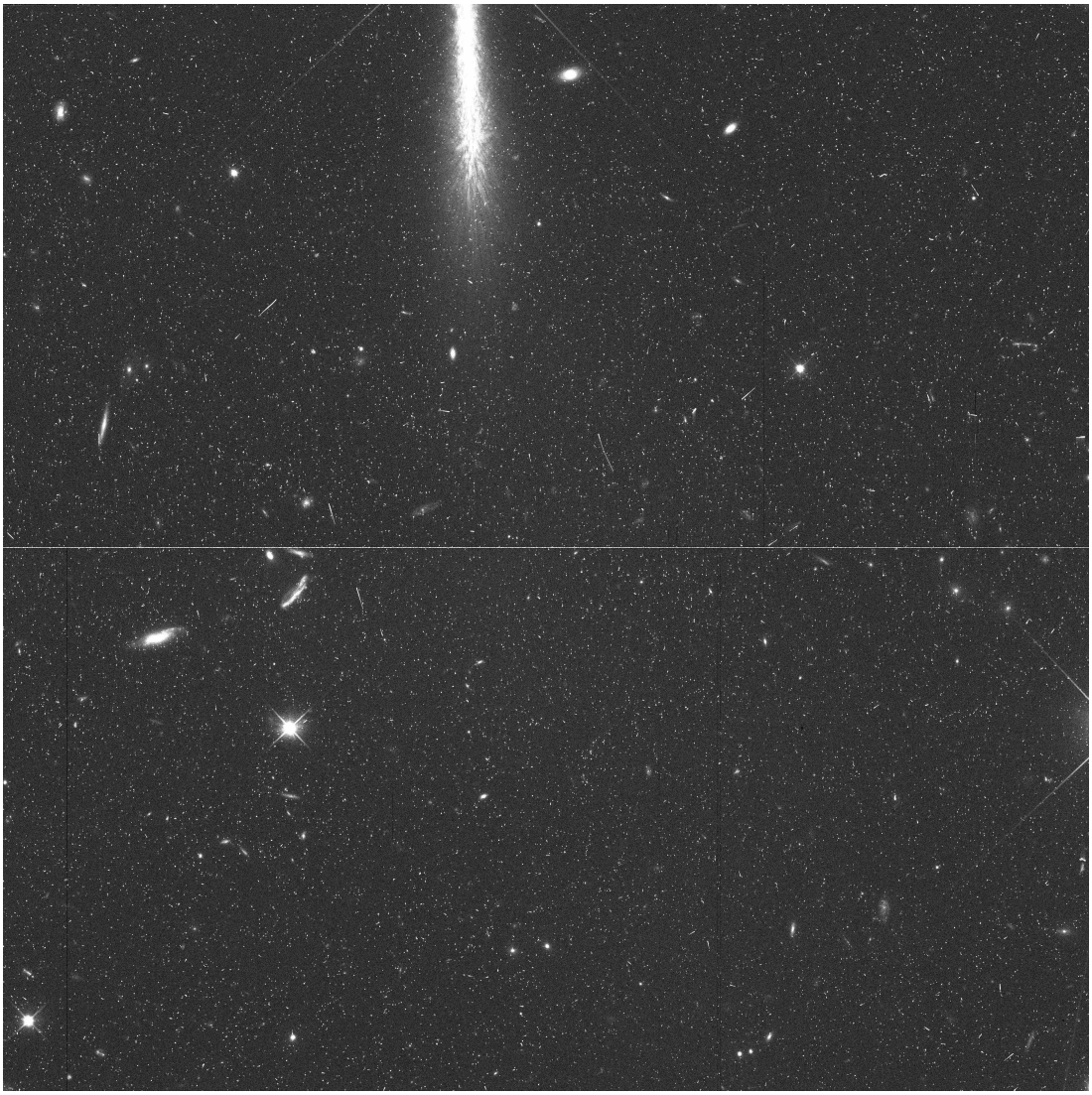

Figure 18 – Dragon's breath in UVIS image `iboa86p3q_flt.fits`.

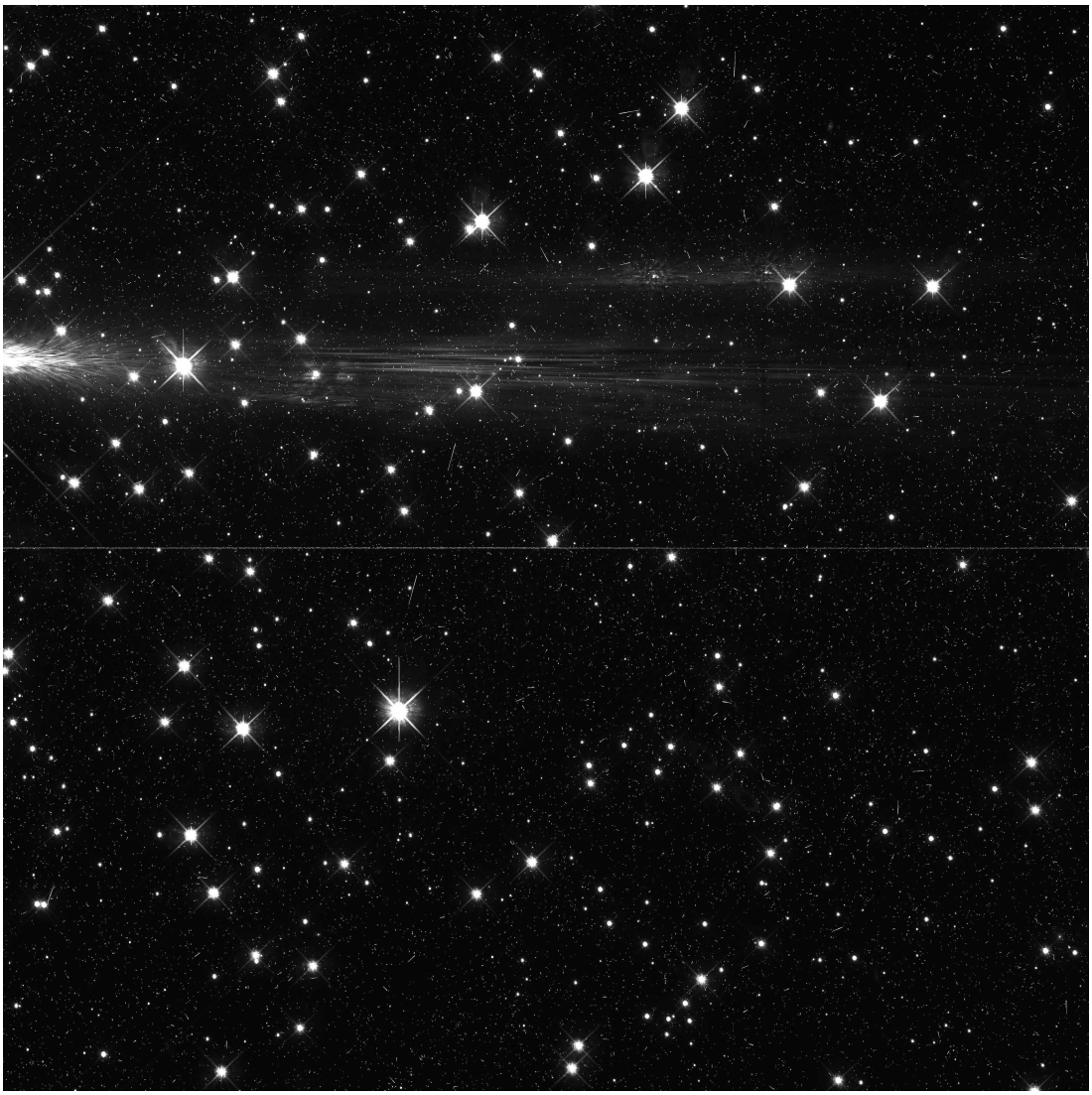

Figure 19 – Dragon's breath in UVIS image `ibop04gaq_flt.fits`*. Scattered light is also visible above it.*

3.4 Earth Limb/Shine (IR)

Earth limb (also called Earth shine or scattered Earth light) is stray light that appears as a higher background on the left of the IR detector, always of the shape shown in Figure 20. It is dependent on HST's pointing direction (Hilbert and McCullough, 2009). It can be avoided by using the LOW-SKY special requirement parameter (STScI, 2017) but many observers choose not to do so since it significantly reduces the available orbital visibility. This philosophy of eschewing the LOW-SKY requirement is often applied in deep-field grism programs, where a direct image is taken first or last in the orbit because the extra light is acceptable for their purpose of identifying sources that disperse in the pro- or preceding

grism images (for example, see program 14227). Thus, most Earth limb examples flagged in current data are intentional. This was not always the case! As depicted in Figure 71 of the Appendix, in 2009-2010, right after WFC3's installation, the effect was not as well characterized and it intruded on a greater percentage of IR observations.

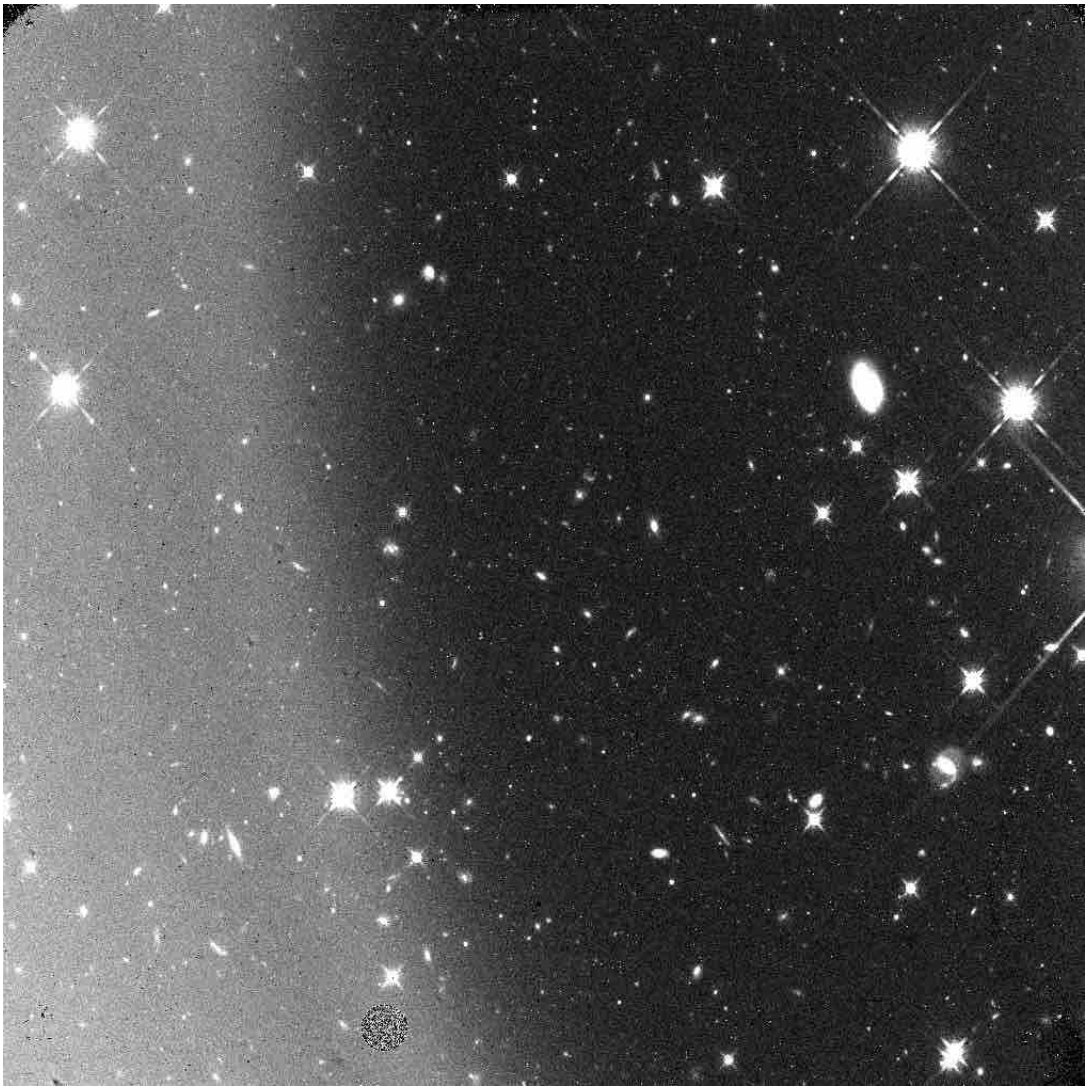

Figure 20 – Earth limb in IR image `ic2j03d2q_flt.fits`.

3.5 Figure-8 Ghost (UVIS)

Figure-8 ghosts occur on a diagonal from a bright source observed in UVIS quad D, and so are most often found in quad A. They are caused by reflections off the CCD detector window and their confined appearances across the quad A-to-D diagonal is due to the detector's tilt. Figures 3 through 8 in McCullough (2011) show diagrams of how and where figure-8 ghosts can arise. In the lowermost right corner of quad D, a single source can cause more than one ghost; see, for example, Figure 22.

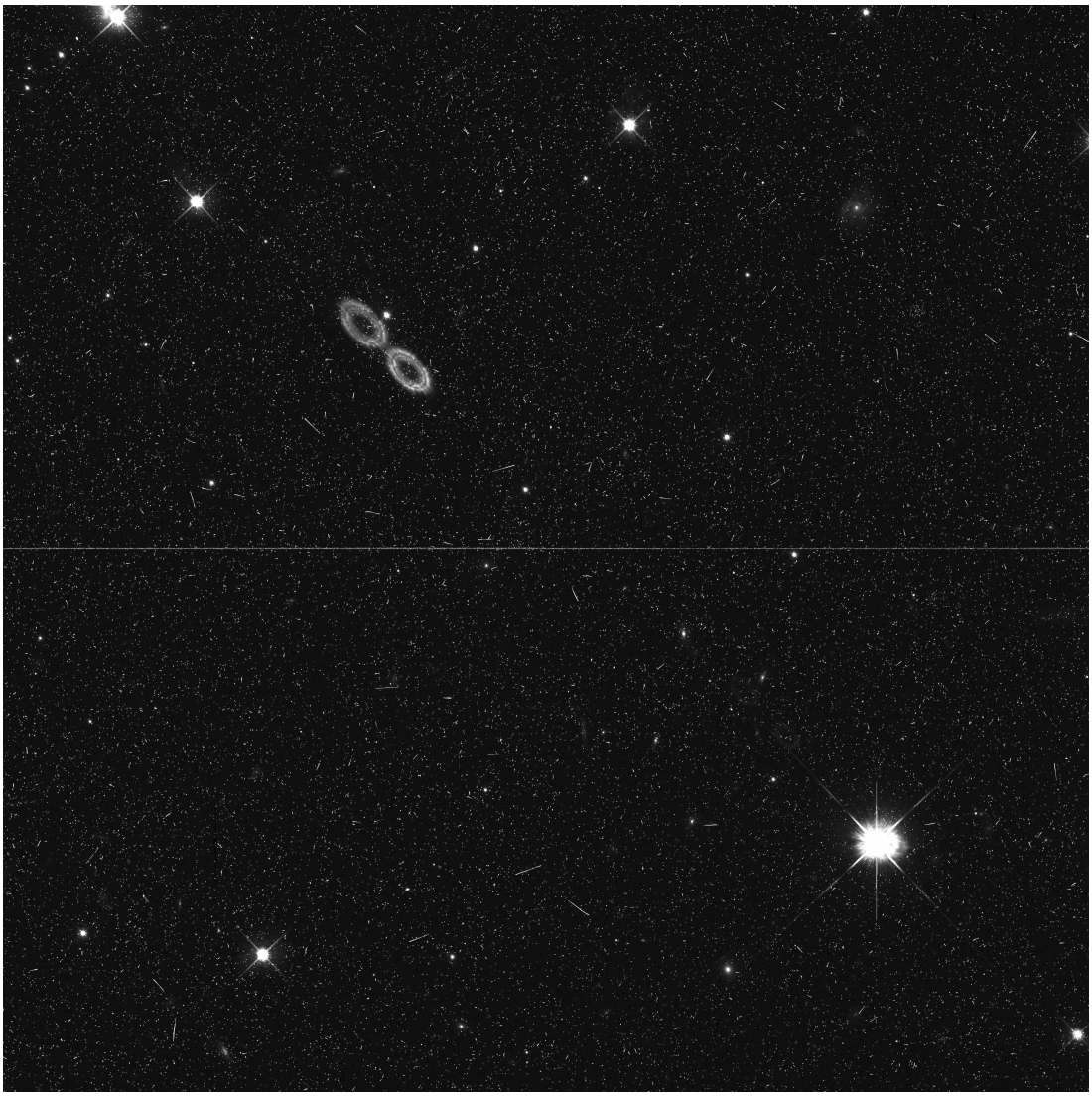

Figure 21 – Figure-8 Ghost on image `ibit12fnq_flt.fits`.

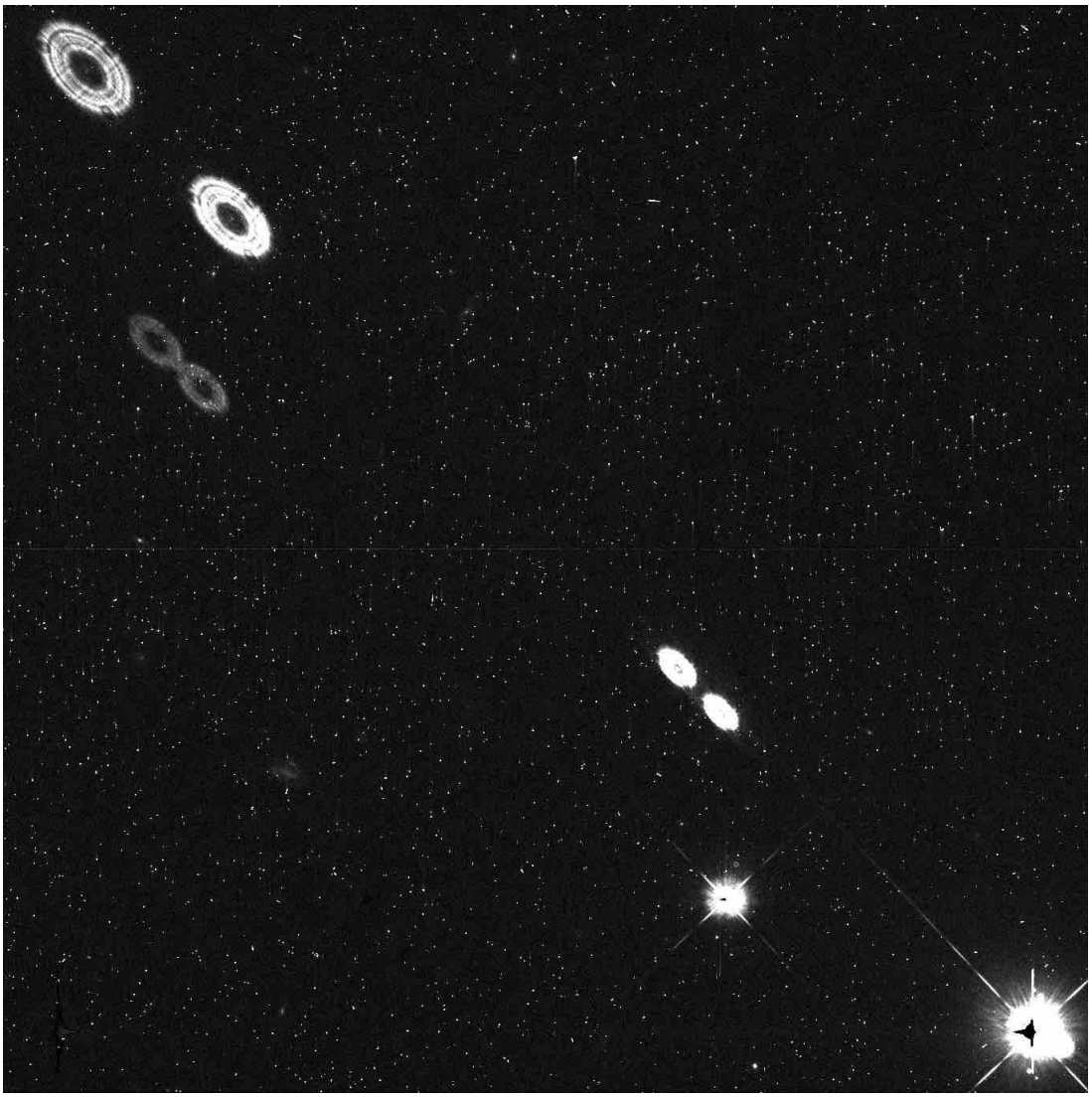

Figure 22 – Multiple figure-8 Ghosts (two from the brightest star and one from the second brightest) on image `ibvk02ccq_flt.fits`.

3.6 Filter Ghost (UVIS)

Not to be confused with the detector-filter ghost, a filter ghost is a small, donut-shaped reflection just off the filter that appears near or within the source's PSF. It is caused by a reflection off layers in the filters.

To illustrate the feature, Figure 23 shows it manifest on a very bright star on a subarray. More frequently the filter ghost is subtle, as shown in Figure 24. If you look carefully, you can spot ghosts on most of the brighter stars on the upper half of the image.

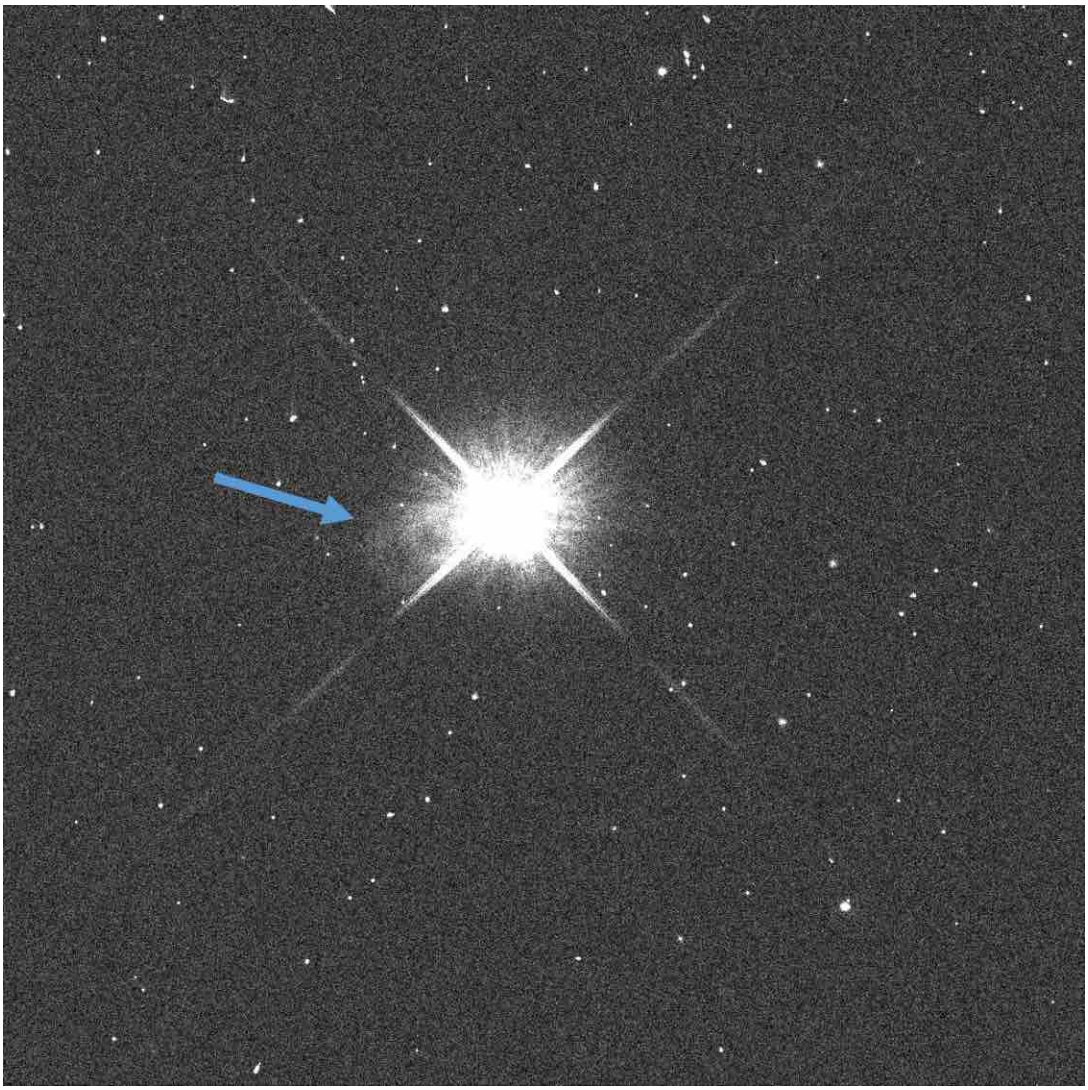

Figure 23 – Filter ghost on UVIS image `ic9t32gbq_flt.fits`.

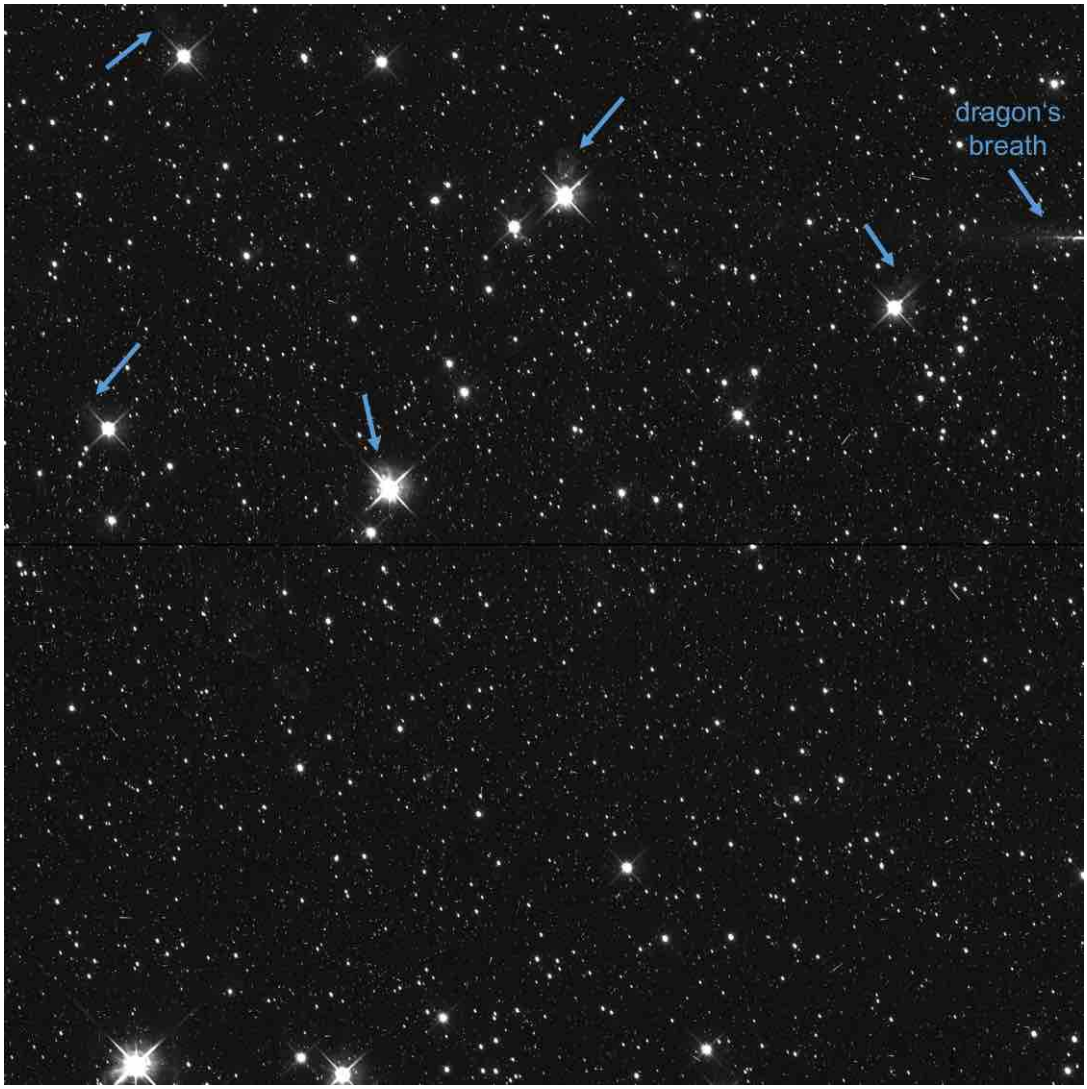

Figure 24 – Filter ghosts on UVIS image `icze18k6q_flt.fits`*. A small spout of dragon's breath is on the upper right edge.*

3.7 Fringing (UVIS)

Fringing on UVIS is a pattern of constructive and destructive interference created by multiple reflections between the CCD detector surfaces (Wong, 2010). It is seen at wavelengths longer than 650 nm because only then does the silicon of the CCD become transparent enough - that is, the absorption efficiency decreases enough - to allow the reflections to occur. Because fringing is sensitive to the thickness of the silicon surface layer, fringing's amplitude, phase, and quantum efficiency also vary across of the detector. On top of this, fringing is highly wavelength dependent. Narrow-band red filters (especially F953N, FQ889N, FQ906N, FQ924N, and FQ937N) generally show the strongest fringing. Fringing can even be seen in

wide-band filters if the source has a narrow emission line spectrum. These effects combined yield the unique "wood-grain" patterns shown in Figure 25 and in the redder quad filters in Figure 58. Section 5.6.5 of Deustua (2016) gives a broader overview of fringing.

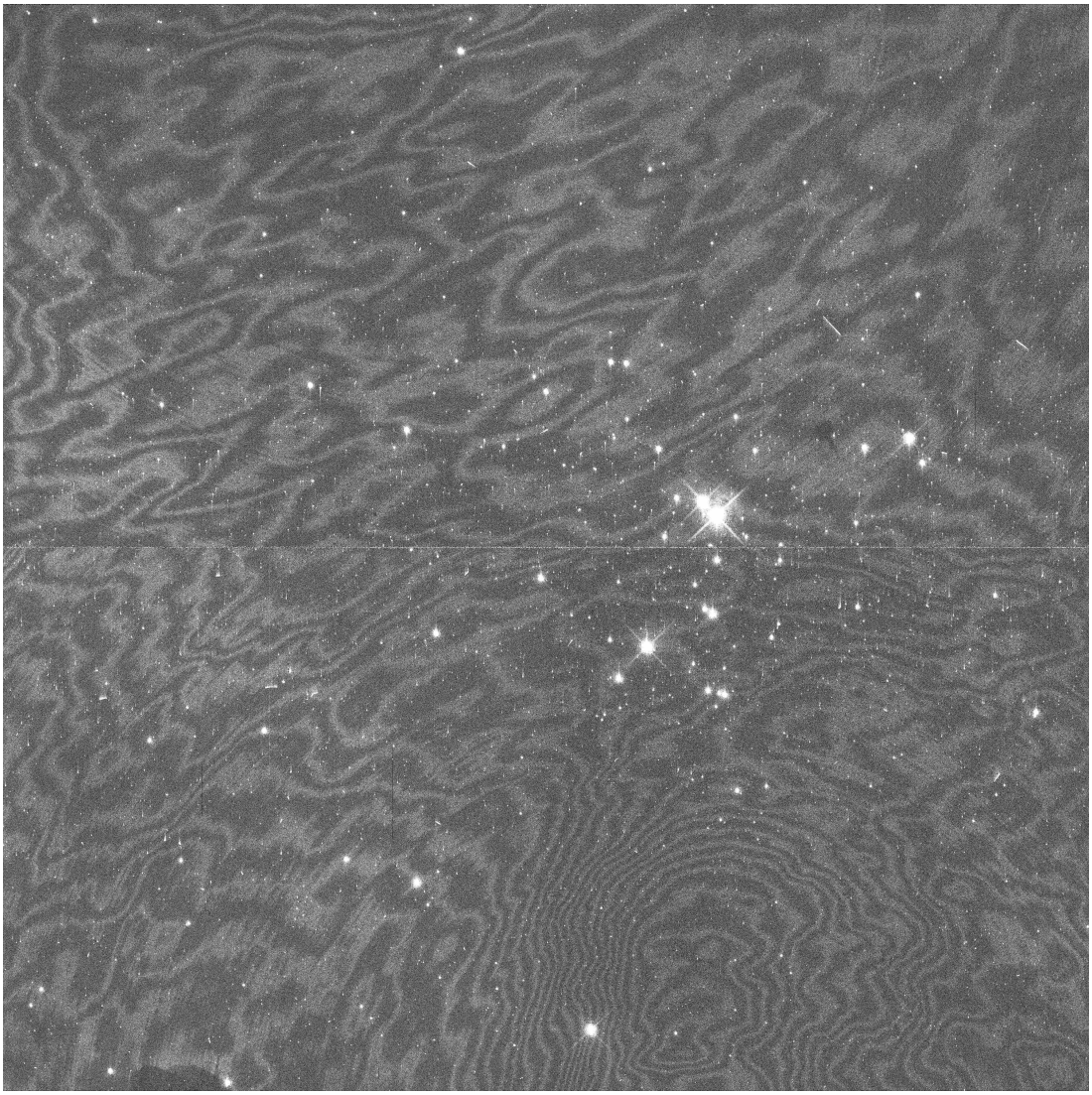

Figure 25 – Fringing in UVIS image `icwh01emq_flt.fits`.

3.8 Light Hedge (IR)

The cause of the uniquely-patterned IR light hedge is unknown. It appears to be scatter off the edge of the IR detector's baffle, perhaps a more extreme form of the light spike from atypically bright objects sitting on the edge of the IR detector's frame.

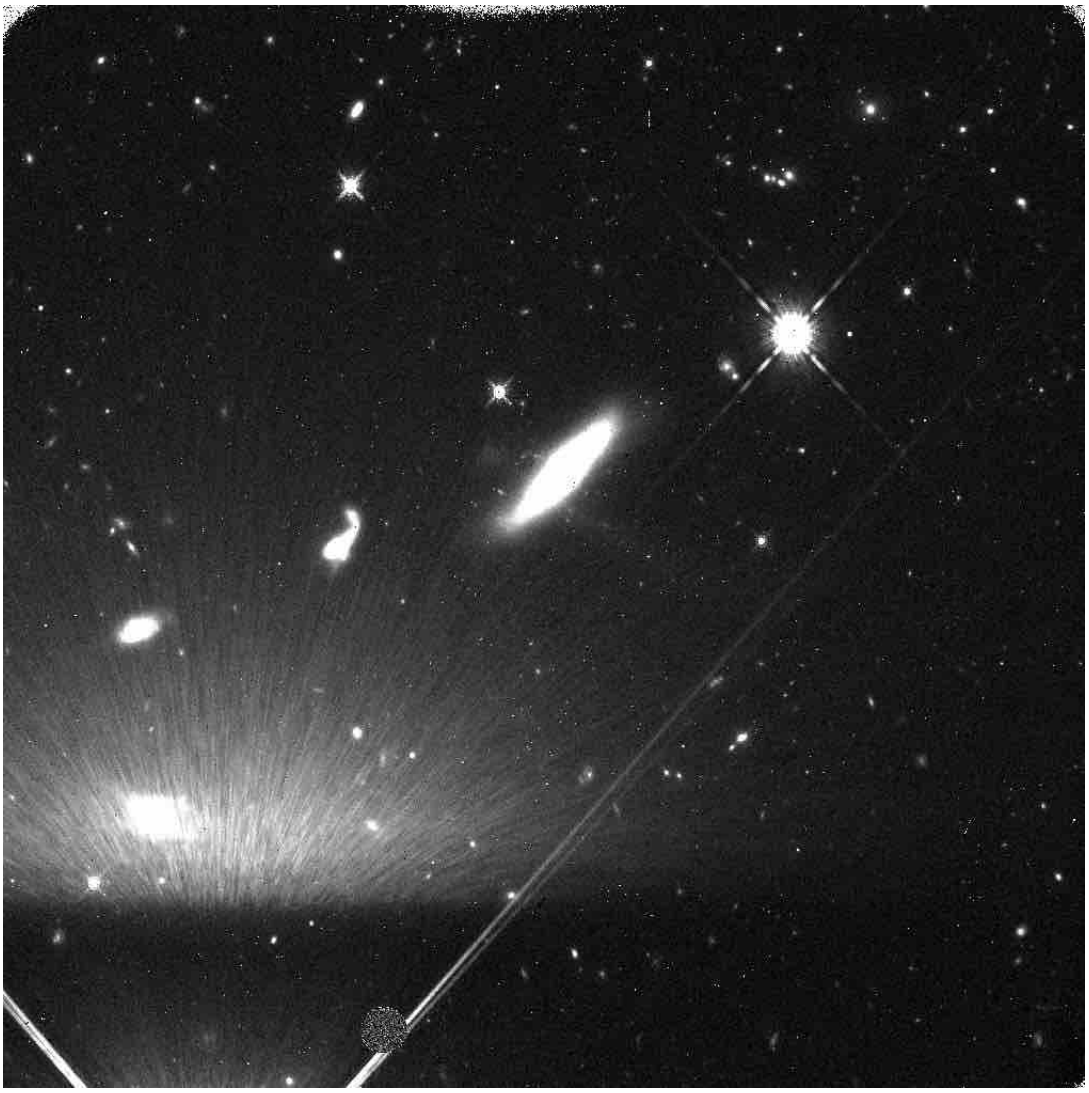

Figure 26 – Light hedge in IR image `ia1e27jzq_flt.fits`.

3.9 Light Spike (IR)

A light spike is a glint on the IR detector, occurring when a bright source hits the edge of the baffle in the detector's assembly (Brown, 2008). It can look similar to a diffraction spike (lower left side in Figure 27) or a more imposing triangle of light (bottom left in Figure 28). The spike is always perpendicular to the detector frame.

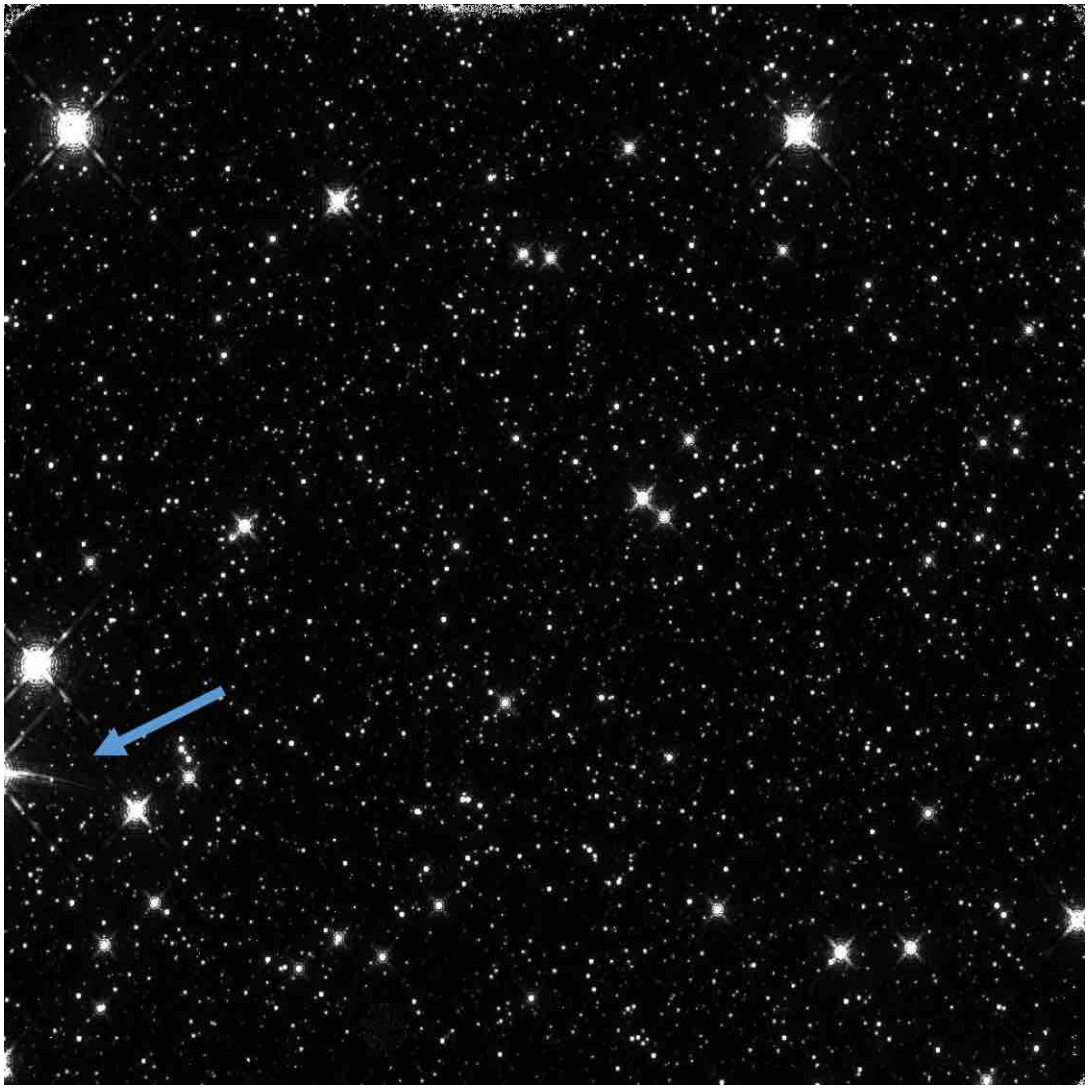

Figure 27 – Light spike in IR image `ib2k52d0q_flt.fits`.

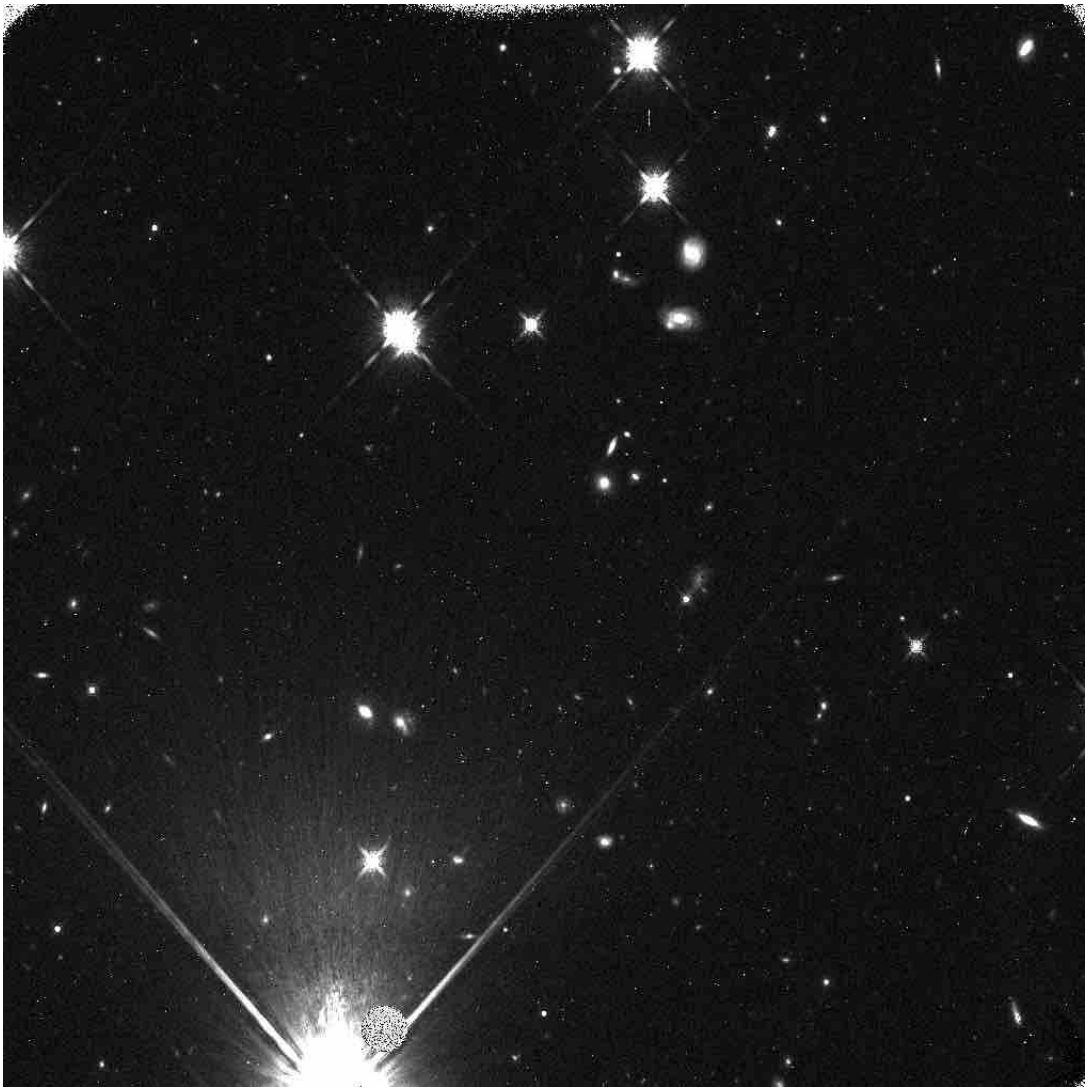

Figure 28 – A more intense light spike in IR image `ibjv77lsq_flt.fits`.

3.10 Off-Frame Diffraction Spike (IR & UVIS)

WFC3 diffraction spikes are always offset, in both the IR and UVIS detectors, 45 degrees in the detector frame. These are flagged by WFC3 quicklookers only if the source is outside of the frame.

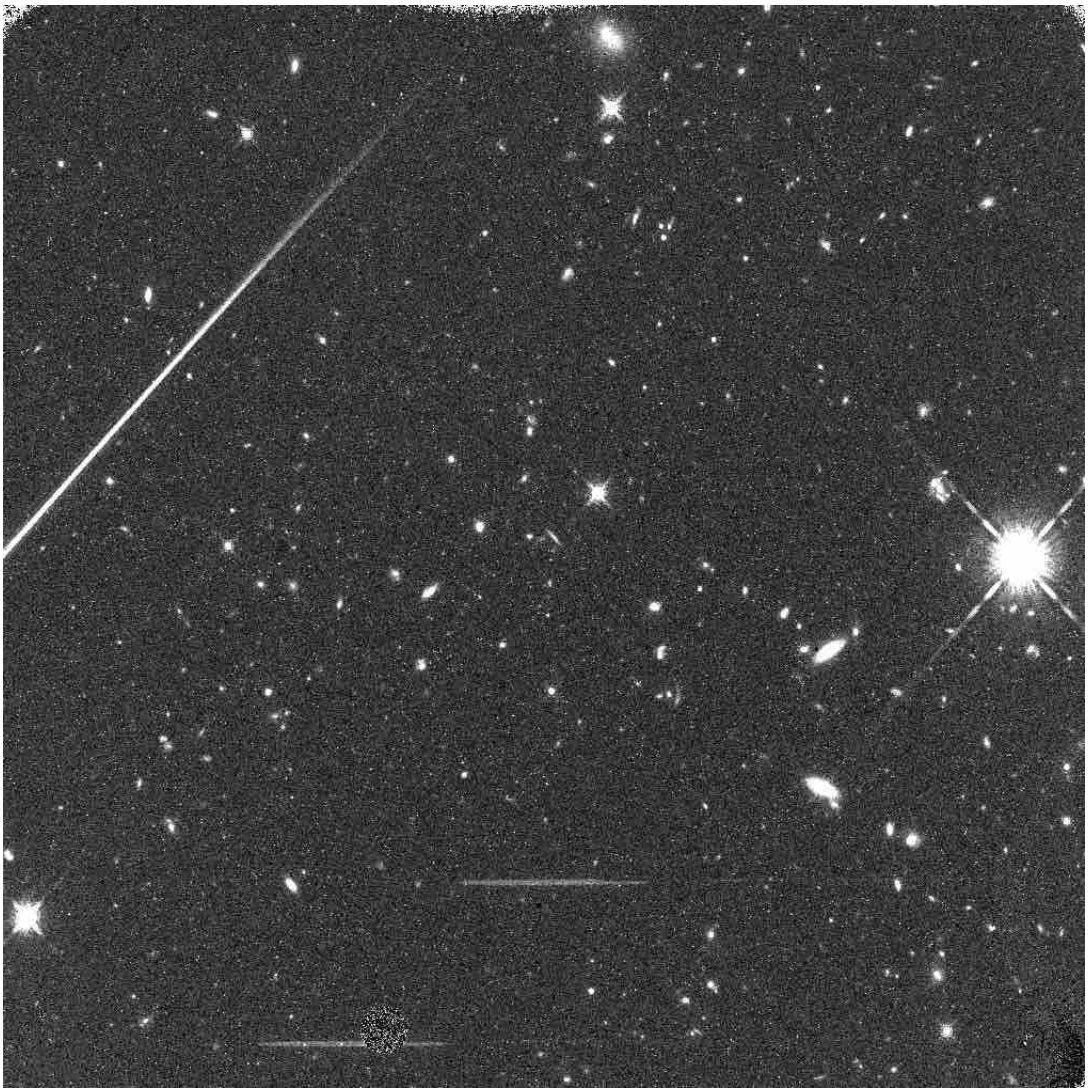

Figure 29 – Off-frame diffraction spike in IR image `icw413xkq_flt.fits`*. Notice also the persisting grism traces.*

3.11 Scattered Light (UVIS)

Scattered light on UVIS is a similar phenomenon to dragon's breath (Fowler et al., 2017); however, it emerges in the middle of the detector as opposed to just off the frame, and the offending source is not always as easily identifiable.

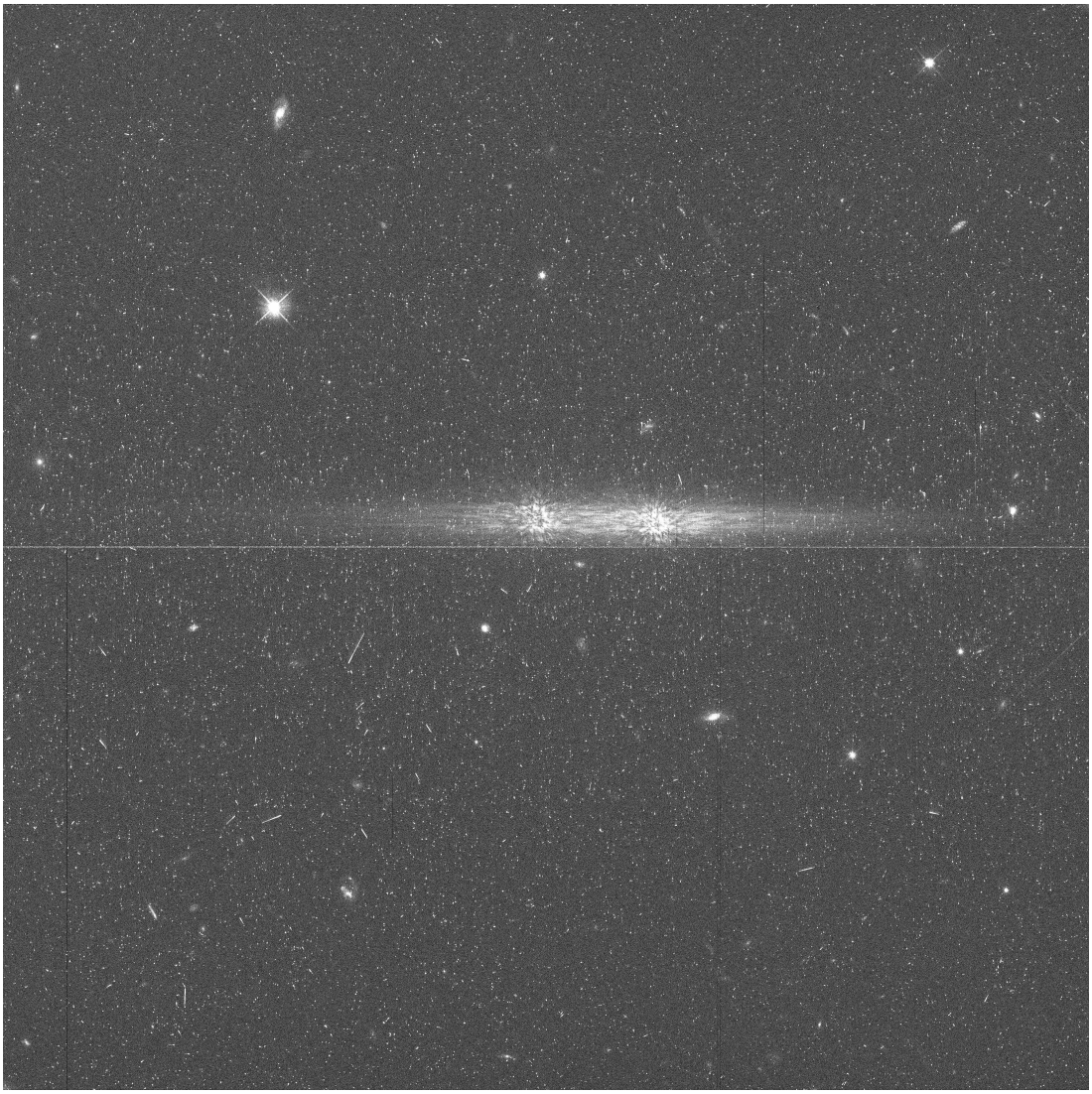

Figure 30 – Scattered light in UVIS image `ibsp04n9q_flt.fits`.

4 Other Anomalies

In the section are some anomalies that are caused by neither the detector nor the optics. Many of these are acts of nature out of the control of the program coordinators.

4.1 Data Dropout (IR & UVIS)

Sometimes data are completely lost and unrecoverable (dropped) during transfer. The dropped data are detected in OPUS, Hubble's telemetry-processing system, and constant-values are inserted in their place (S. Baggett, private communication). As consequence, the missing data appear as black pixels such as shown in Figure 31. The data dropouts will usually be flagged in the DQ array. While Figure 31 is a more typical example of data dropout, Figure 32 is more abnormal because it looks like data transfer error. We can tell there were in fact data dropouts by looking at the IMA file, where we see that the dropout regions shift in different reads (SCI extensions 4, 5, and 6) and that OPUS filled the dropped data with constant values. Their close semblance to data transfer error is due to `calwf3`'s up-the-ramp fitting.

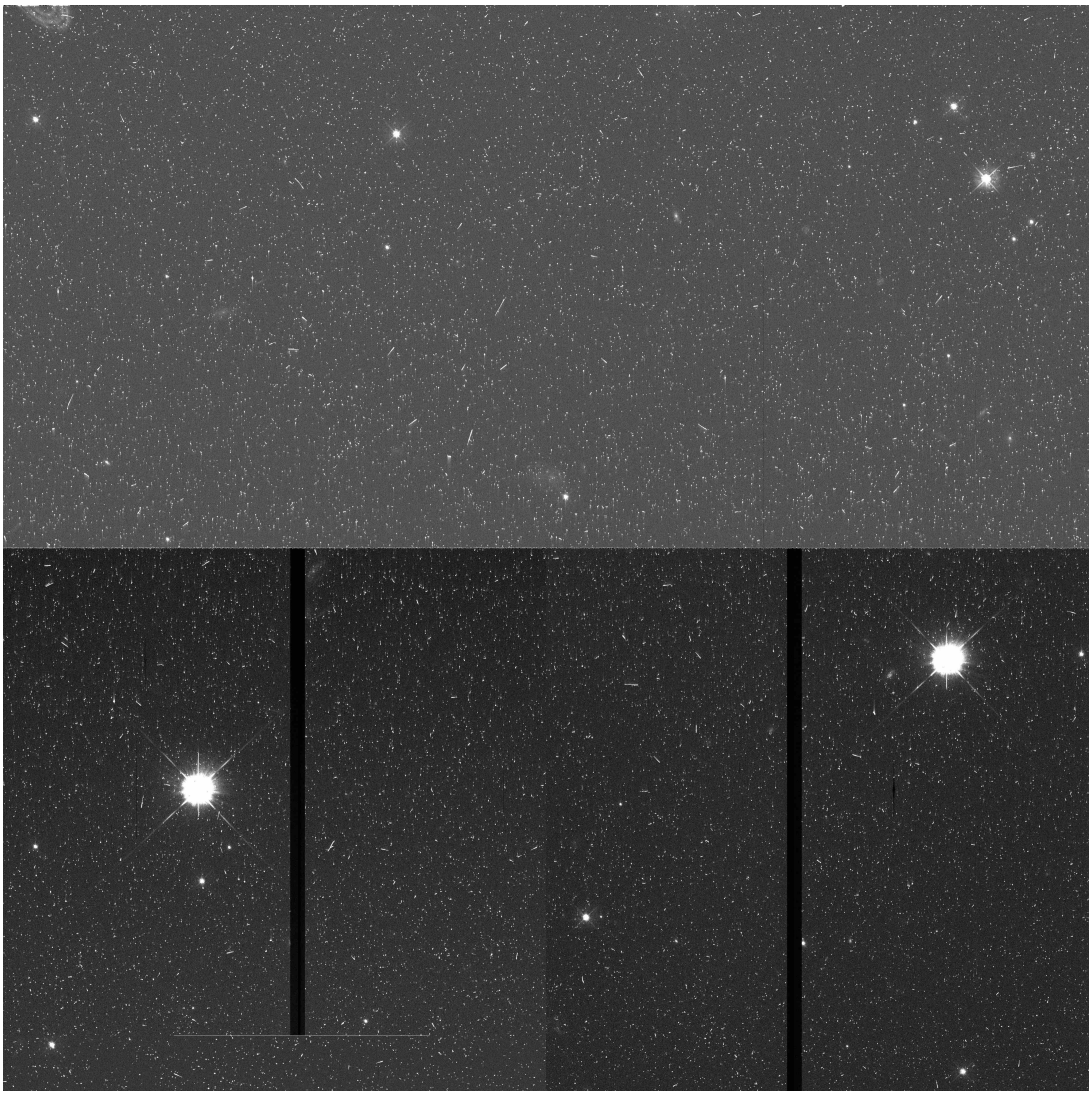

Figure 31 – Data dropout regions in UVIS image `icnp12qgq_flt.fits`.

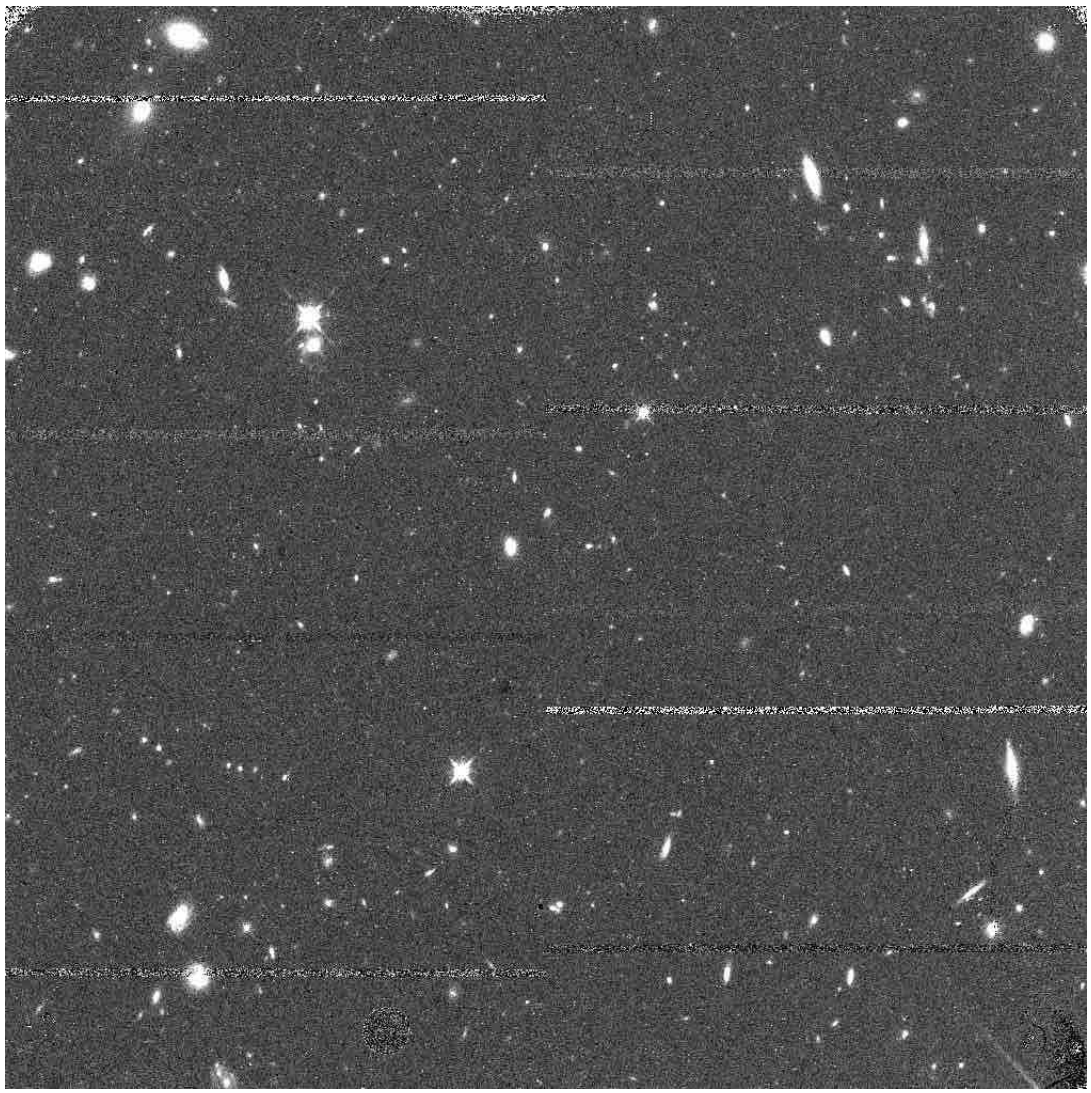

Figure 32 – Bands of data dropout on IR image `ibwjqacoq_flt.fits`.

4.2 Data Transfer Error (IR & UVIS)

Data transfer error occurs when the data encounter noise during transmission. But unlike in data dropout, OPUS does not consider the values to be dropped or bad and therefore doesn't insert constant-value fill data (S. Baggett, private communication). It is characterized by horizontal striping that often are often boxed in quadrants, looking similar to the retired UVIS mode of charge injection.

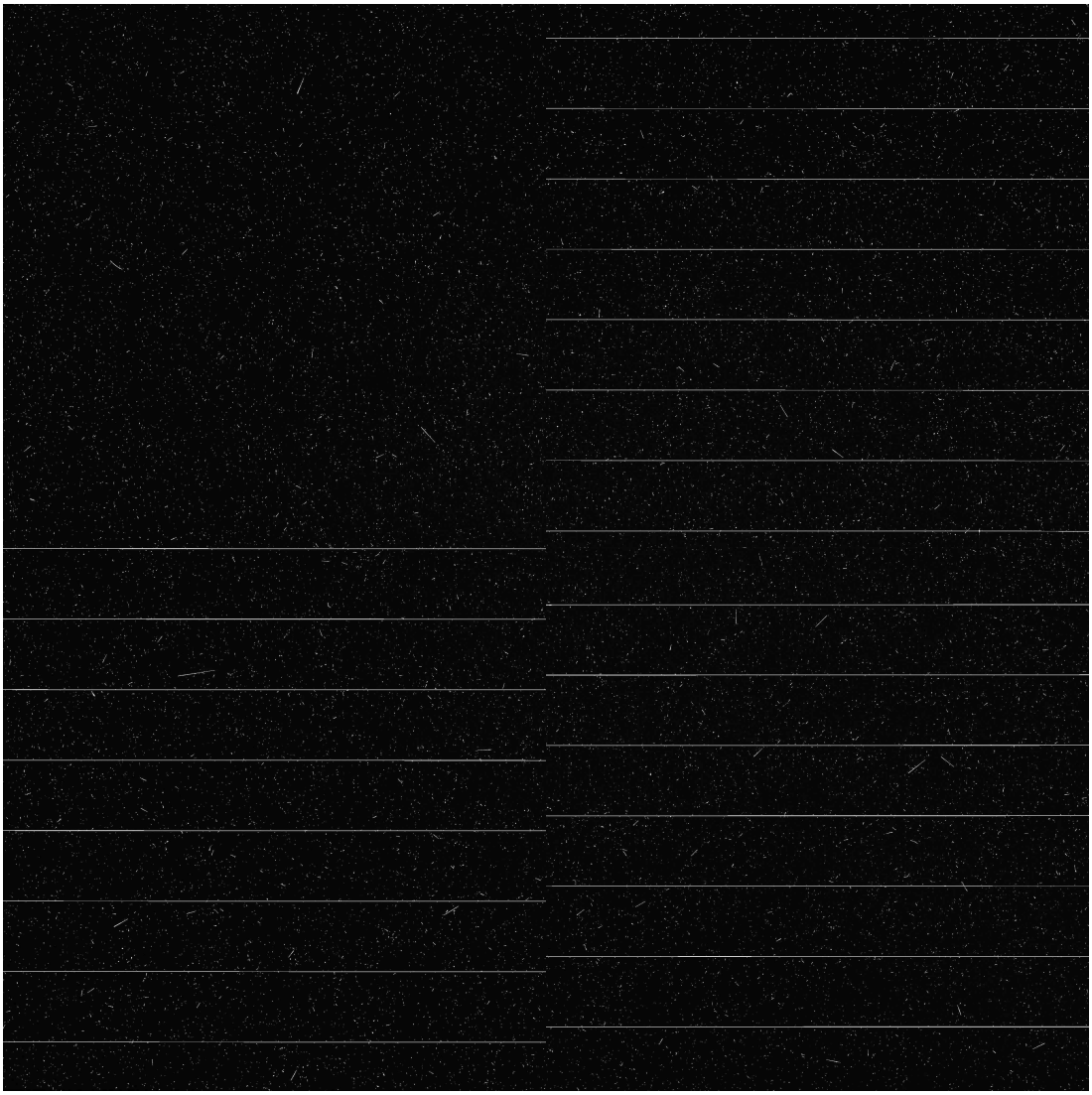

Figure 33 – Stripes of data transfer error on UVIS image `icfc87ngs_flt.fits`.

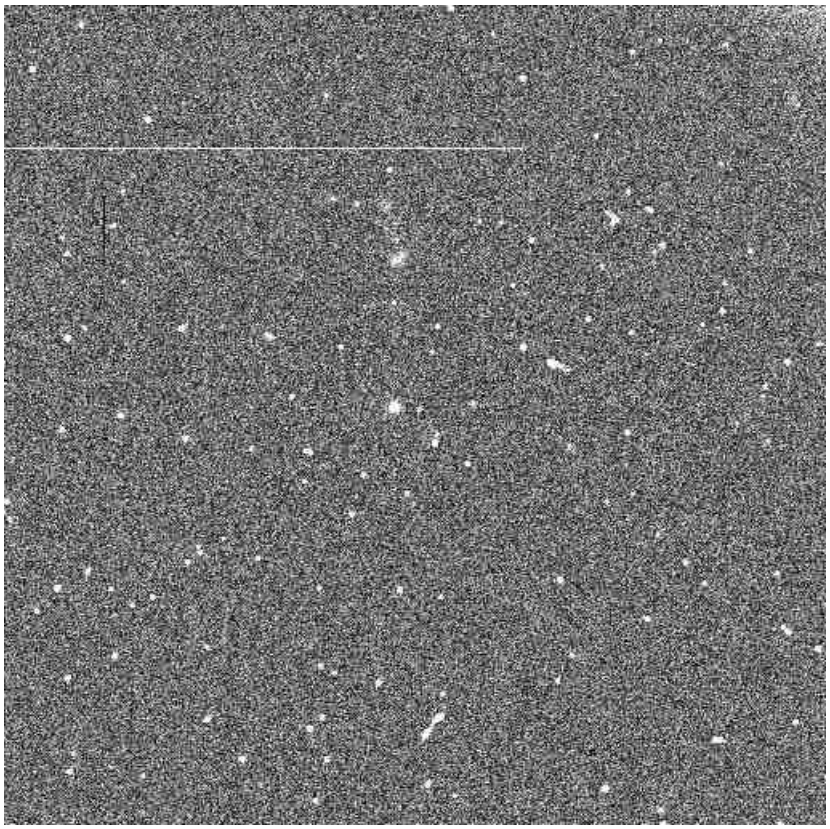

Figure 34 – The white horizontal line is a small region of data transfer error on UVIS subarray image `ib3504r8q_flt.fits`.

4.3 Guidestar Failure (IR & UVIS)

In the event of a guidestar failure, the PI will be automatically notified. Guidestar failures can cause all sources to be streaked in parallel across the field of view. Earth flat, moving target, and spatial scanning observations have source trails that mimic those you would observe in a guidestar failure. If you're uncertain, the quickest check for a guidestar failure is the header keyword EXPFLAG, which will be set to "TDF-DOWN AT EXPSTART" or "INDETERMINATE." But be careful because the converse is not always true: these values for EXPFLAGs are also used in internal calibration images such as darks and biases or unique modes such as spatial scanning. The surest check for a guidestar failure is to inspect the proposal's visit status information from `http://www.stsci.edu/hst/scheduling/program_information`.

Figure 35 – Guidestar failure in IR subarray image `icyta4rxq_flt.fits`.

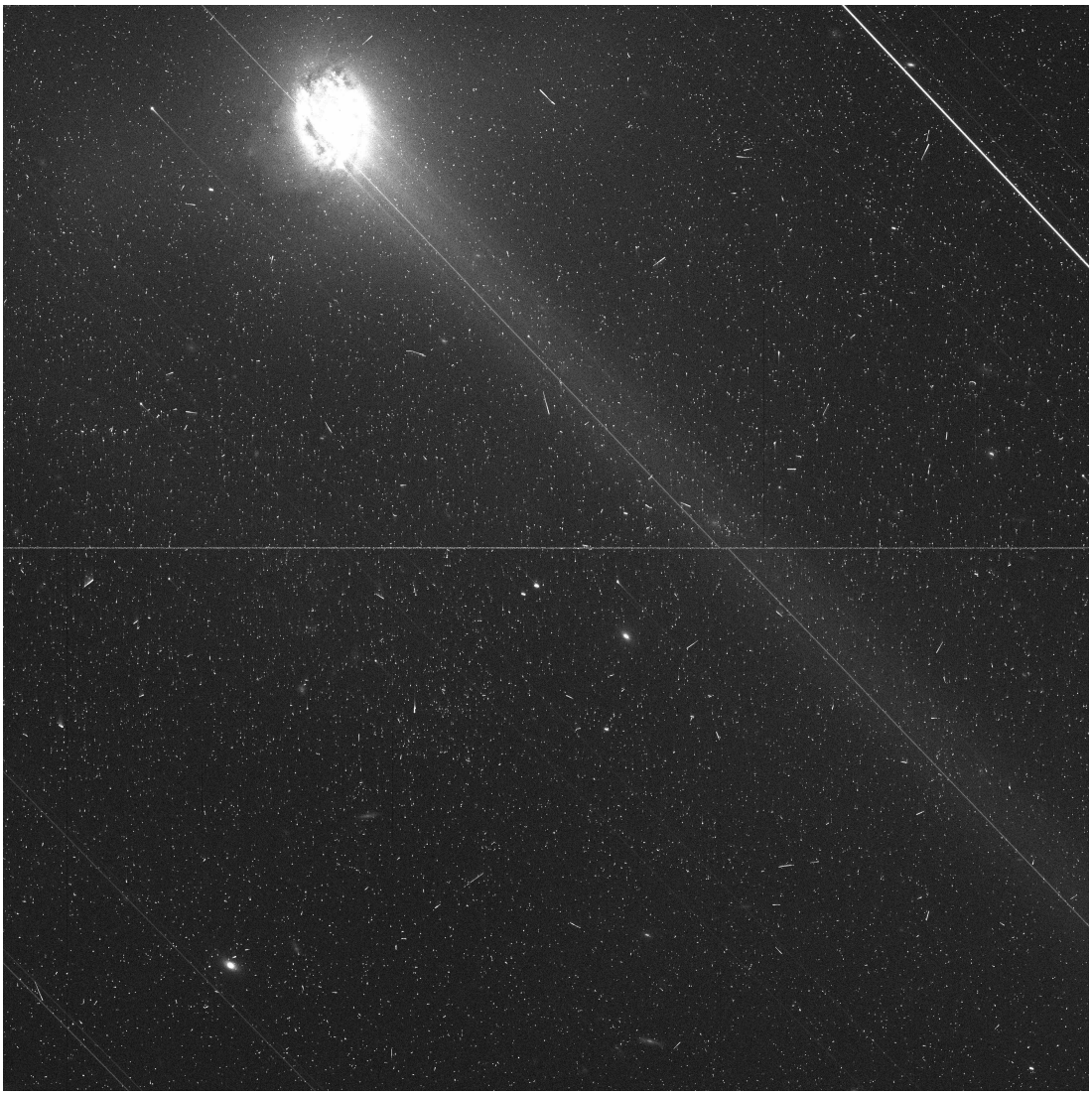

Figure 36 – Guidestar failure in UVIS image `icdm11giq_flt.fits`.

4.4 Satellite Trail (IR & UVIS)

Hubble is in low-Earth orbit and satellites quite frequently intersect with the area of sky being observed. They don't always appear as uniform lines. Sometimes in UVIS tumbling satellites can cause dashed-line trails, but most often they appear as single strong lines as in Figure 37. In IR images, `calwf3` can sometimes cause the trail to look blacked-out (Figure 38) because it tries to fit up-the-ramp a source that appears suddenly in a read. In IR grism images, such as in Figure 39, the satellite will be dispersed. You can, if necessary, mask the trails out, and if your science target is affected badly enough, in IR images you can remove the affected read(s) and re-calibrate. You may need to mask or remove several reads because

satellite trails can cause persistence and thus appear in subsequent reads.

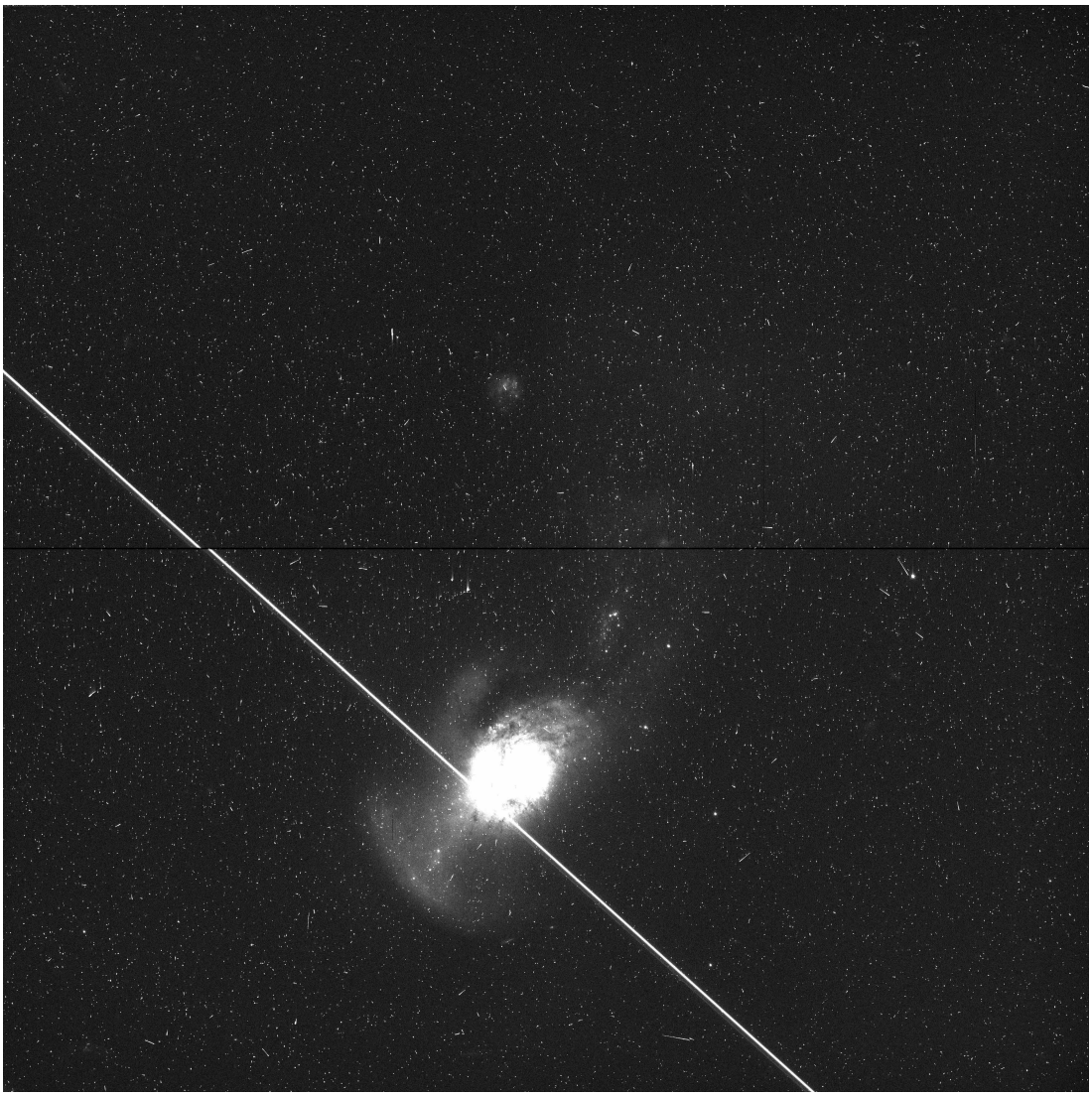

Figure 37 – Satellite trail, broken by the chip gap, on UVIS image `icx107qnq_flt.fits`*. The extent of the chip gap is an artifact of how the two UVIS chips are stitched together in the JPG and is not to scale with the chips.*

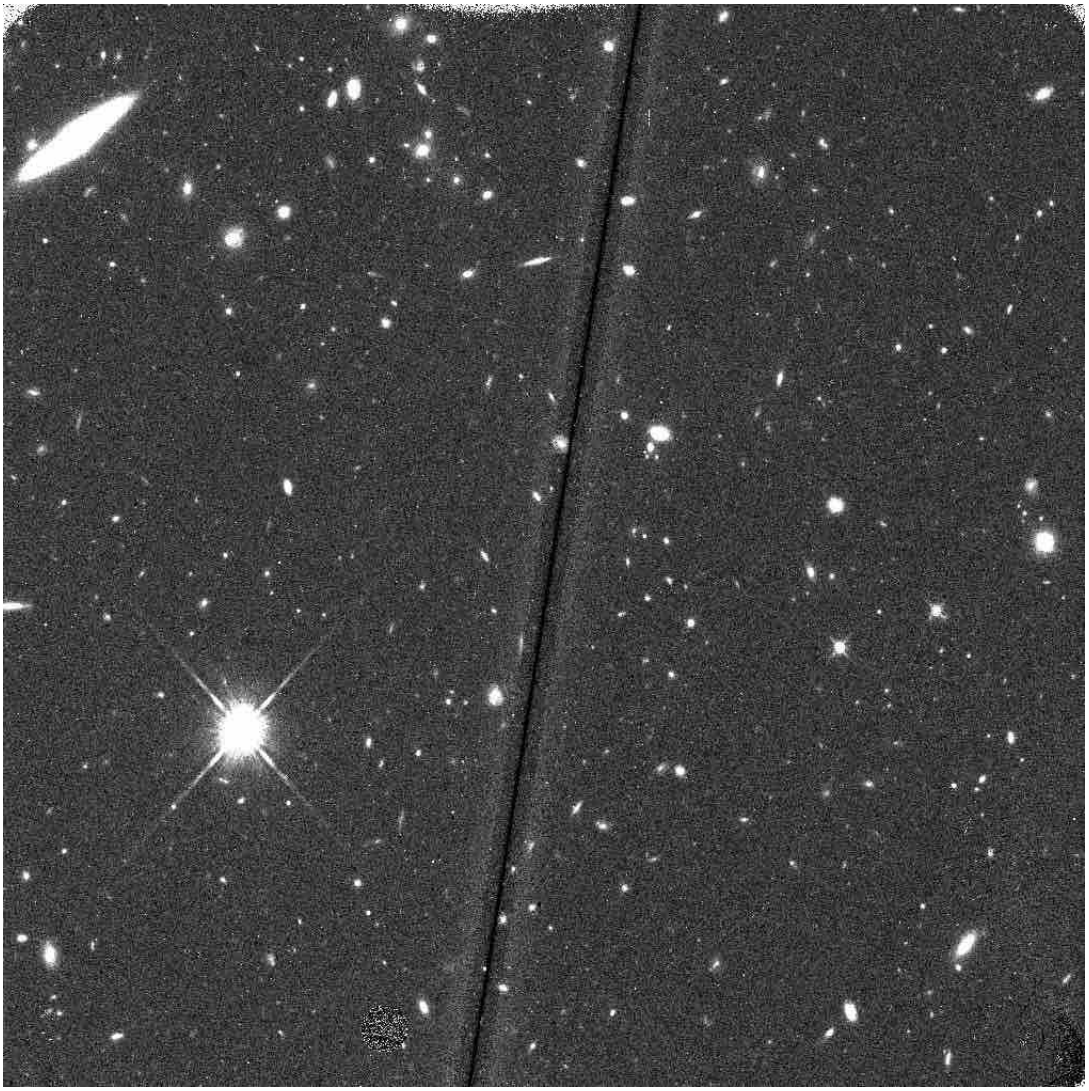

Figure 38 – Satellite trail in IR image `ia2g02pbq_flt.fits`*. The dark, fuzzy appearance is due to* `calwf3`*'s up-the-ramp fitting.*

Figure 39 – Dispersed satellite trail in IR grism G102, image `ibtt50g5q_flt.fits`.

4.5 Space Trash and Asteroids (IR & UVIS)

Some moving targets are clearly not satellites because they move more slowly and/or have more obviously curving paths.

In the first example, Figure 40, the white-bordered string of beads on the center left of the image is, in fact, moving. Each "bead" is the location of a single object on an individual read (see Figure 42). If you flip through the remaining Visit 05 images of this program (12553) you see the object continue to move. In UVIS, a moving target such as an asteroid or space trash would just be a streak, sometimes indiscernible from a satellite trail or cosmic ray. In IR, the moving target will move read-to-read (unlike most satellites or cosmic rays, depending on the read rate) and because `calwf3` fits the ramps to produce the final FLT,

they can be flagged and therefore masked out (appear as black smudges) in the final FLT. It's for this more dramatic appearance in the IR that the Quicklook team seems to find more moving targets in IR than in UVIS.

A report by Sunnquist et al. (2017) highlights 87 examples of serendipitous astroid observations from WFC3/IR images in the Frontier Fields program. In a rarer, more dazzling example, Figure 41 shows a bright asteroid (top smudge) that moved into the WFC3/IR frame during a grism exposure. This asteroid was later identified as 1036 Ganymed.

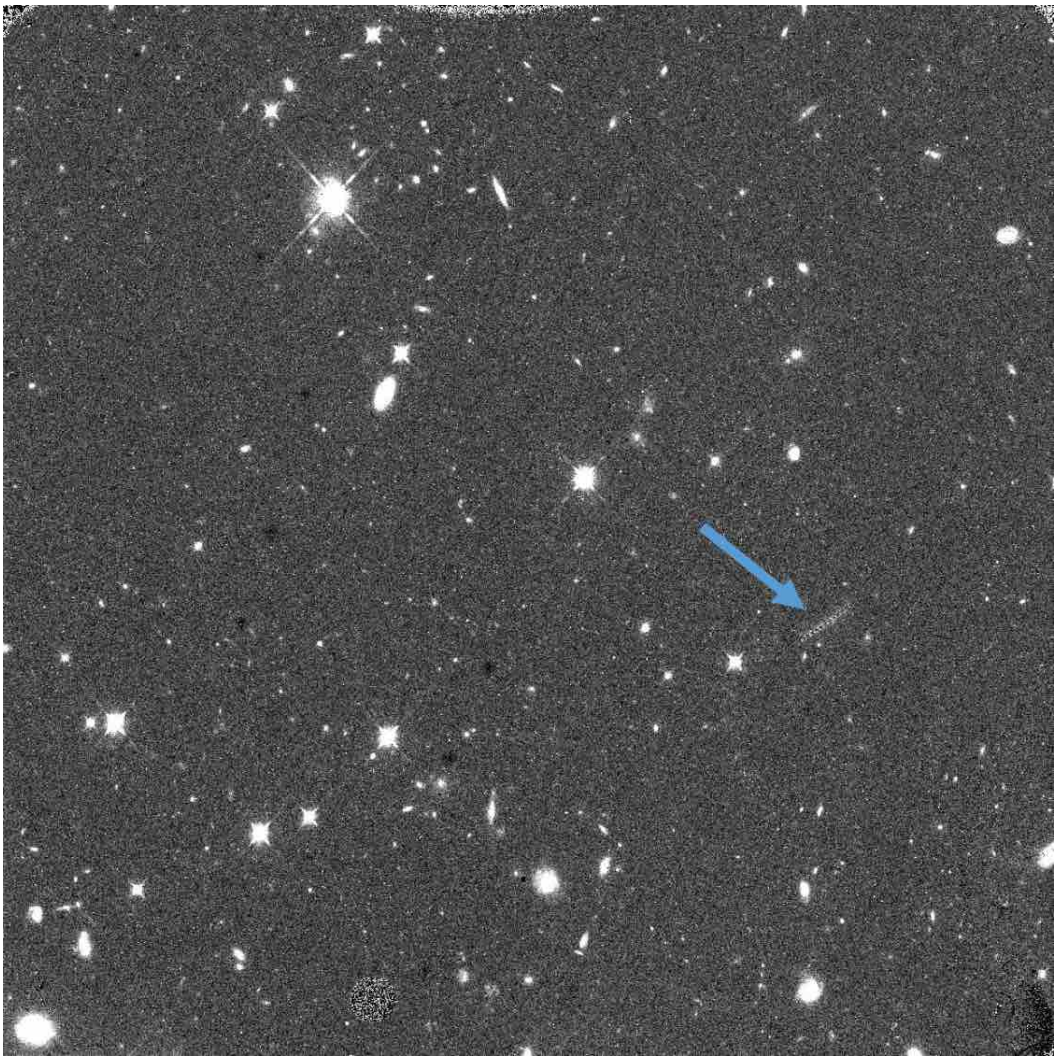

Figure 40 – Potential space trash or asteroid in IR image `ibpp05e0q_flt.fits`*. The read-to-read progression of the object in the IMA file is shown in Figure 42.*

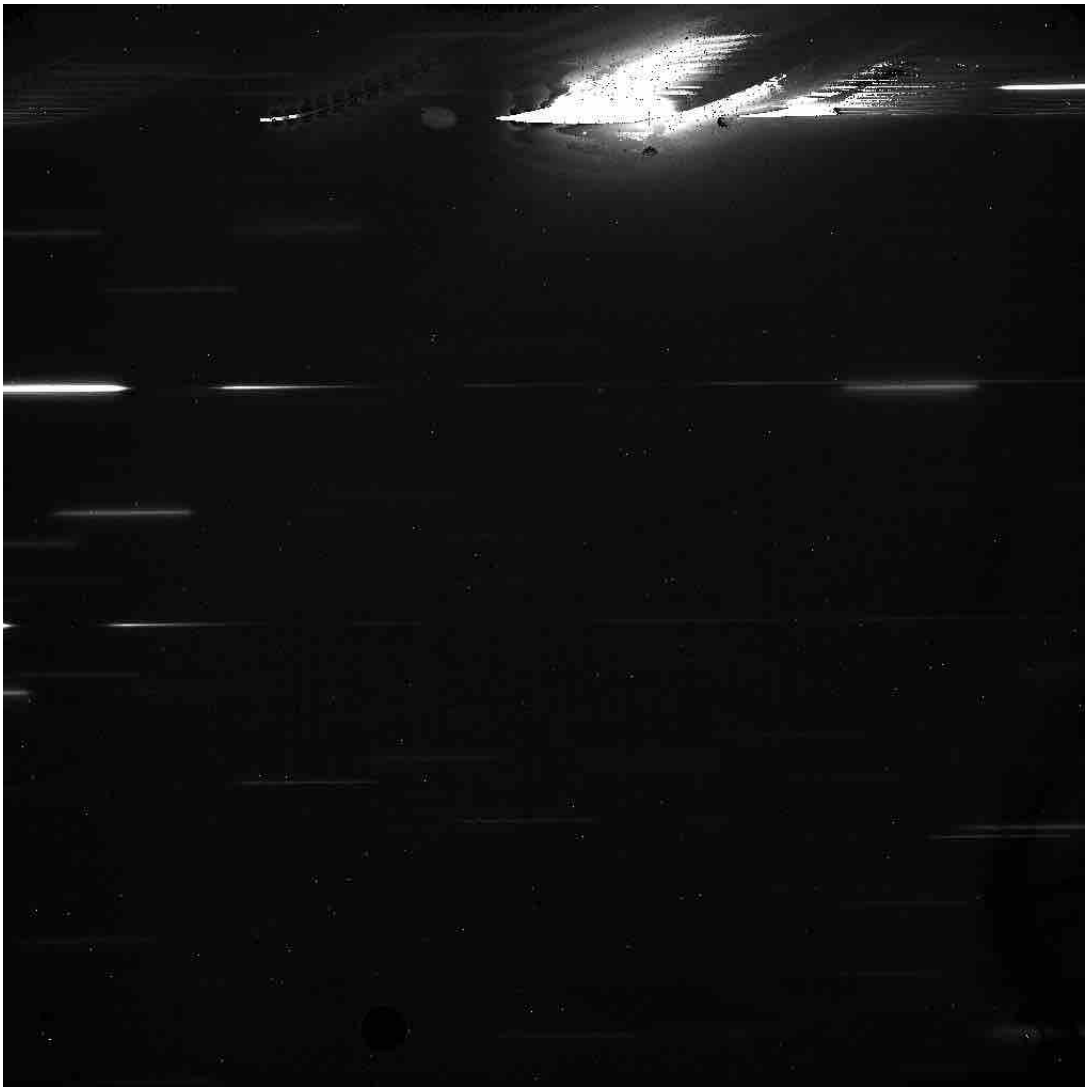

Figure 41 – At top, the serendipitous capture of Mars-scrossing asteroid 1036 Ganymed in IR grism image `ibhm12udq_flt.fits`*. Also visible are grism bright object bands from the dispersed diffraction spikes. The read-to-read progression of the asteroid in the IMA file is shown in Figure 42.*

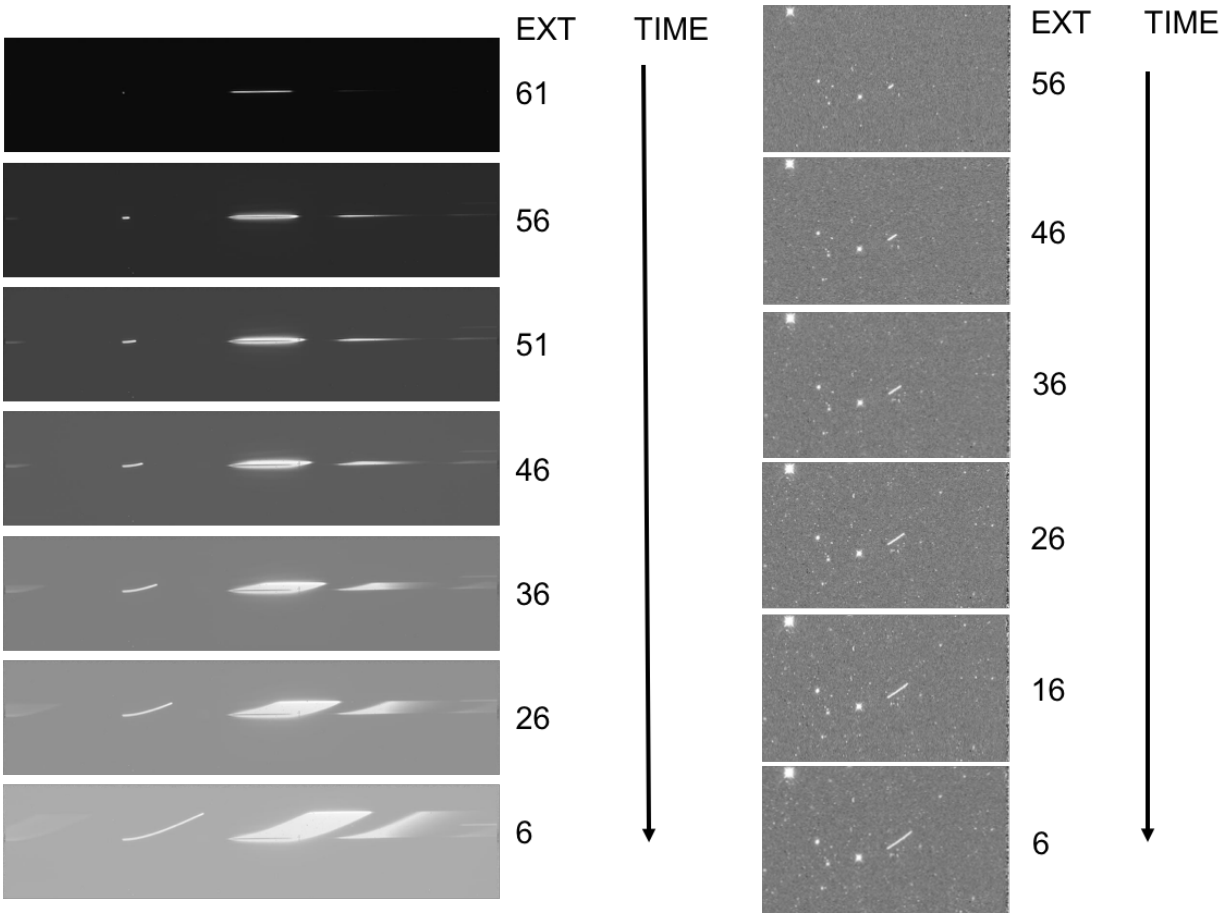

Figure 42 – Asteroid 1036 Ganymed (left) and unidentified space debris or asteroid (right) moving read-to-read in the IMA files. The IMA extension numbers are listed; note that they decrease as time increases! The objects streak as time progresses because they are being continuously integrated up the ramp.

5 Known Detector Defects

The following are known (hence, not "anomalous") detector defects that are for the most part corrected for in the calibration pipeline `calwf3`, and in the case of CTE decay and new blobs, are tracked by specific monitoring scripts rather than by daily quicklooking. Therefore images in which known detector defects appear are not flagged by the Quicklook team as containing anomalies.

5.1 Blobs (IR)

Figure 43 shows the application of the blob mask. See Section 2.7 for more about blobs.

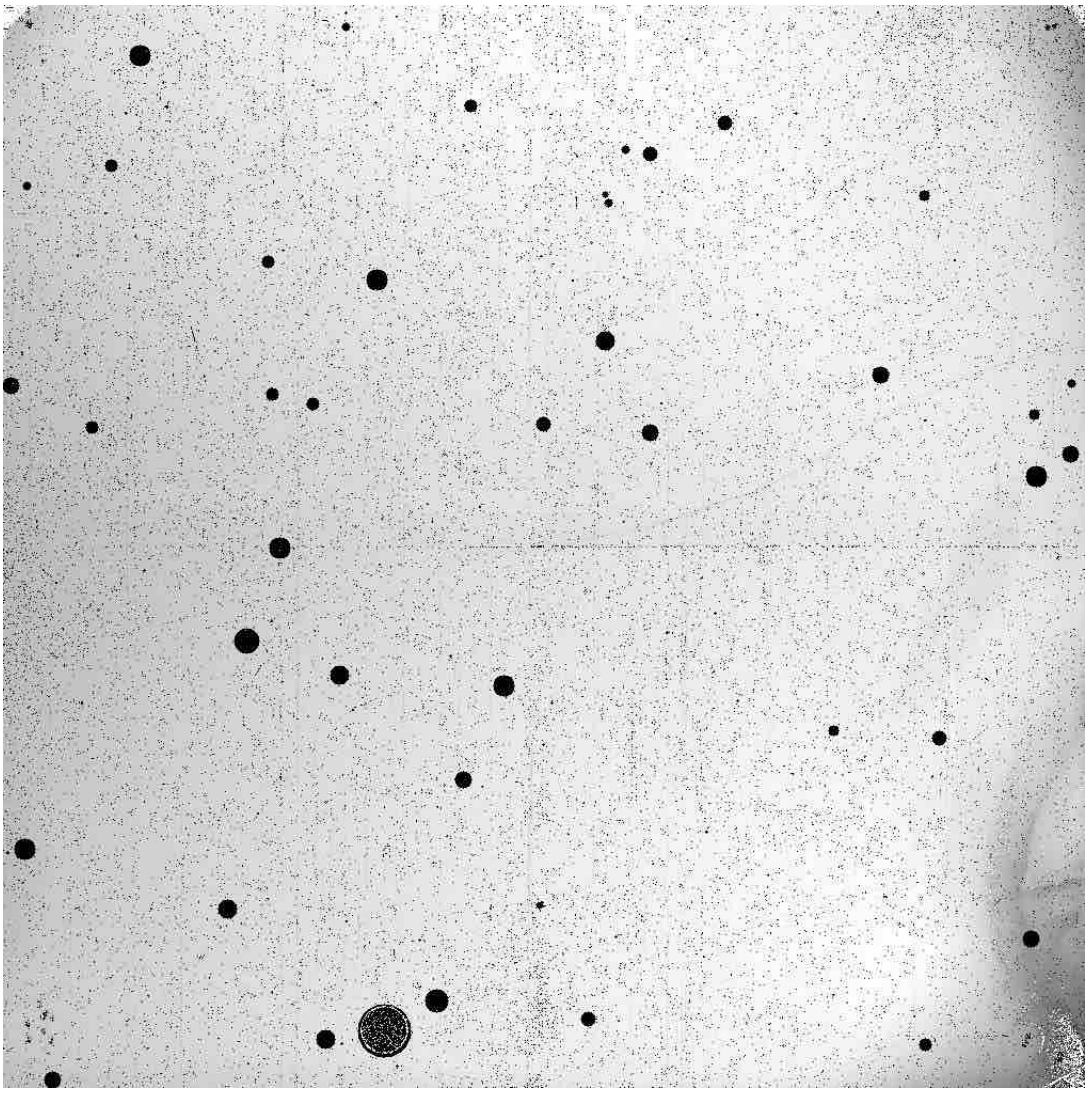

Figure 43 – Application of an IR blob mask in IR image `ic5j16e3q_flt.fits`.

5.2 CTE Trails (UVIS)

Charge transfer efficiency (CTE) trails are a consequence of ongoing radiation damage to the silicon lattice of the UVIS detector, decreasing its ability to transfer charge without losing it to traps. Figure 44 shows an extreme case of bad CTE due to short exposure time and no post-flash, making the sources in the image appear to be melting toward the center. This illusion is due to charge on readout having to journey through more traps the farther it is from the corner amplifiers (see illustration in Figure 1). CTE losses are fairly straightforward to mitigate for most science cases. You can increase the background, in effect filling potential traps, via either filter choice, post-flash, or longer exposure time. In addition, you can use the CTE-corrected analogs of FLT files, the FLC files, which have been run through a software, now part of the `calwf3` pipeline, that pushes charge back to its source. Chapter 6 in Deustua (2016) provides more details.

Because CTE losses are a characteristic of the detector, bad CTE is not flagged as an anomaly. Like other detector characteristics, however, its evolution is monitored with yearly programs (Gosmeyer and Baggett, 2017).

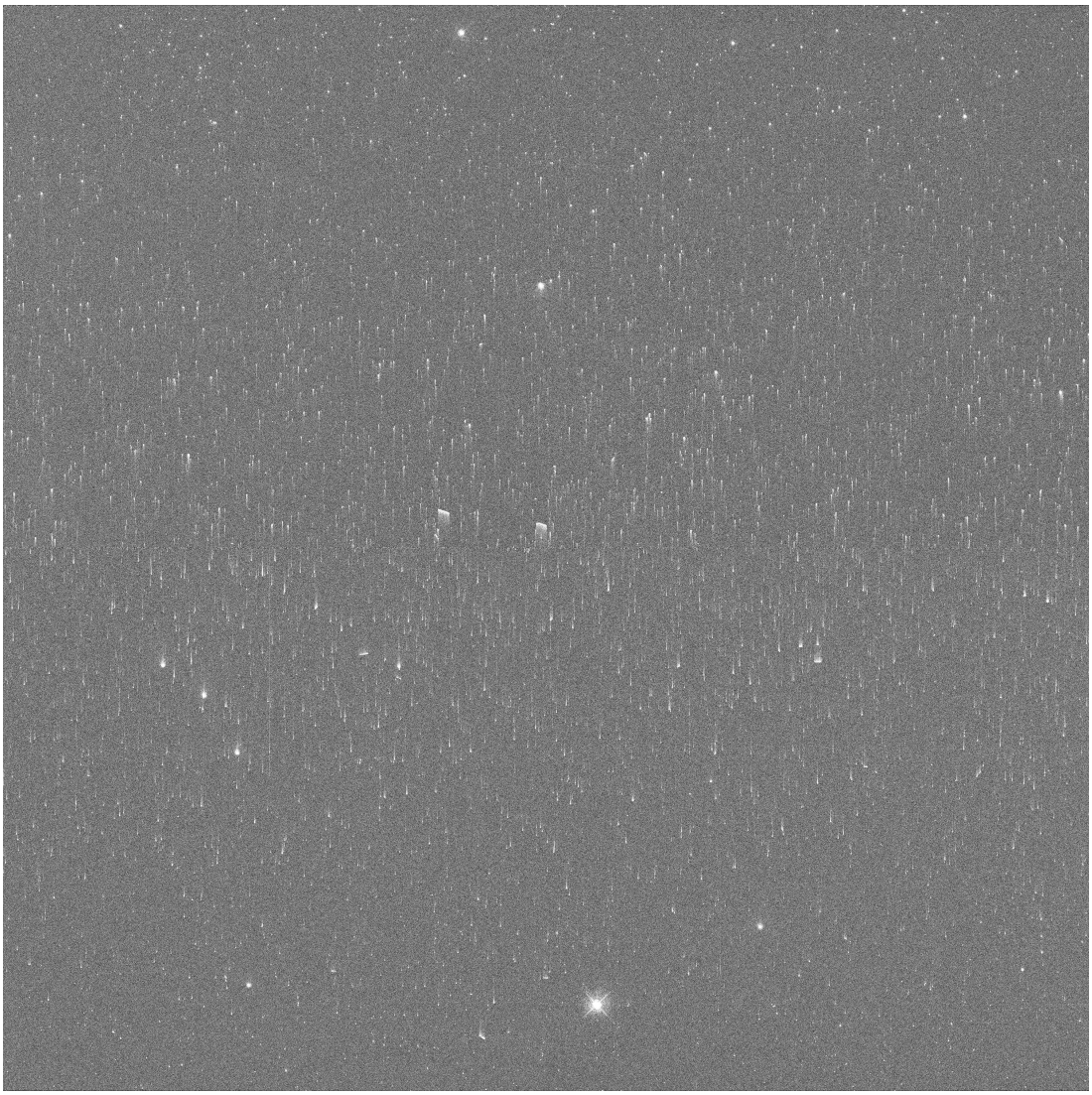

Figure 44 – CTE trails on a low-background UVIS image `icqu01elq_flt.fits`.

5.3 IR Flat Field

The IR flat field shows unique defects, such as the arc-shaped "Wagon Wheel" and circular "Death Star," which are stable regions of low quantum efficiency with mild wavelength dependency (Bushouse, 2008). The scratch in the mid-right and unbonded pixels in the upper corners and center are also known defects.

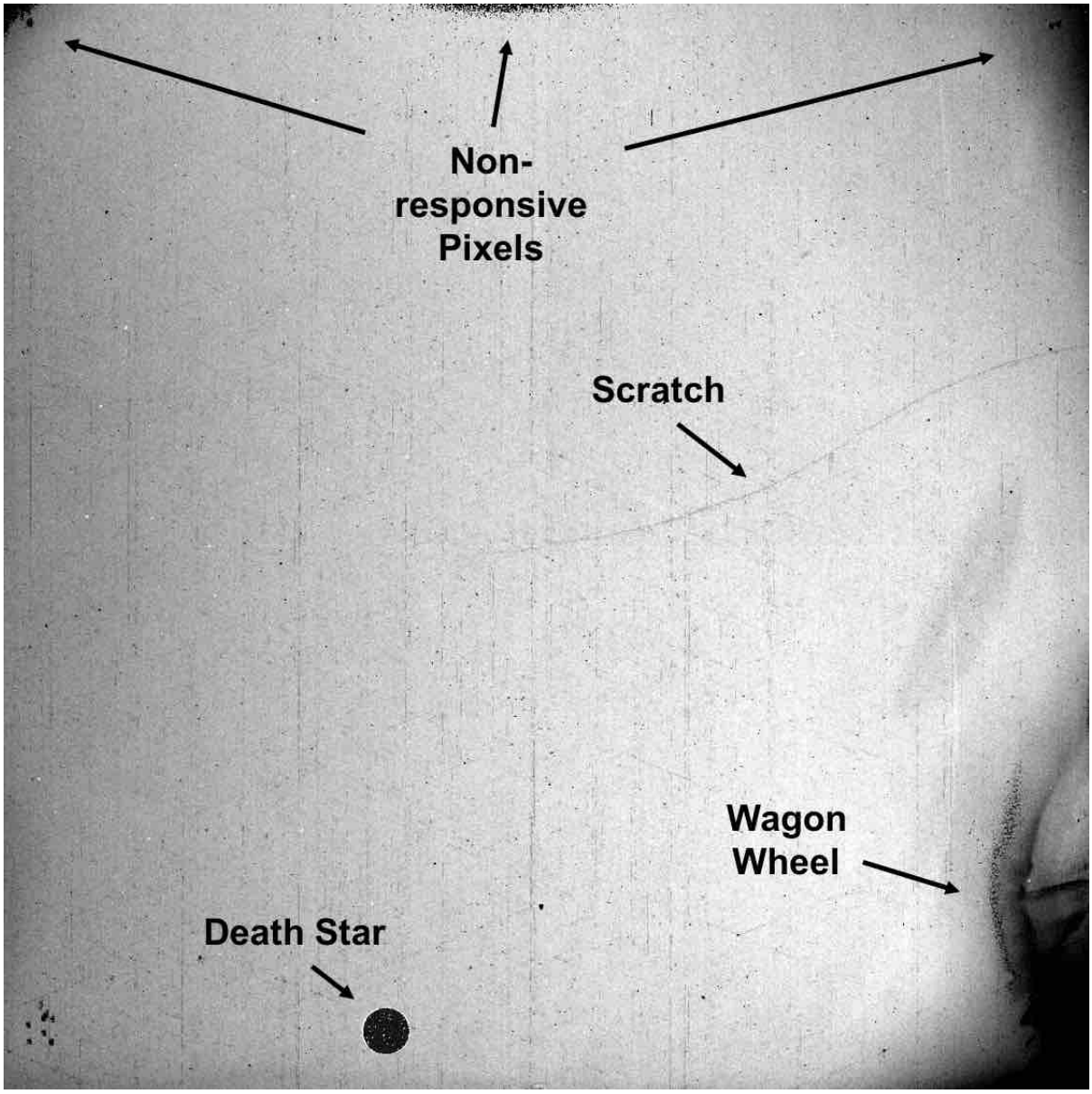

Figure 45 – IR flat field image `ic5n01hvq_flt.fits` *clearly showing the Wagon Wheel, Death Star, scratch, and upper non-responsive pixels.*

5.4 Snowballs (IR)

IR snowballs are transient events, believed to be caused by radioactive decay within the detector or surrounding materials that randomly and instantaneously deposit at least 200,000 electrons over an area of up to 40 pixels (Durbin et al., 2015). They are treated as cosmic rays in the pipeline and thus often do not appear in the final calibrated FLT file. However, sometimes snowballs will be incompletely removed, as shown in the example in Figure 46. A list of all snowballs recorded to have appeared 2009-2015 is available at `http://www.stsci.edu/hst/wfc3/ins_performance/anomalies/ir_snowball_table.txt`.

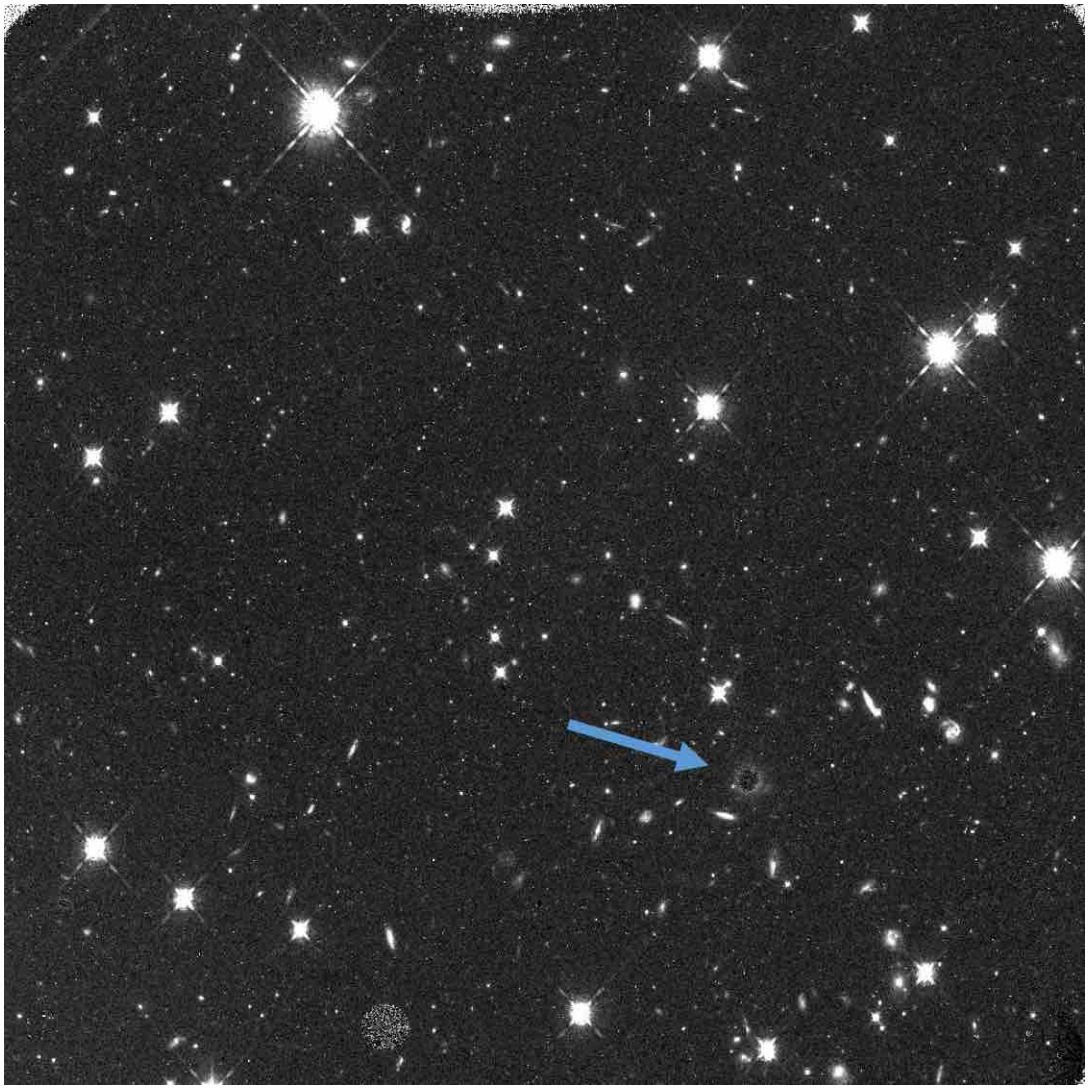

Figure 46 – An incompletely removed snowball in IR image `ib8d95lpq_flt.fits`.

5.5 UVIS Bad Pixel Columns

Seven columns in UVIS are known to be defective and are flagged in the DQ array. In pre-2016 flats the bad columns were set to 0, and therefore would show up in images as black dataless lines. In the 2016 version of the flats the bad columns were interpolated so that they no longer appear in images (Mack et al., 2016). You might still see them in images calibrated with a pre-2016 version of `calwf3`, which you can check with the header keyword CAL_VER.

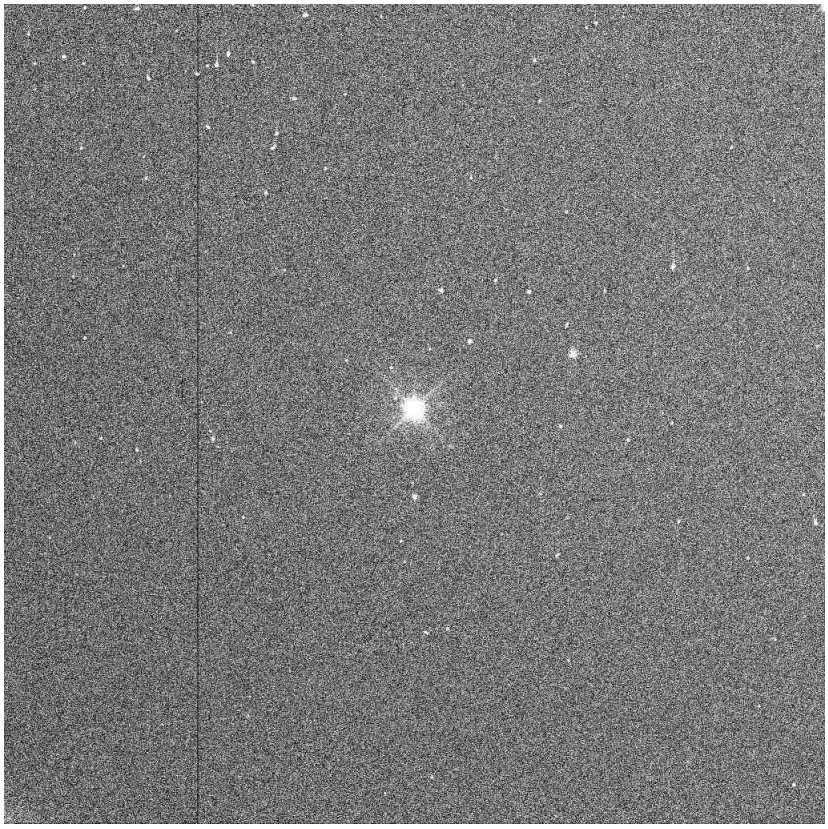

Figure 47 – A bad pixel column in UVIS subarray image `ic1r14lmq_flt.fits`.

5.6 UVIS Internal Flat Field

On the UVIS internal flat field you can see an overall gradient from the upper left to the lower right and bright "arclets" across the quadrants, as well as smaller features such as the white "droplets" (almost-in-focus dust on the CCD window), dark "dust motes" (fuzzy out-of-focus circular features from dust on the filters), scratches in the upper center of chip 1, bad columns, and the chip gap (Baggett et al., 2009).

Many of these features are due to the calibration subsystem used to generate the internal flatfields and thus will not appear in the pipeline flatfields.

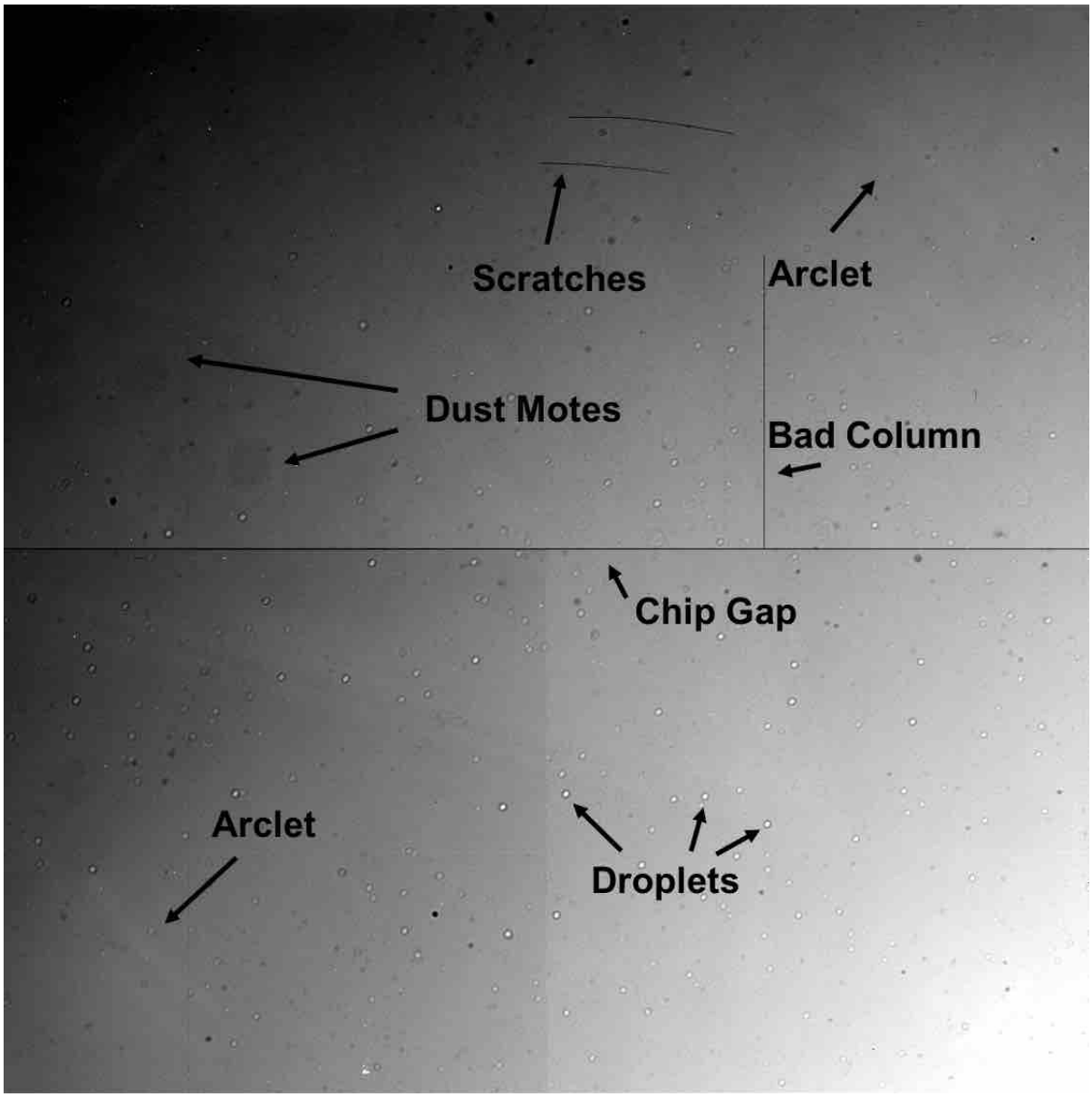

Figure 48 – The UVIS internal flat field, from image `ic3w06i9q_flt.fits`.

6 Non-Standard Modes

In this section are examples of some non-standard modes that can be mistaken for anomalous behavior. They are not flagged by quicklookers.

6.1 Bowtie (UVIS)

In a monitoring observation called a "bowtie," the UVIS detector is allowed to saturate ∼9 times full-well, yielding the bowtie shape seen in Figure 49. The purpose of these observations is to condition the detector and check for hysteresis, the quantum efficiency deficit across the UVIS chips (Bourque and Baggett, 2013).

Figure 49 – Bowtie observation, UVIS image `icq101kyq_flt.fits`.

6.2 Charge Injection (UVIS)

In Cycles 17 and 18 charge injection (CI) was tested as a method to reduce charge transfer efficiency (CTE) decline in UVIS images. Ultimately, post-flash became the standard method for mitigating CTE, and CI was retired. The signature stripes in CI images can be mistaken for data transfer error. However, in CI the stripes are always horizontal and parallel entirely across the frame (resembling the screen of an old analog television), and furthermore, any CI you would see would be in 2010-2011 archived images.

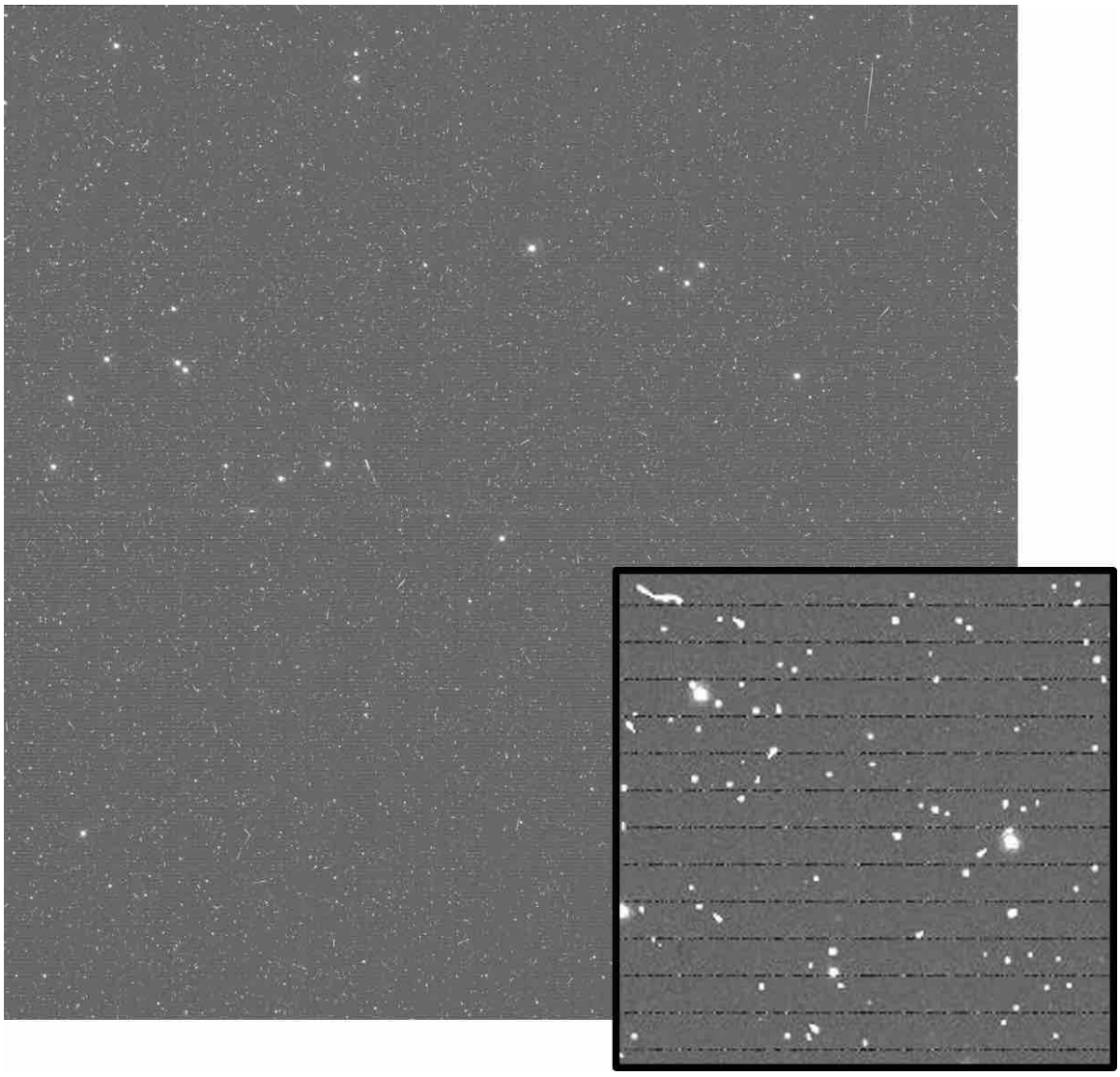

Figure 50 – Charge injection in an external UVIS image `ibnh13gaq_flt.fits`*. The close-up is included to highlight the characteristic stripes of the charge injection mode.*

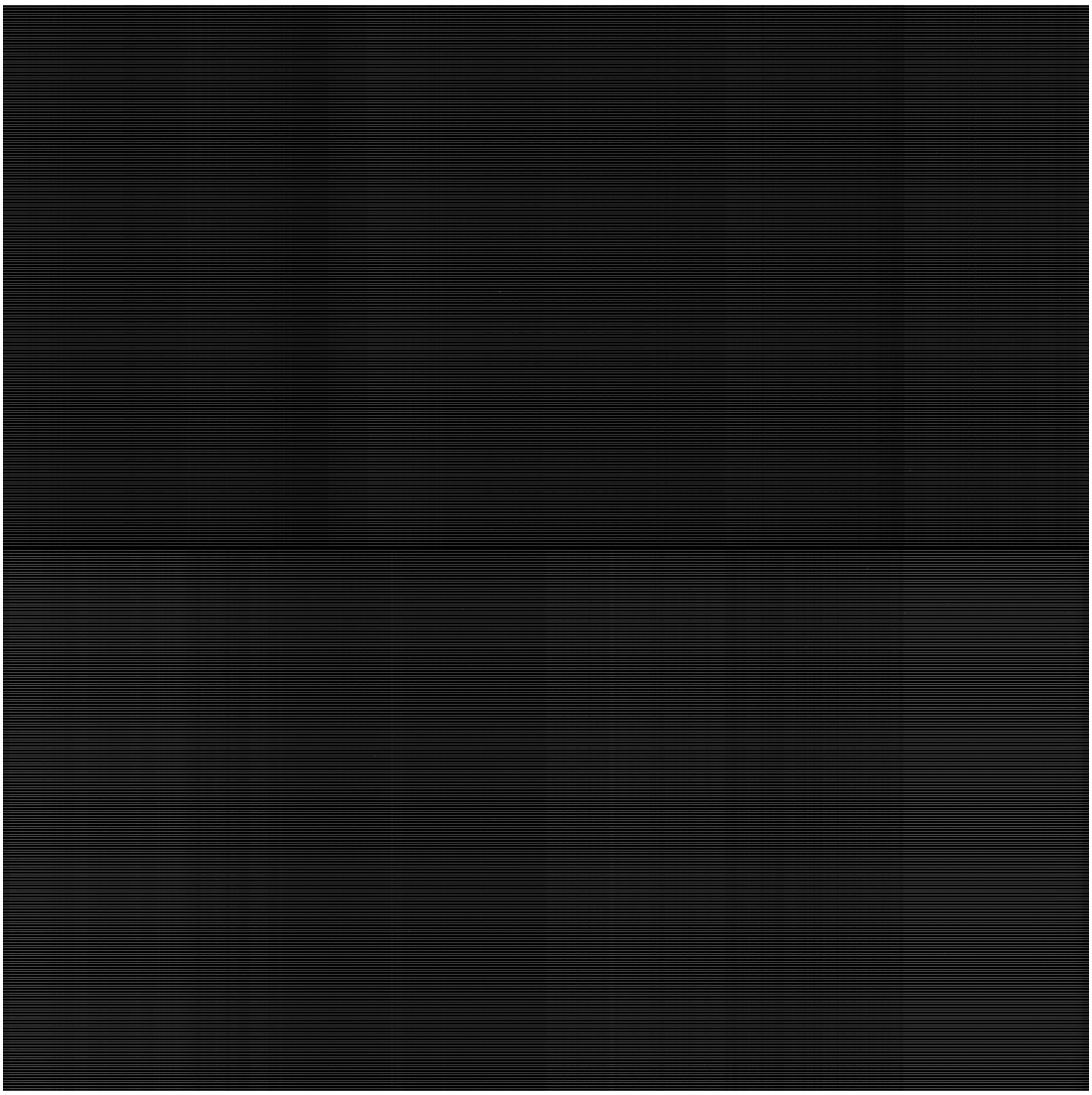

Figure 51 – Charge injection in UVIS bias image `iblk76fbq_flt.fits`.

6.3 Earth Flats (IR)

The purpose of Earth flats is discussed in Section 2.7 and an image with persistence from an Earth flat is in Figure 13. They can be distinguished from real anomalous behavior, such as a guidestar failure, by checking header keywords. An Earth flat is only ever taken as part of a calibration (CAL) proposal and the IMAGETYP keyword will be set to "DARK-Earth-CALIB."

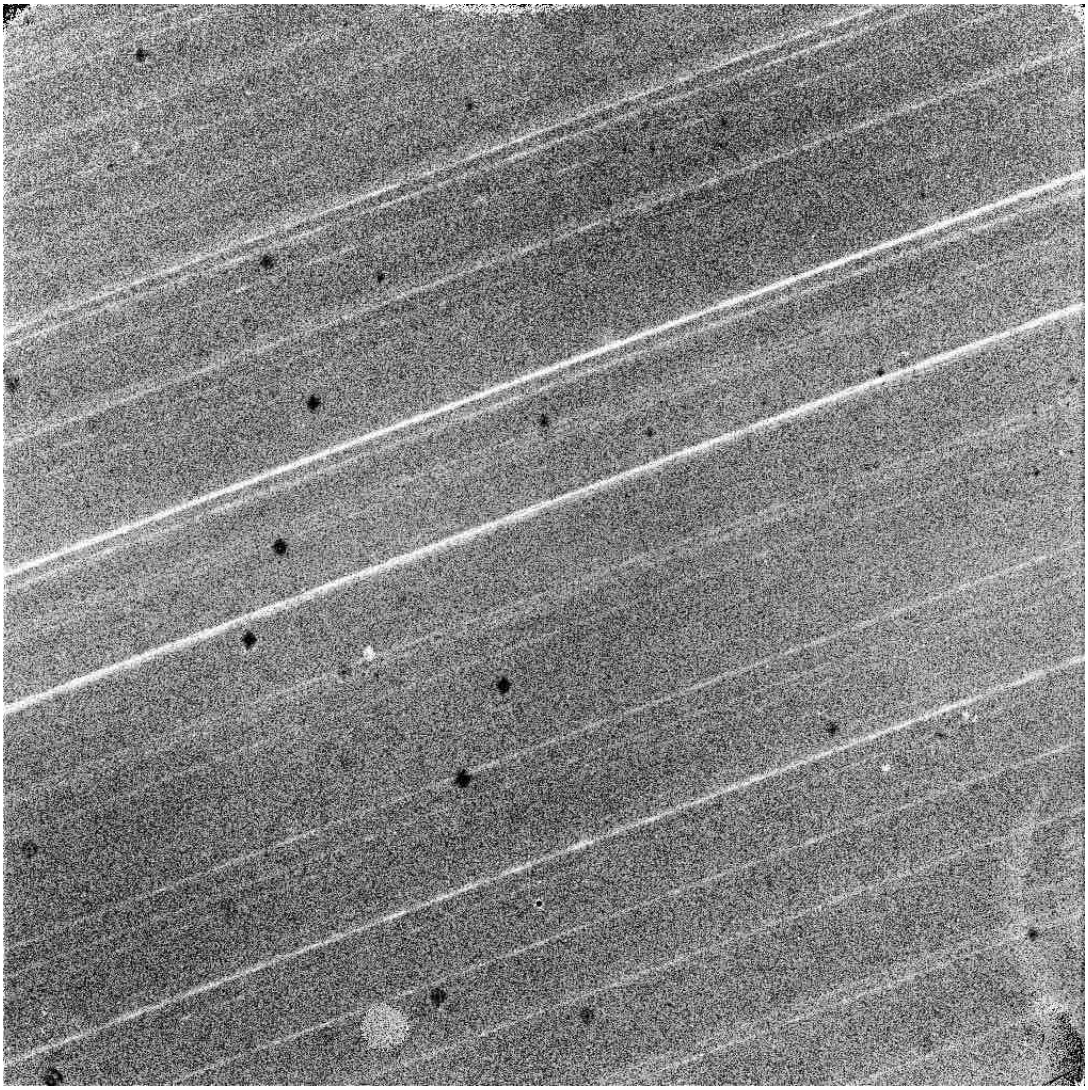

Figure 52 – Earth flat, UVIS image `ic5i02dkq_flt.fits`*. Note also the prominent blobs.*

6.4 Grism Bright Object Bands (IR)

The diffraction spikes of bright objects dispersed in the IR grisms can appear as bands on the top and bottom of the bright object's 1st order trace. A good example is on the bottom left of Figure 53.

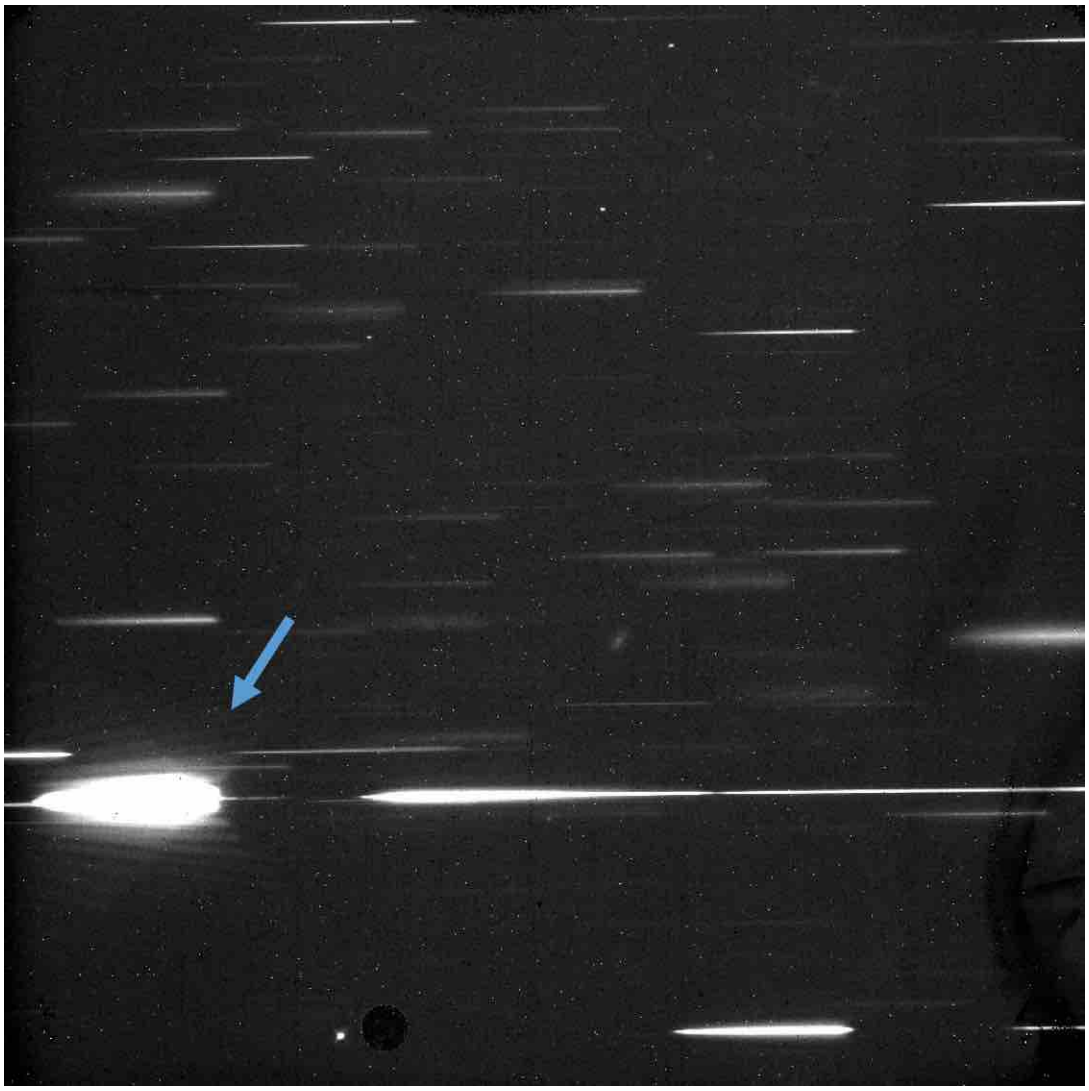

Figure 53 – Bands from dispersed diffraction spikes of a bright object in IR grism image `icat14icq_flt.fits`.

6.5 Grism+Spatial Scanning (IR)

Spatial scanning IR grism images can throw off a nominal run of `calwf3`, which assumes a linearly increasing signal in each pixel and therefore fits up-the-ramp to produce the final FLT. But for sources that move from ramp-to-ramp (scanned data, moving targets, satellite trails), up-the-ramp fitting is not ideal. As a workaround, the current version of `calwf3` sets the cosmic-ray correction step CRCORR to "OMIT" in scanned images, disabling the up-the-ramp fitting. The resulting FLT file will be a semi-reasonable output of first-minus-last read, better for previewing images (Figure 54). In older versions of `calwf3`, CRCORR was always set to "PERFORM" and hence the outcome of scanned grism images would be the more bizarre outcome of up-the-ramp fitting (Figure 55). Since they are such a special case, teams that take scanned grism images generally write their own software to properly process them.

Figure 54 – Grism spatial scanning in IR image `icpp01acq_flt.fits`*, with the current version of* `calwf3` *where by default the keyword CRCORR is set to "OMIT" in spatial scanning images.*

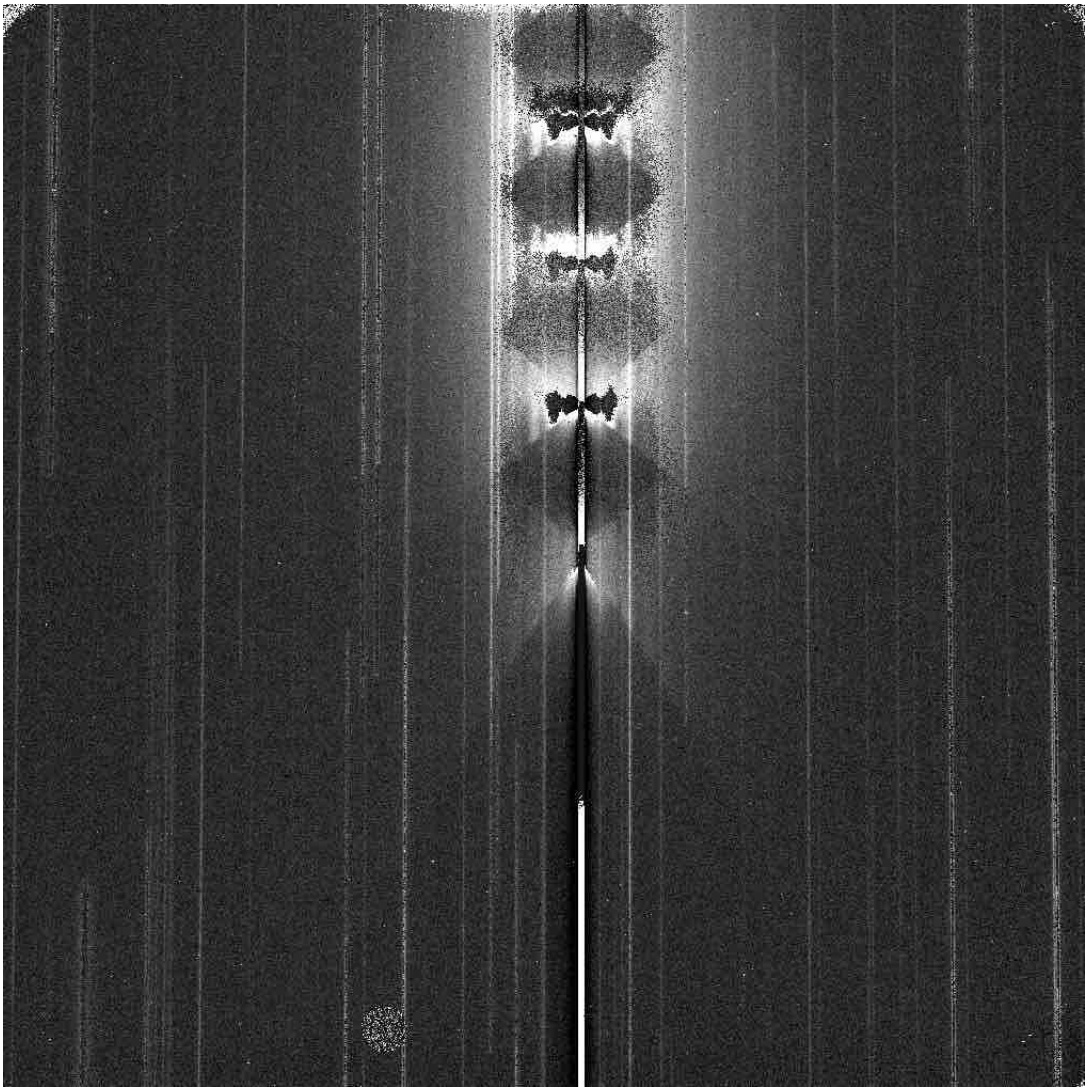

Figure 55 – Grism spatial scanning in IR image `icpp01acq_flt.fits`*, with an older version of* `calwf3` *where keyword CRCORR was set to "PERFORM."*

6.6 Moving Target Observation (IR & UVIS)

A deliberate moving target observation (as opposed to a serendipitous one) will track on the moving target (comets, asteroids, moons), letting the background stars streak. To be sure it is a moving target observation, and not, for instance, a guidestar failure, check the TARGNAME keyword for a comet or asteroid name or the MTFLAG keyword, which will equal "T" if a moving target.

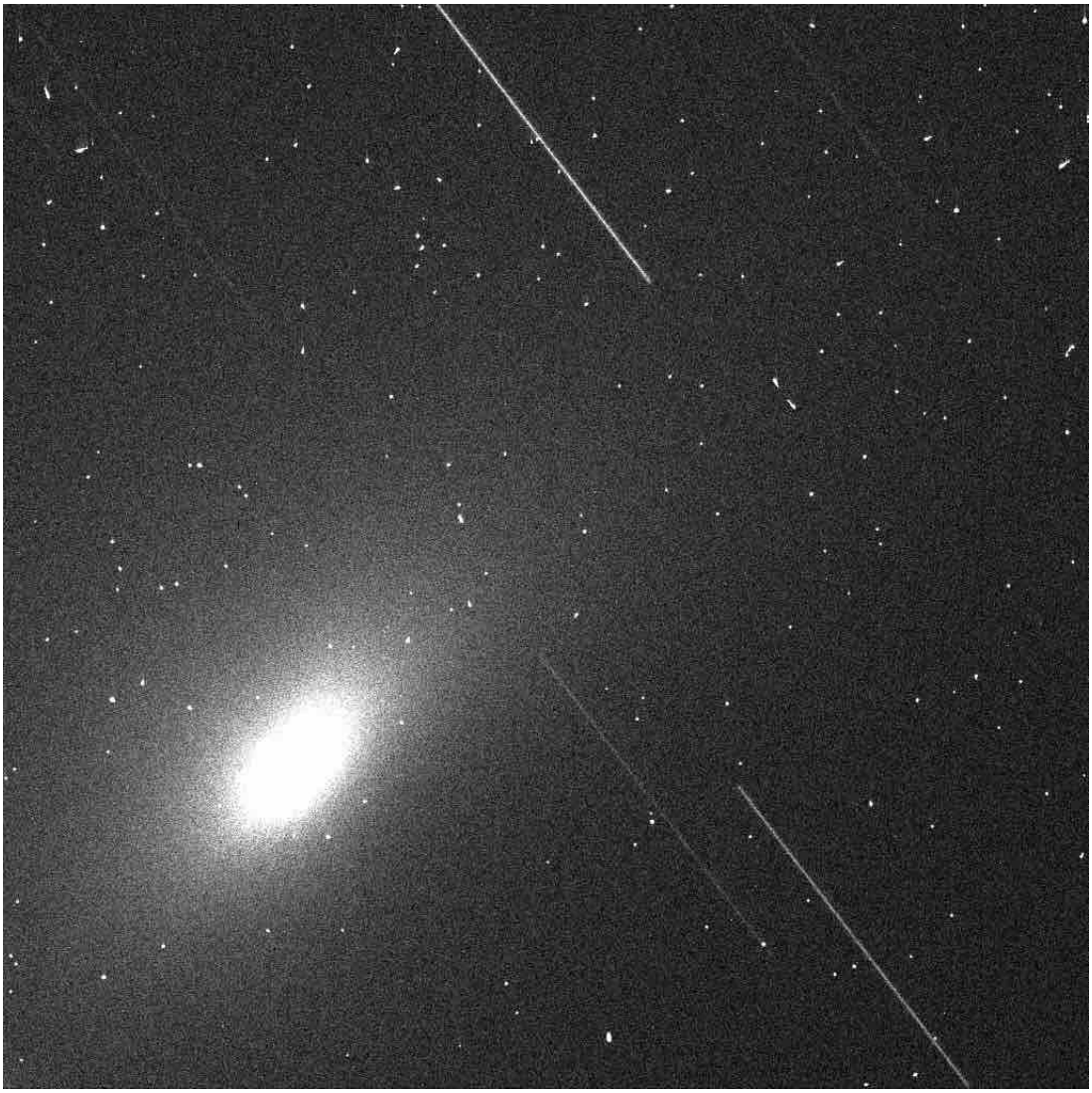

Figure 56 – Moving target in IR image `icvba1alq_flt.fits`.

6.7 Quad Filters (UVIS)

UVIS has five filters that are in fact four filters in one (distinguished by "FQ" as in quad filter FQ436N), for a total of 20 quad filters. Because of the sharp change in bandpass between quadrants, these quad filter images can look bizarre when taken in full-frame rather subarray mode. The first example (Figure 57) shows a science observation taken in a full-frame, and the second example (Figure 58) shows a flat field. WFC3 filters are discussed in Section 2.3.2 of Dressel (2017).

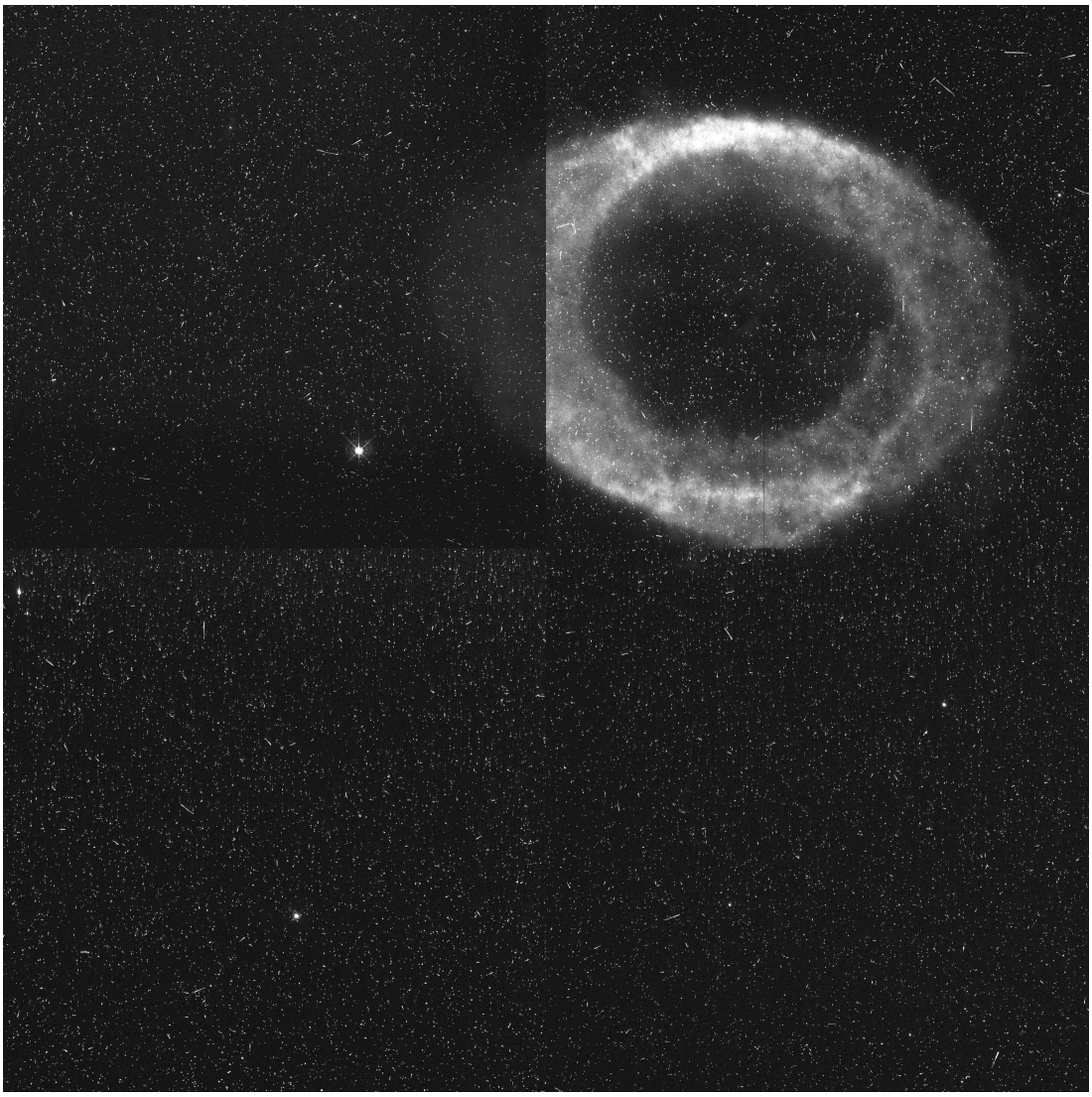

Figure 57 – Example of a science image, `ibh602m6q_flt.fits`*, using a UVIS quad filter.*

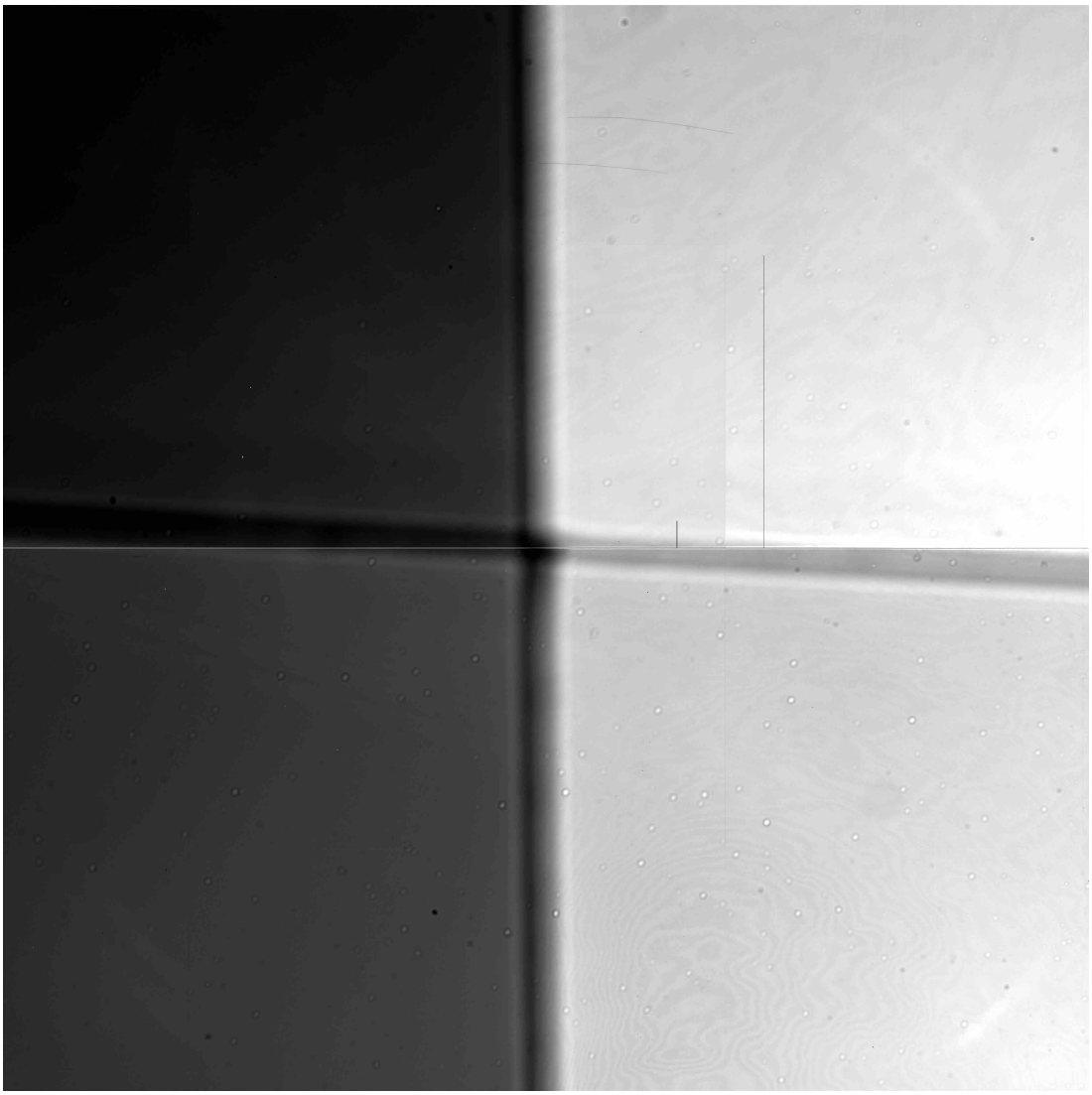

Figure 58 – Example of a UVIS quad filter flat field, image `icqs11dmq_flt.fits`*. Fringing is also visible in the two right quads, FQ750N (quad B) and FQ727N (quad D).*

6.8 Spatial Scanning (IR & UVIS)

Spatial scanning is a special mode available for both IR and UVIS where the detector is deliberately scanned across the scene in order to collect more charge from a source that might otherwise quickly saturate and to increase precision in photometry or astrometry (McCullough and MacKenty, 2012). Scanned images can look a lot like Earth flats or guidestar failures, and like guidestar failures the keyword EXPFLAG might say "TDF-DOWN AT EXPSTART" or "INDETERMINATE." If you have doubts, check the keyword SCAN_TYP. It should equal "C" if the observation was programmed to be a spatial scan, while "normal" staring mode images will have SCAN_TYP of "N." Grisms can also be used in scanning mode; see the examples in Section 6.5.

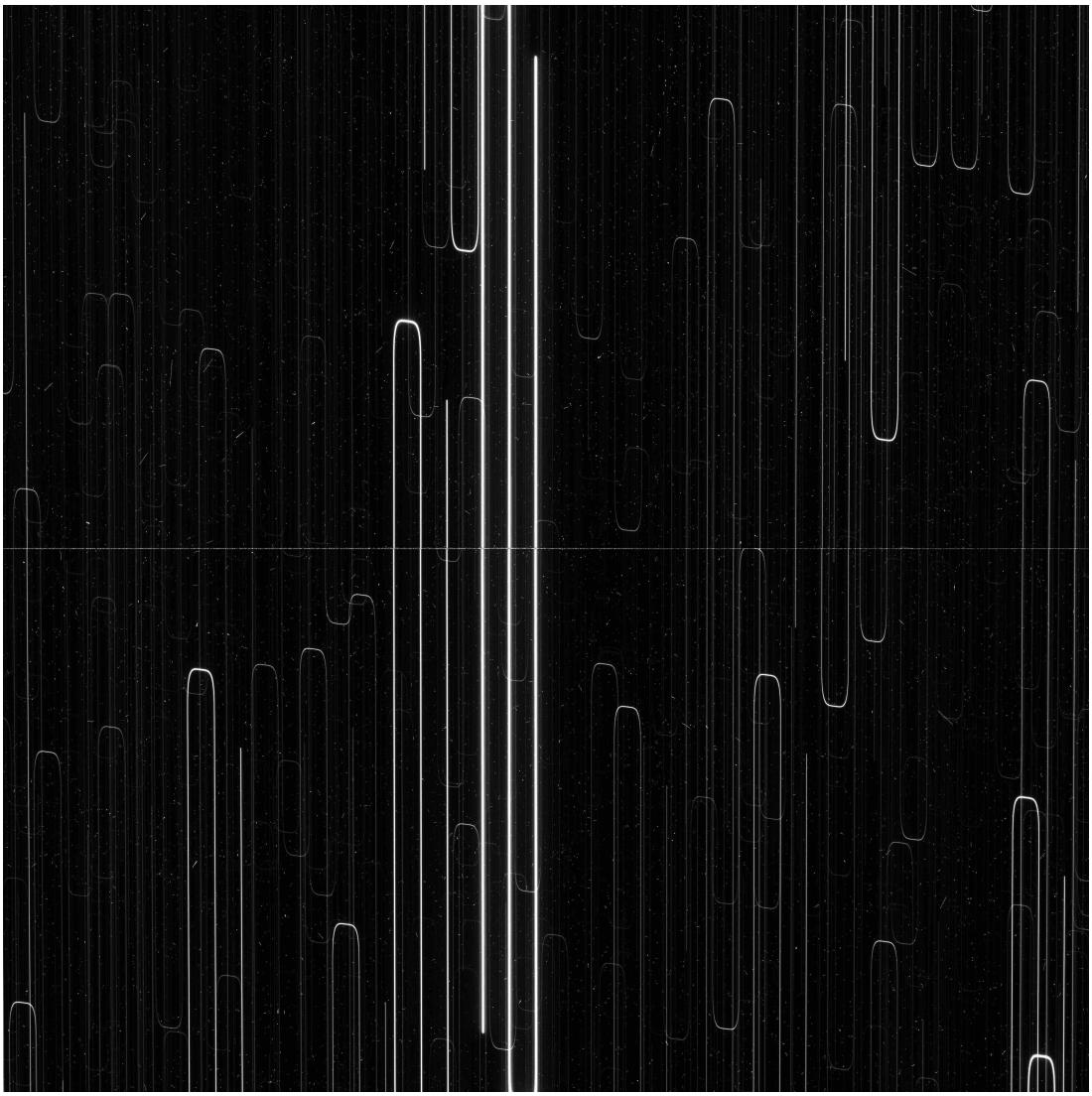

Figure 59 – Example of a "plow pattern" spatial scan in UVIS image `ibzc03wlq_flt.fits`.

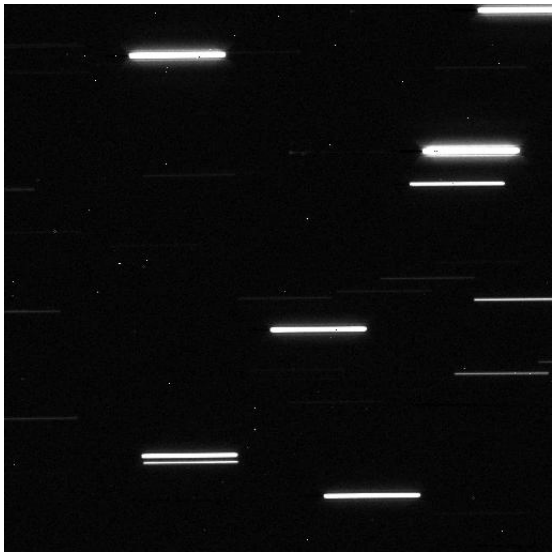

Figure 60 – Example of a horizontal spatial scan in IR subarray image `icro03kaq_flt.fits`.

6.9 UVIS Grism

The UVIS grism G280 disperses light in "wings" on either side of the source. The spectra are curved, with negative orders to the left and positive orders to the right. Figure 2 in Kuntschner et al. (2009) gives a schematic of the spectral orders in the traces up to orders ±8.

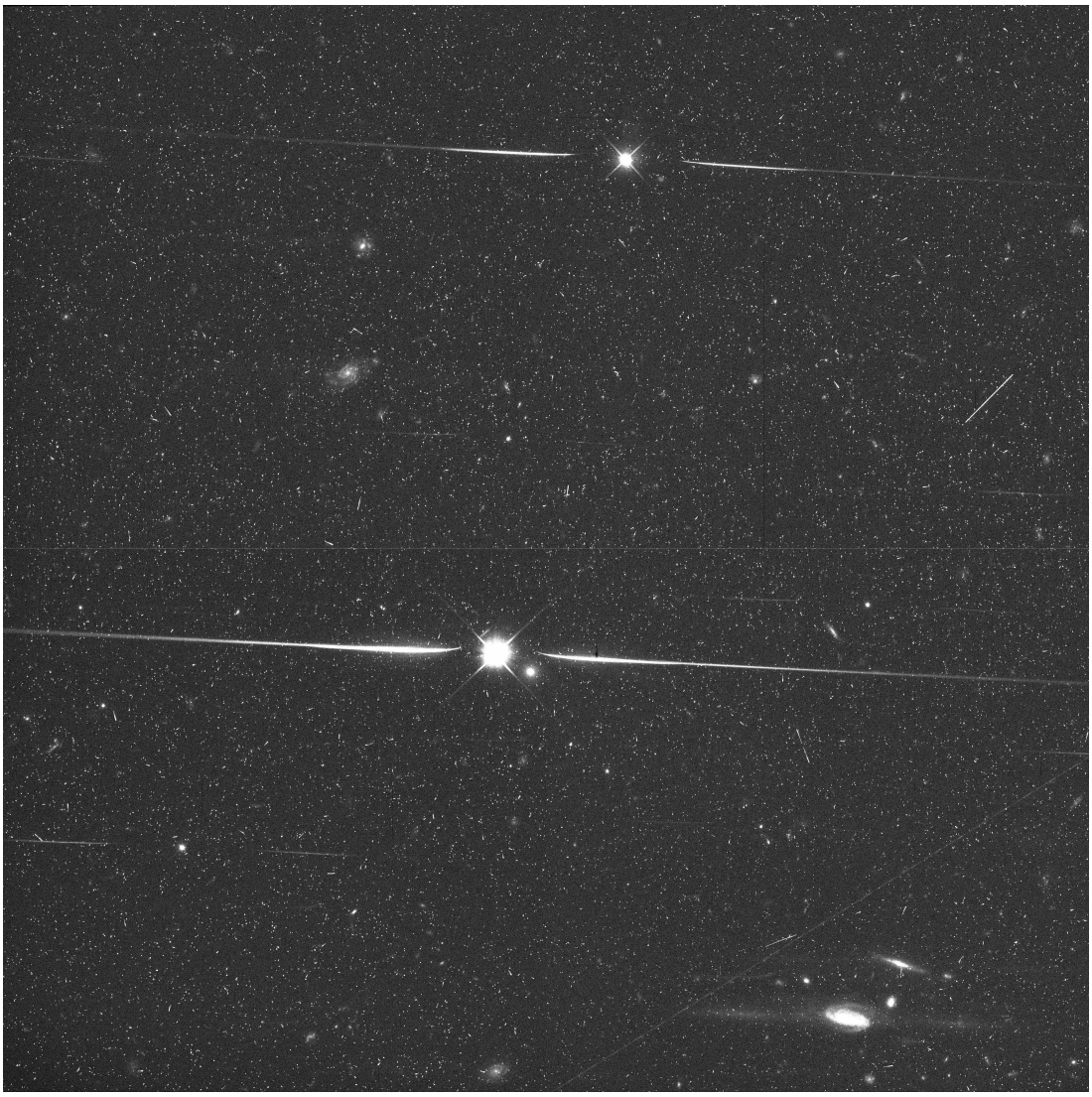

Figure 61 – Example of the UVIS grism G280, image `ibk321u7q_flt.fits`*. The sources are dispersed into positive and negative "wings." A satellite trail is also present in the lower right corner.*

7 Conclusions

Already the WFC3 Quicklook anomalies database table has contributed to detector studies, including a 2016 Space Astronomy Summer Program student project in which dragon's breath and scattered light were characterized from the dozens of examples flagged (minute 36:00 in Markwardt (2016)). This study was expanded and summarized in an instrument science report, Fowler et al. (2017), and in the creation of an interactive dragon's breath/scattered light map, which UVIS proposers can reference to avoid placing bright stars in a hot spot likely to trigger the light scatter (`http://www.stsci.edu/hst/wfc3/ins_performance/anomalies/bokeh_dragon.html`). Other analysis projects could be powered by the anomalies table. For example, it would now be possible to characterize the IR diamond feature using the over 200 examples so far flagged. Further examples of the utility of the anomalies table are discussed in the Appendix.

James Webb Space Telescope instrument teams should consider utilizing a Quicklook system similar to WFC3's to keep track of the expected as well as the inevitable unexpected optical and detector anomalies. Having it in place by commissioning should help expedite in that critical time diagnosing issues and detecting trends.

Quicklook-Related Software

The primarily Python-based software packages governing the Quicklook database, detector monitoring scripts, and website can be found in the STScI Github repositories `automated_scripts`, `detectors`, `pyql`, and `ql-website`. Please email `wfc3_ql@stsci.edu` for access and `help@stsci.edu` for general questions about WFC3 anomalies.

Acknowledgements

We thank all past and present members of the Quicklook team for their contributions to software and image checking: Varun Bajaj, Matthew Bourque, Ariel Bowers, Mike Dulude, Meredith "Website" Durbin, Jules Fowler, Heather Gunning, Harish Khandrika, Heather Kurtz, Larissa Markwardt, Catherine Martlin, Myles McKay, Abi Rajan, Clare Shanahan, Ben Sunnquist, and not at all the least, Mr Quicklook himself, Alex Viana. We give special thanks to Sylvia Baggett for the never-failing help on detector questions. Both Sylvia Baggett and Matthew Bourque were reviewers of this report and we thank them again for their time.

References

Baggett, S. (2009). WFC3 TV3 Testing: UVIS-1 Crosstalk. *WFC3 Instrument Science Report 2009-03*.

Baggett, S., Sabbi, E., and McCullough, P. (2009). WFC3 SMOV Proposal 11422/11529: UVIS SOFA and Lamp Checks. *WFC3 Instrument Science Report 2009-27*.

Bourque, M. and Baggett, S. (2013). WFC3/UVIS Bowtie Monitor. *WFC3 Instrument Science Report 2013-09*.

Bourque, M., Bajaj, V., Bowers, A., Dulude, M., Durbin, M., Gosmeyer, C. Gunning, H., Khandrika, H., Martlin, C., Sunnquist, B., and Viana, A. (2016). The HST/WFC3 Quicklook Project: A User Interface to Hubble Space Telescope Wide Field Camera 3 Data. *Proceedings of the International Astronomical Union*.

Brown, T. (2007). UVIS Channel Filter Ghosts after Filter Replacement. *WFC3 Instrument Science Report 2007-09*.

Brown, T. (2008). WFC3 TV3 Testing: IR Channel Baffle Scatter. *WFC3 Instrument Science Report 2008-06*.

Bushouse, H. (2008). WFC3 IR Ground P-Flats. *WFC3 Instrument Science Report 2008-28*.

Clette, F. (2017). Sunspot Index and Long-term Solar Observations. http://www.sidc.be/silso/datafiles#total.

Deustua, S., editor (2016). *WFC3 Data Handbook, Version 3.0*. Baltimore: STScI.

Dressel, L., editor (2017). *Wide Field Camera 3 Instrument Handbook, Version 9.0*. Baltimore: STScI.

Dulude, M., Baggett, S., Bushouse, H., and Hilbert, B. (2011). WFC3/IR Banding. *WFC3 Instrument Science Report 2011-04*.

Durbin, M., Bourque, M., and Baggett, S. (2015). IR "Snowballs": Long-Term Characterization. *WFC3 Instrument Science Report 2015-01*.

Durbin, M. and McCullough, P. (2015). The Impact of Blobs on WFC3/IR Stellar Photometry. *WFC3 Instrument Science Report 2015-06*.

Fowler, J., Markwardt, L., Bourque, M., and J., A. (2017). Analysis of Dragon's Breath and Scattered Light Detector Anomalies on WFC3/UVIS. *WFC3 Instrument Science Report 2017-02*.

Fürst, F., Wilms, J., Rothschild, R. E., Pottschmidt, K., Smith, D. M., and Lingenfelter, R. (2009). Temporal variations of strength and location of the South Atlantic Anomaly as measured by RXTE. *Earth & Planetary Science Letters*.

Gilliland, R., Rajan, A., and Deustua, S. (2010). WFC3/UVIS Full Well Depths, and Linearity Near and Beyond Saturation. *WFC3 Instrument Science Report 2010-10*.

Gosmeyer, C. and Baggett, S. (2015). WFC3 IR Gain from 2010 to 2015. *WFC3 Instrument Science Report 2015-14*.

Gosmeyer, C. and Baggett, S. (2017). WFC3/UVIS External CTE Monitor: 2016 Updates on Coefficients and Analysis Pipeline. *WFC3 Instrument Science Report 2017-09*.

Hilbert, B. and McCullough, P. (2009). Wfc3 smov results: Ir channel dark current, read-noise, and background signal. *WFC3 Instrument Science Report 2009-21*.

Kuntschner, H., Bushouse, H., Kummel, M., and Walsh, J. R. (2009). The ground calibrations of wfc3/uvis g280 grism. *WFC3 Instrument Science Report 2009-01*.

Long, K. S., Baggett, S. M., and MacKenty, J. W. (2013a). Characterizing Persistence in the WFC3 IR Channel: Finite Trapping Times. *WFC3 Instrument Science Report 2013-06*.

Long, K. S., Baggett, S. M., and MacKenty, J. W. (2013b). Characterizing Persistence in the WFC3 IR Channel: Observations of Omega Cen. *WFC3 Instrument Science Report 2013-07*.

Mack, J., Dahlen, T., Sabbi, E., and Bowers, A. (2016). UVIS 2.0: Chip-Dependent Flats. *WFC3 Instrument Science Report 2016-04*.

Markwardt, L. (2016). Annual SASP Symposium 2016 (Space Mission Support & Software Development). https://webcast.stsci.edu/webcast/detail.xhtml?talkid=5167&parent=1.

McCullough, P. (2011). Geometric Model of UVIS Filter Ghosts in WFC3. *WFC3 Instrument Science Report 2011-16*.

McCullough, P., Mack, J., Dulude, M., and Hilbert, B. (2014). Infrared Blobs: Time-dependent Flags. *WFC3 Instrument Science Report 2014-21*.

McCullough, P. and MacKenty, J. (2012). Considerations for using Spatial Scans with WFC3. *WFC3 Instrument Science Report 2012-08*.

Ryan, R. and Baggett, S. (2015). The Internal Flat Fields for WFC3/IR. *WFC3 Instrument Science Report 2015-11*.

STScI (2017). HST Cycle 25 Phase II Proposal Instructions. http://www.stsci.edu/ftp/documents/p2pi/p2pi.pdf.

Sunnquist, B., Mack, J., and Khandrika, H. (2017). Asteroids in the WFC3/IR Frontier Fields Images. *WFC3 Instrument Science Report 2017-18*.

Viana, A. and Baggett, S. (2010). WFC3 TV3 Testing: IR Crosstalk. *WFC3 Instrument Science Report 2010-02*.

Wong, M. (2010). Amplitude of Fringing on in WFC3/UVIS Narrowband Red Filters. *WFC3 Instrument Science Report 2010-04*.

Appendix: The Power of the Quicklook Database

The FITS header information of all WFC3 images ever taken are stored as tables in the Quicklook database. To provide a visual for the number of WFC3 images contained in the database, we plot the total number images, with and without anomalies, taken in every filter of IR (Figure 62) and UVIS (Figure 63), from June 2009 up to 10 August 2017. The total number of IR and UVIS observations are 112,823 and 95,256, respectively, with 11% and 8% flagged for containing at least one anomaly. With the addition of the anomalies table in the WFC3 Quicklook internal database, it is easy to plot the frequency of features. Here we briefly show off the potential of the database for detector analysis and hope to seed a few questions that may be worth follow-up study.

Because the anomalies table can be joined with other tables containing the FITS header information, including filter names, we can can plot the number of images per filter that contain UVIS optical anomalies: detector-filter ghost (Figure 64), figure-8 ghost (Figure 65), filter ghost (Figure 66), dragon's breath (Figure 67), and scattered light (Figure 68). It is not surprising to see that the most used filters (F275W, F350LP, F475X, F606W, F814W) also show the most anomalies. Fringing, known to be wavelength-dependent, unsurprisingly frequents only certain red filters (Figure 69). A little more surprising is that the IR diamond feature prefers the F110W and F098M filters over the most-overall-used F160W (Figure 70). This perhaps has to do with the diamond feature's apparent correlation with saturated sources.

We go now to simply plotting frequencies of anomalies with time. In Figure 71 we plot a histogram of images over WFC3's lifetime containing Earth limb/shine. The number of Earth limb-blasted images spikes in 2010 and then settles down, a consequence of more judicious scheduling, not because there were more IR images - see the left plot in Figure 75.

We plot the number of cosmic ray showers flagged in external UVIS images in Figure 72. If we overplot the number of sunspots (monthly mean total sunspot number file from Clette (2017)) as a proxy for solar activity, the number of cosmic ray shower events appears to anti-correlate with solar activity. If this is true, it is not a new result. The anti-correlation between solar activity and cosmic ray frequency is well-known (e.g., on Hubble's instruments, charge transfer efficiency degradation has been shown to increase with decreased solar activity (Gosmeyer and Baggett, 2017)). The theory is that higher solar activity heats the upper atmosphere, increasing the neutral atmospheric density in the altitude of zones of high radiation that low-Earth-orbit satellites like Hubble pass through, providing them with more shielding from cosmic rays (Fürst et al., 2009). In the figure, there appears to be higher counts of cosmic ray showers when the solar cycle was near minimum around 2010. As the

cycle is apparently waning again, it remains to be seen whether another jump in cosmic ray showers occurs. It might be better to normalize to exposure time and do a more in-depth analysis once quicklooking of the full archive has been completed.

We plot guidestar failures against date, per detector (Figure 73), and as expected, the distribution appears random, divided fairly equally between IR and UVIS. However, if we plot counts of satellite trails per detector a somewhat surprising pattern emerges for what should be a random event. Per date bin, 2-3× more IR images have satellite trails than UVIS (Figure 74), even if we discount all subarrays and compare only full frame images. Not only should this be random, bear in mind too, the IR detector ($136'' \times 123''$) covers less sky area than the two UVIS chips ($162'' \times 162''$). The discreprancy cannot necessarily be explained by more IR images or more cumulative IR exposure times; as the plots in Figure 75 show, neither the total exposure time nor the total number of images in IR is consistently 2-3× UVIS. We offer a few speculations. First, there may be a detection bias since satellite trails are more obvious to quicklookers on the IR detector because of their poor up-the-ramp fitting, whereas on UVIS they can be tough at times to distinguish from long cosmic rays. Second, many of the satellite trails flagged in the IR images are not unique; some trails are just persistence caused by real trails in earlier images, and thus a single trail might be counted multiple times. A final consideration is the packing of orbits. IR observations are able to be packed more closely than UVIS images per orbit, which means the same satellite has a greater opportunity to appear in multiple IR images than in multiple UVIS images. These speculations could be definitively verified by an analyses of the over 1200 examples flagged in the database.

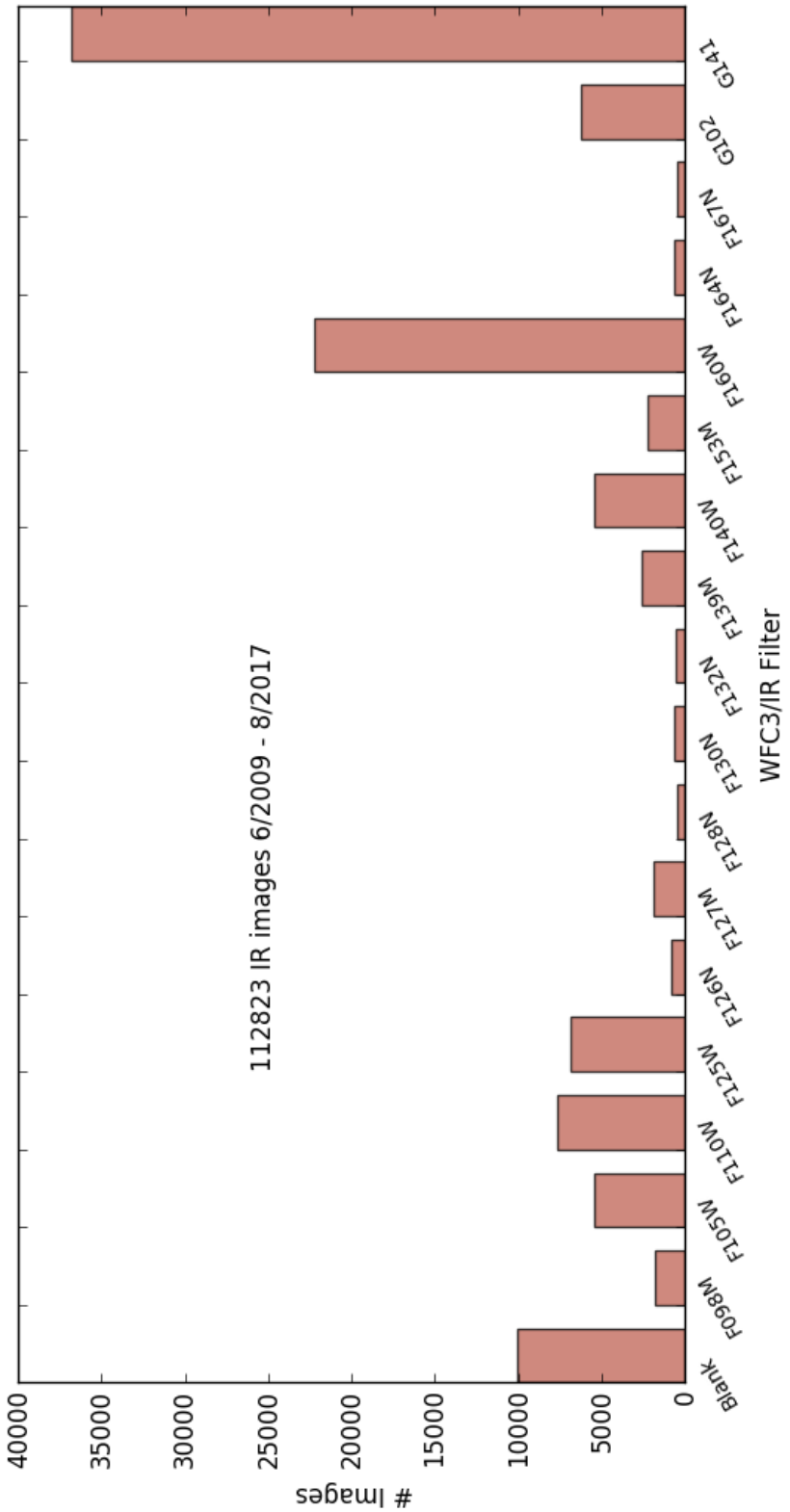

Figure 62 – Total number of images, with and without anomalies, in each IR filter from June 2009 to August 2017.

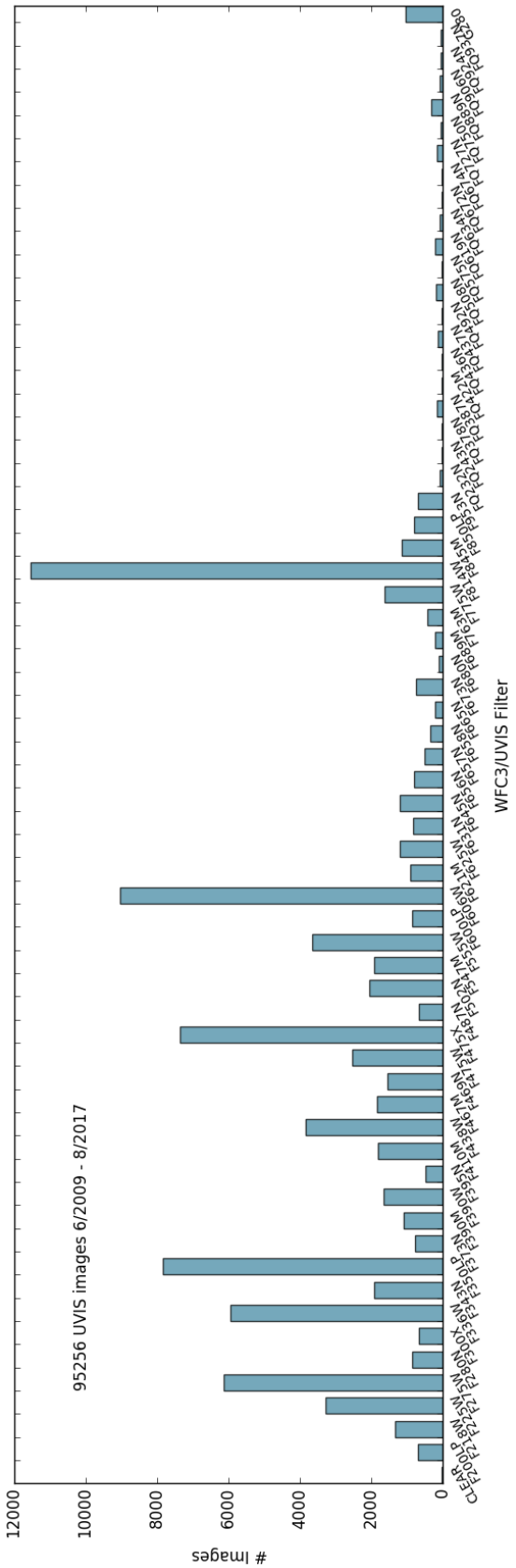

Figure 63 – Total number of images, with and without anomalies, in each UVIS filter from June 2009 to August 2017.

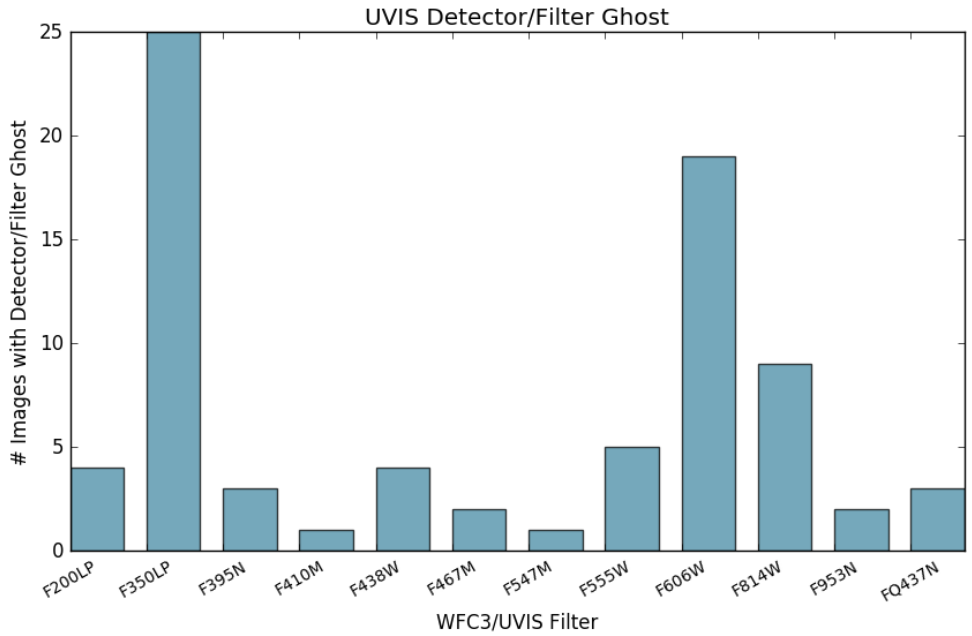

Figure 64 – Number of UVIS images, per filter, so far flagged by the Quicklook team for containing a detector-filter ghost.

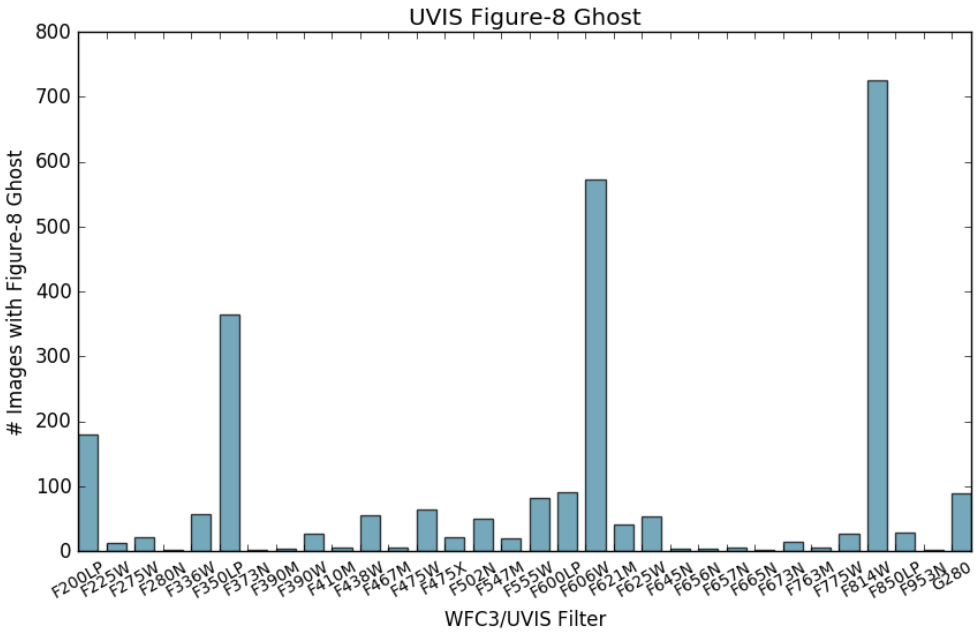

Figure 65 – Number of UVIS images, per filter, so far flagged by the Quicklook team for containing a figure-8 ghost.

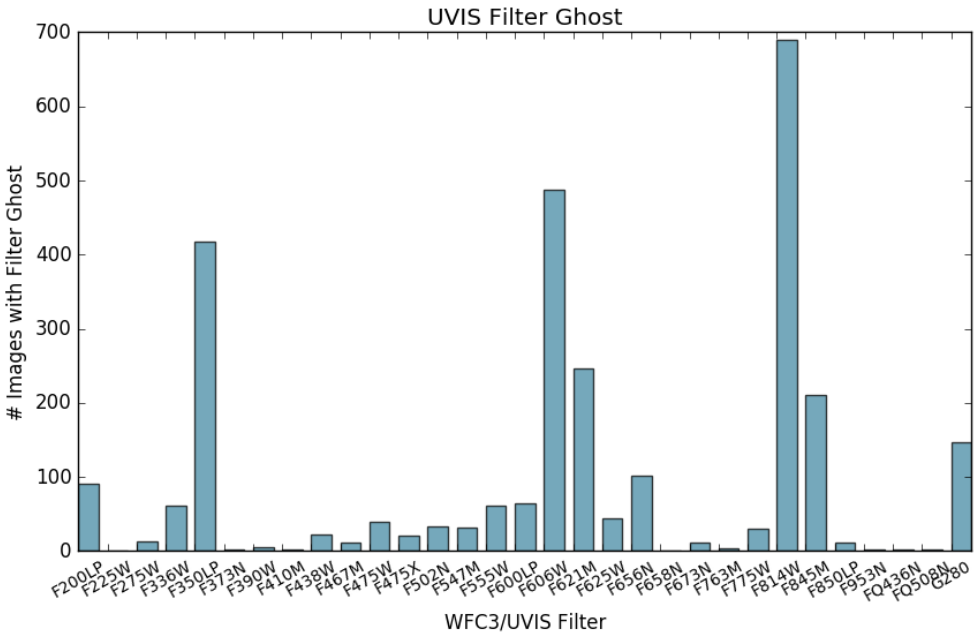

Figure 66 – Number of UVIS images, per filter, so far flagged by the Quicklook team for containing a filter ghost.

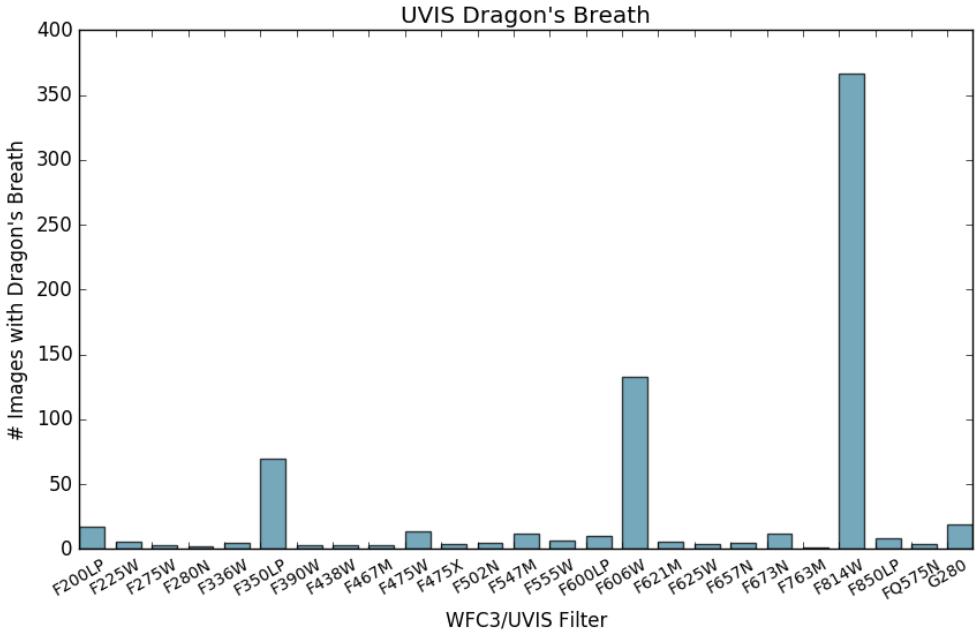

Figure 67 – Number of UVIS images, per filter, so far flagged by the Quicklook team for containing dragon's breath.

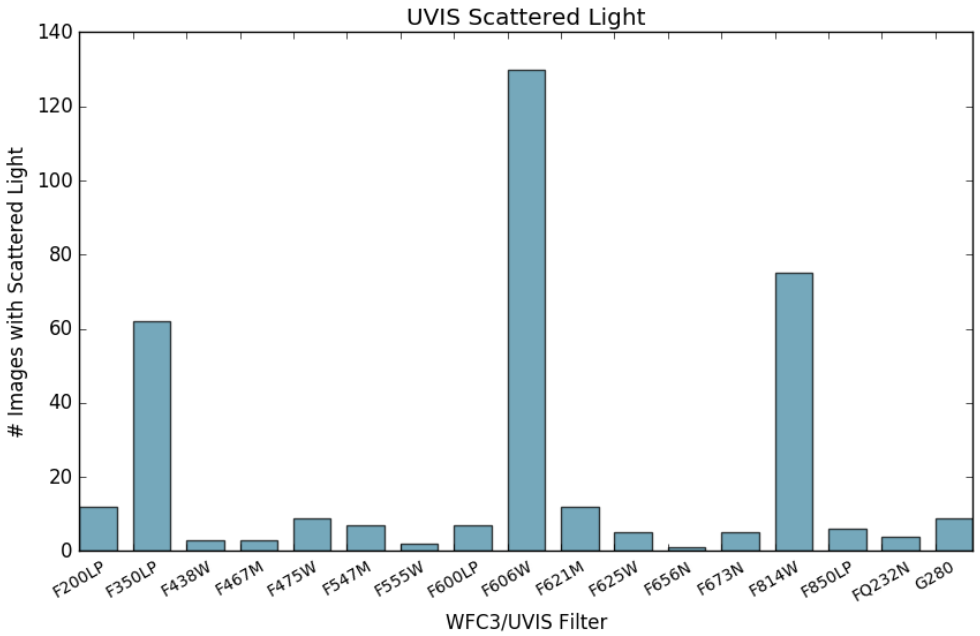

Figure 68 – Number of UVIS images, per filter, so far flagged by the Quicklook team for containing scattered light.

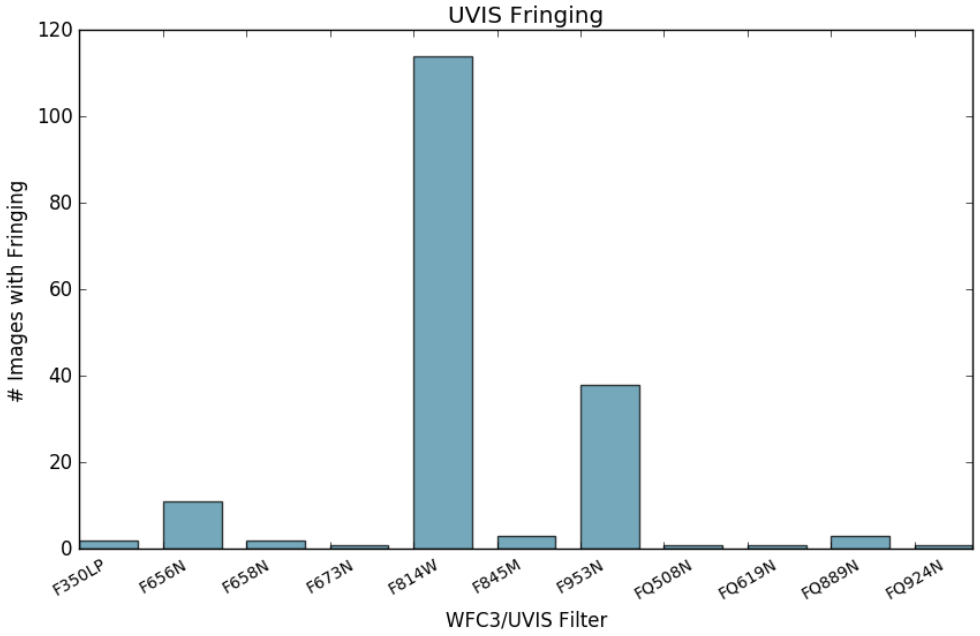

Figure 69 – Number of UVIS images, per filter, so far flagged by the Quicklook team for containing fringing.

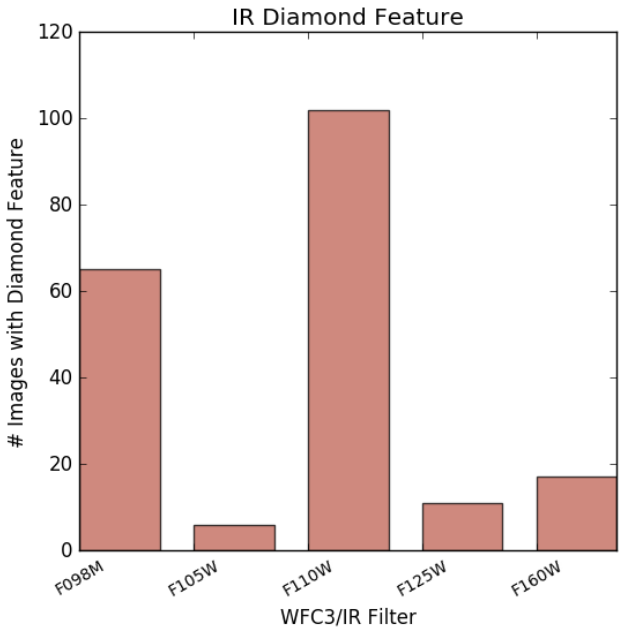

Figure 70 – Number of IR images, per filter, so far flagged by the Quicklook team for containing a diamond feature.

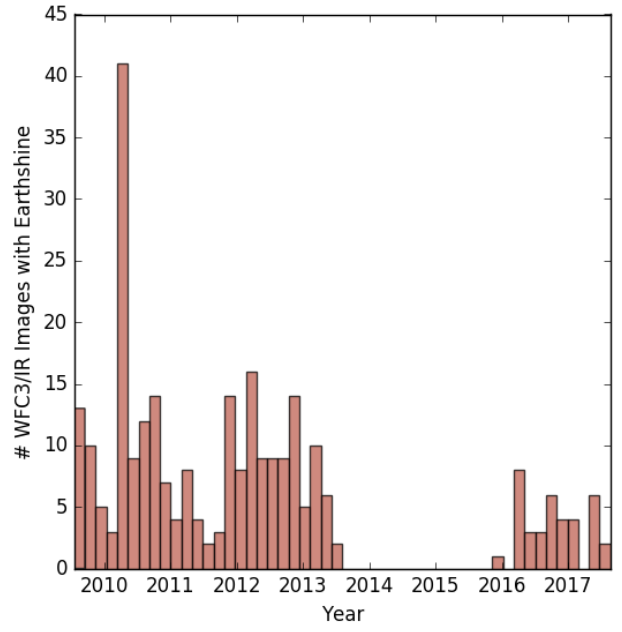

Figure 71 – Histogram of IR images so far flagged by the Quicklook team for containing Earth limb/shine, where each bin is roughly 1.7 months. The 2014-2015 gap represents archived images the Quicklook team has not yet finished flagging.

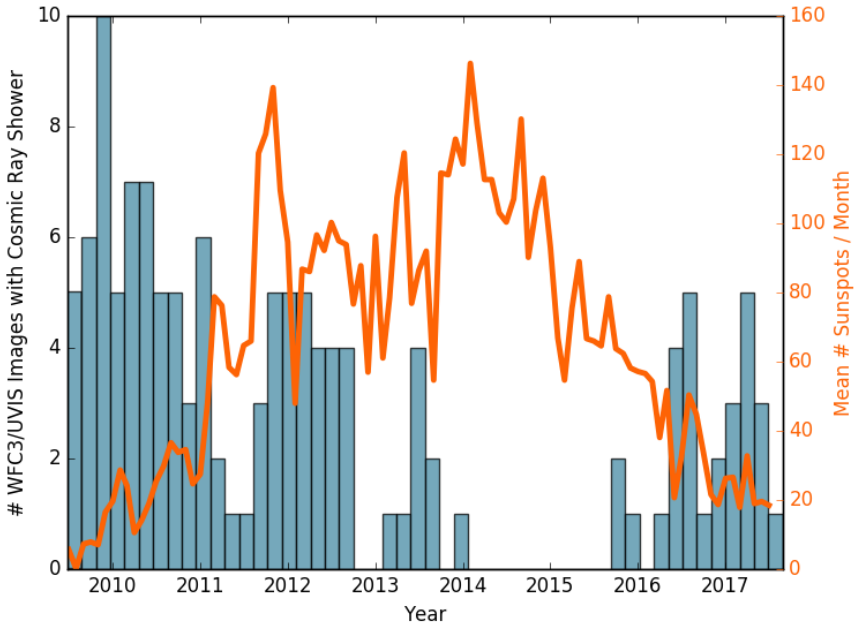

Figure 72 – Histogram of external UVIS images so far flagged by the Quicklook team for containing cosmic ray showers, where each bin is roughly 1.7 months. Overplotted are the mean sunspot counts per month. The 2014-2015 gap in the histogram represent archived images the Quicklook team has not yet finished flagging.

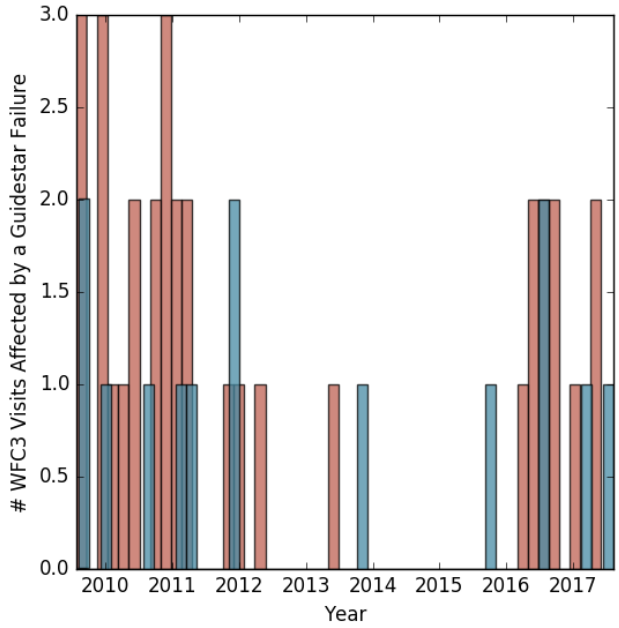

Figure 73 – Histogram of IR (red) and UVIS (blue) visits so far flagged by the Quicklook team as containing a guidestar failure. Each bin is roughly 1.7 months. The 2014-2015 gap represents archived images the Quicklook team has not yet finished flagging.

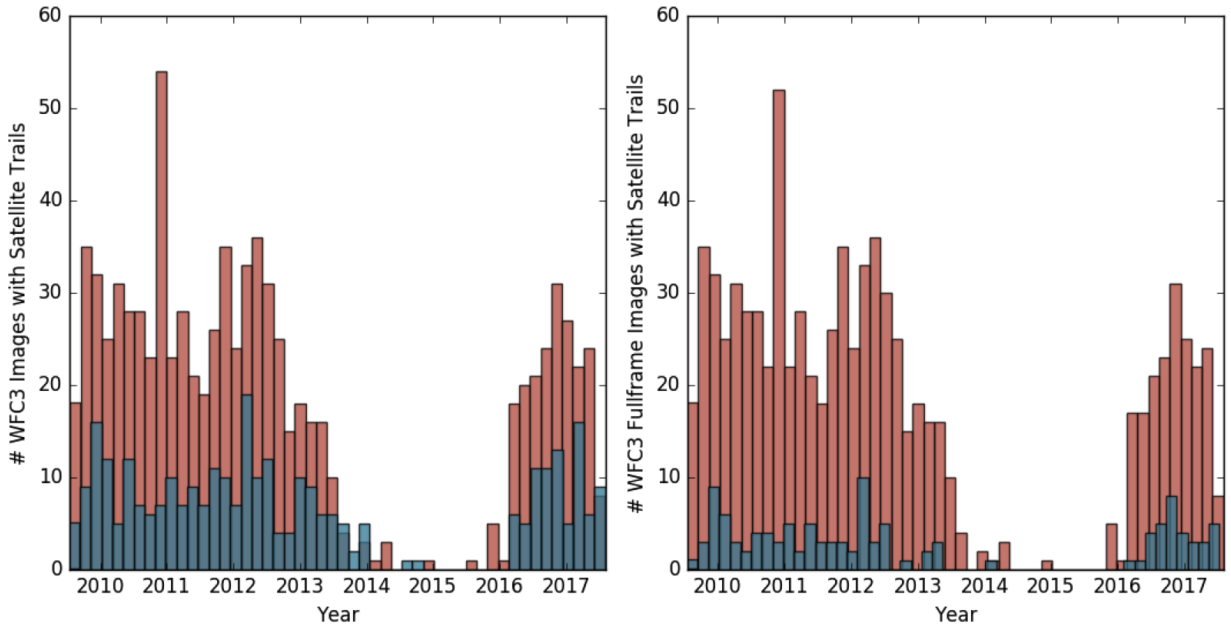

Figure 74 – Histogram of IR (red) and UVIS (blue) images flagged for satellite trails, where each bin is roughly 1.7 months. The left plot shows all images, including subarrays, and the right plot shows only full frame images. The 2014-2015 gap represents archived images the Quicklook team has not yet finished flagging.

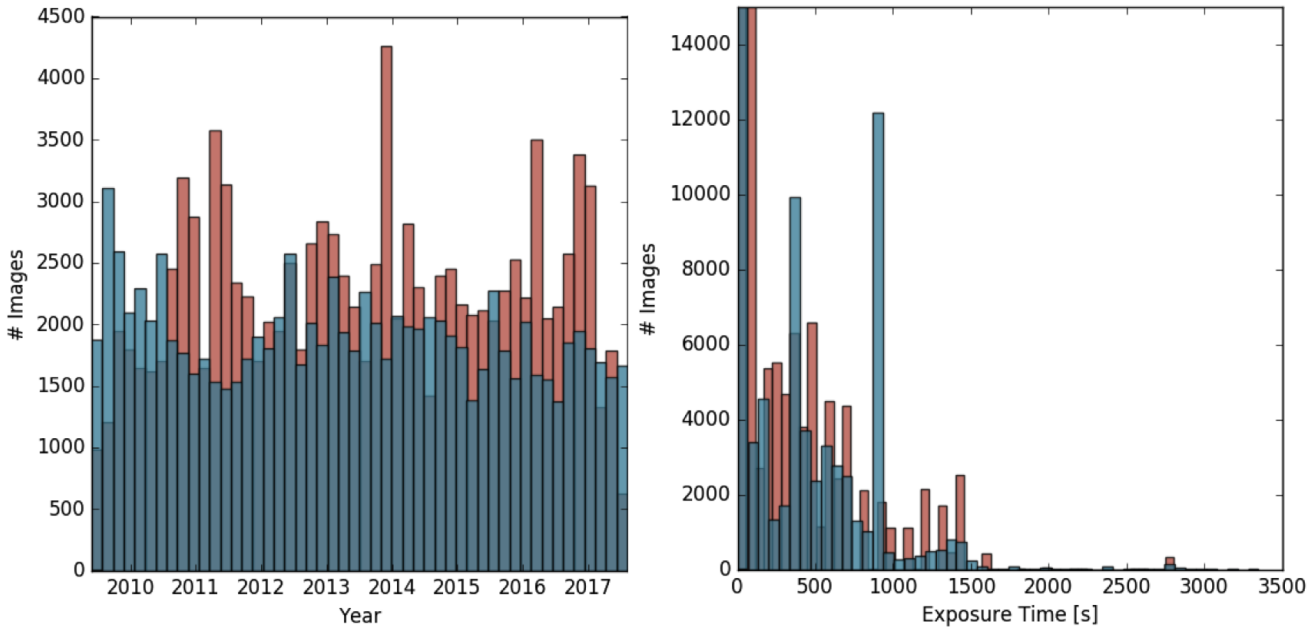

Figure 75 – On the left, the total number of IR (red) and UVIS (blue) images over time, where each bin is roughly 1.7 months. On the right, the total number of IR and UVIS images in bins of exposure time.